

Galaxy Truncations

Introducing 2 techniques to aid in the search

Stephan Peters

December 19, 2009

Abstract

Two new techniques have been developed to determine the surface brightness profiles in galaxies. *Equivalent profiles* is a re-implementation of an old technique used by for example (de Vaucouleurs et al., 1968). A second technique is the *Principle Axis Summation*. This technique performs a reprojection of the data as if the galaxies is seen edge-on. A major benefit of PAS is the independence of inclination. These techniques are analysed against the sample of Pohlen and Trujillo (2006) and found a valid measures of surface brightness profiles. The PAS system is then used as a tool for measuring and mapping dust extinction in galaxies.

Contents

1	Introduction	2
2	Techniques matter	4
2.1	Introduction	4
2.2	Equivalent Profiles	5
2.3	Principle Axis Summation	11
2.4	Profile fitting	13
2.4.1	Scalelengths	13
2.4.2	Break fitting	14
3	Pohlen & Trujillo dataset	15
3.1	Description	15
3.2	Results	16
4	Mapping dust	21
4.1	Introduction	21
4.2	NYU value-added catalog	22
4.3	Results	24
5	Discussion & Conclusions	29
6	Acknowledgements	31
A	The Pohlen & Trujillo dataset	35
A.1	Derived Parameters	35
A.2	Main parameters	37
A.3	Plots for each galaxy	41

Chapter 1

Introduction

The surface brightness of a galaxy can be seen as the amount of light a small area of a galaxy is emitting. One of the nice properties of the surface brightness is its independence of distance. While the light intensity decreases with distance as $1/r^2$. The angular size decrease with $1/r$. The area thus scales with $1/r^2$. The intensity decrease by distance is thus compensated by the same decrease of area, making the surface brightness a distance independent measure.

Surface brightness profiles depict the surface brightness as a function of the distance to the center of a galaxy. It was found early-on that the intensity decline follows an exponential decay [de Vaucouleurs (1959) and Freeman (1970)]. These conclusions were drawn from face-on galaxies.

van der Kruit (1979) performed the same analysis on edge-on galaxies. He finds that galaxies not only exhibit an exponential decline in intensity, but sometimes also show a strong truncation. This truncation appears as a sharp break in the profile. At this point the intensity no longer slowly decreases, but instead make a sharp downward bend and rapidly declines to zero. In later years the untruncated galaxies would be named type I, while the truncated would be named type II.

Using face-on galaxies Erwin et al. (2005) find that besides the type I and II galaxies there also exists a type III. In these, the intensity first declines normally. At the radius of the break it then changes direction and starts to decline less rapidly. A further subclassification is proposed. The original truncated galaxies of van der Kruit (1979) become *type II-CT galaxies* in this scheme. It is believed that the concept of a truncation is not a true truncation, but instead details a point beyond which there still exists a rapidly decreasing brightness profile.(Florido et al., 2007)

It is yet unclear what the exact physical cause of the profiles is. Various possible sources of truncations have been proposed. These range from local star formation density thresholds (Schaye, 2004), to angular momentum distribution (van der Kruit, 1987) and the influence of a magnetic field (Florido et al., 2007). Interestingly truncations have also been detected in hydrodynamic cosmological models (Sánchez-Blázquez et al., 2009). The reader is referred to (van der Kruit, 2008) for a review of all theories.

The physical cause of truncations is thus still unknown. As such, it is interesting to develop new ways of analysing the data. These might provide new insights into the data. In this report two techniques have been developed for that exact reason.

Chapter 2

Techniques matter

2.1 Introduction

A well known problem in many fields of science is the impact the act of observing has on an observation. By observing, the observer changes the observed. In astronomical observations this phenomena is not of much influence. Stars do not get dimmer because some of their light is taken by the camera. Spectral lines do not disappear once they have been seen.

An analog of this problem does work in astronomy: the way we observe changes what we think we observe. Techniques are the key, and with each more advanced one more *assumptions* will have to be made which can have an impact on what one thinks is observed.

In the field of surface brightness profiles, there are now two techniques for different situations. For edge-on galaxy a simple surface brightness measurement along the main axis is sufficient for a surface brightness plot. In sufficiently deep exposures one can even make separate profiles for various heights in the disk.

The observed surface brightness is a result of a line-of-sight integration of all light-sources along that line of sight, combined with inevitable dust extinction. Light from stars at the back of the galaxy will suffer from a long path through the galaxy and as such will suffer from much extinction. Another problem is that the light on one line of sight originates in various regions (in terms of distance from the galaxy center). If the brightness of the galaxy decreases monotonically with radius, one could deal with this problem. In reality it will never be this simple, as the existence of spiral arms proves. Impressive steps are un-

dertaken to deal with this by decomposing the galaxy (e.g. Pohlen et al. (2007)), but assumptions will always play a role.

In face-on galaxies the situation is completely reversed. Where in the edge-on galaxies one deals with a line-of-sight integration along the radial axis of the galaxy, one now deals with a line of sight along the far shorter height of the galaxy. Dust will be of far less importance and the substructure in the galaxy can easily be seen. But what exactly is a radial profile in this situation? A simple average of all light observed at each radius, thus ignoring the substructure? Or separate profiles for both the spiral arms and the inter-spiral regions need to be defined, as for example in the bachelor thesis of Janssens (2009).

Most authors prefer the simple averaging over all substructure. Several techniques exist for this. In the beginning authors made use of elliptical averaging. Only perfectly face-on galaxies will appear circular and so one almost always fits ellipses to a galaxy with the shape of the ellipse being a (indirect) function of the inclination. A more recent innovation is the use of elliptical isophote fitting, in which the ellipses can be free to rotate and change shape to best fit the observation. This allows for a better treatment of substructure.

Very different technique thus exists with different approaches and results. In this paper, this importance of technique on result has led to the development of two new approaches to disk observation: Equivalent Profiles and Principal Axis Summation. In the sections 2.2 and 2.3 these techniques will be discussed. In section 2.4 the system used to detect and fit breaks and truncations in the profiles is described.

2.2 Equivalent Profiles

In the early days of modern astronomy one of the primary ways of determining the luminosity profile of a galaxy was by using *equivalent luminosity profiles*. This technique is unique in its approach. While most techniques start with a certain distance r and measure a corresponding intensity I , it works in the opposite way. It is based on the simple assumption that galaxies have a brightness distribution centered around their core, with surface brightness decreasing with radius. For an equivalent luminosity profile one measures the entire area in a galaxy, with surface brightness larger than a certain threshold. For each surface brightness I one calculates a equivalent radial distance r^* . This distance represents the radial distance if all of the luminosity contained within it was above that threshold and all luminosity beyond it was lower.

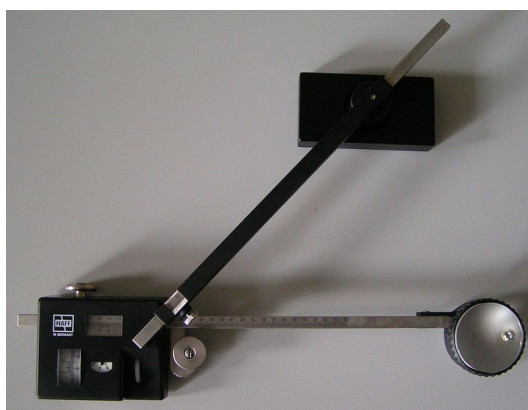


Figure 2.1: An example of a planimeter

In practice this was achieved by creating an isophotal map of a galaxy. By using a device called a planimeter (figure 2.1) one measures the area A covered by each isophote (de Vaucouleurs et al., 1968). The equivalent luminosity profile $I(r^*)$ is then determined using $r^* = (A/\pi)^{1/2}$ (de Vaucouleurs and Davoust, 1980). Inclination is dealt with through the calculation of the area A .

In the last decades the method has fallen from grace when new computerized techniques offered elliptically averaged luminosity profiles (e.g. van der Kruit (1979)).

It is believed that the equivalent profiles still offer interesting and unique insights into galaxy physics. In this report, the technique is therefore re-implemented to make use of the Sloan Digital Sky Survey. In the remainder of this section this setup will be described.

After obtaining the desired source images from the SDSS catalog, each image is masked for all bright stars and objects. These are removed from the image using the IRAF package *fixpix*. An elliptical mask is put around the galaxy. The shape of the ellipse is based on the inclination i which is obtained from literature archives like the NED¹. Each image is checked by hand to ensure that the mask is larger than the maximum radius of the galaxy.

The image is then reprojected into a single dimension and sorted by intensity as array P . This allows for fast data processing. A new array S is made for

¹Available at <http://nedwww.ipac.caltech.edu/>

all possible values of flux f in the range $f \in [\max(P), \min(P)]$ with $S(f)$ being the sum of all pixels in P with values equal or larger than f .

The sky coverage of each SDSS pixel is 0.396^2 arcsec². It is required to reproject all galaxies to a face-on situation. The equation $surface(f) = 0.396^2 S(f) / \cos(i)$ is used for this. To find the equivalent radius r (in arcsec) belonging to a certain flux count f , relation 2.1 is used.

$$r(f) = \sqrt{\frac{surface(f)}{\pi}} = \sqrt{\frac{0.396^2 Q(f)}{\pi \cos(i)}} \quad (2.1)$$

To convert the flux into magnitudes, the standard SDSS scheme as defined in Abazajian et al. (2009) in formula 2.2 is used. The value $flux20$ in formula 2.3 is a value provided for each observation by SDSS in the image header. A better value for $flux20$ can be found by calculating it directly from the airmass, zeropoint aa and extinction coefficient kk . For this, formula 2.4 is used. While the *asinh* magnitudes system would provide benefits for faint objects (Lupton et al., 1999), in this paper *pogson* system will be used. This allows for easier comparison with existing literature.

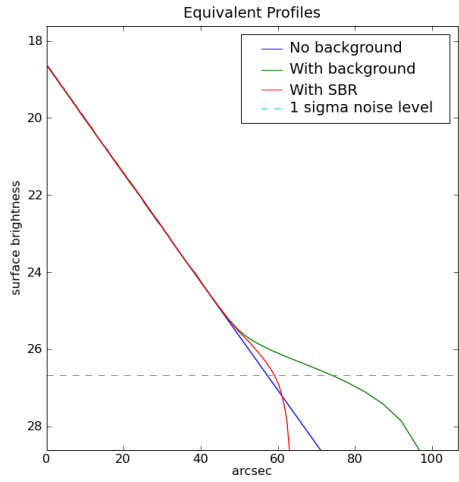
$$\text{mag} = -2.5 \log(f/f_0) \quad (2.2)$$

$$f/f_0 = \frac{f}{10^8 flux20} \quad (2.3)$$

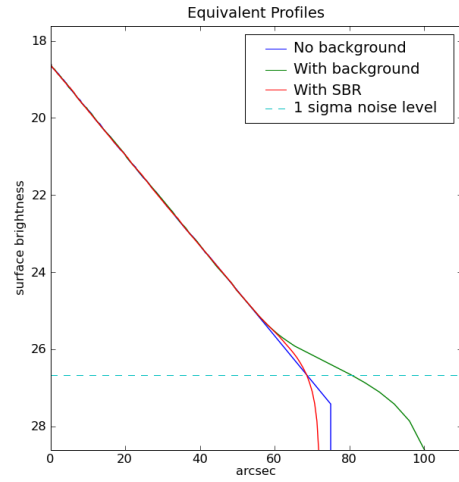
$$flux20 = 53.907456 \times 10^{\frac{20.0}{2.5} - 0.4(aa + kk \times airmass)} \quad (2.4)$$

In figure 2.2 the EP's of 4 simulations of galaxies, with a disk break at various intensities, is shown. The blue line represents a perfect situation without any noise. The green line shows the contaminating effect typical background noise has on the data.

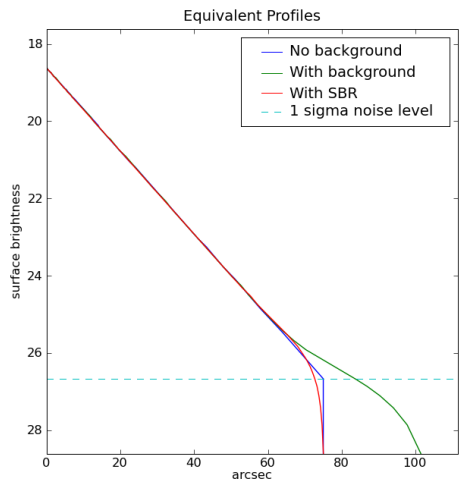
Figure 2.3 also demonstrates this effect. Shown are simulations for a galaxy with a total radius of 250 pixels contained in a mask of 300 pixels radius. In each case, the blue line is the distribution of intensities of the pixels associated with the galaxy, convolved with the noise. The green line denotes the distribution of all pixels associated with the background. The combined effect of these two is shown by the red line. From the height of the combined signal above the galaxy signal, it becomes apparent what a profound effect the background noise has on the technique.



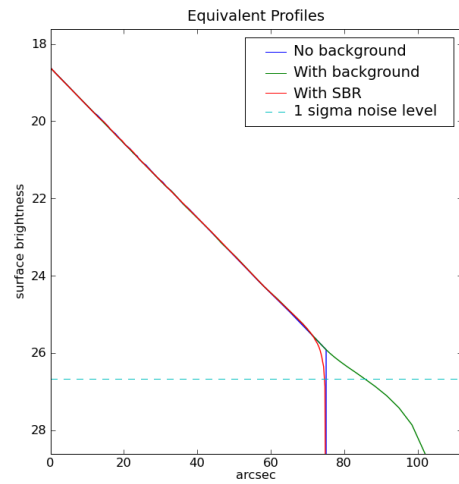
(a) Break at $I = 0.1\sigma$



(b) Break at $I = 0.5\sigma$

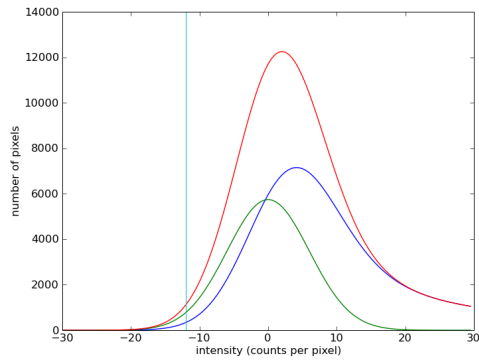


(c) Break at $I = 1.0\sigma$

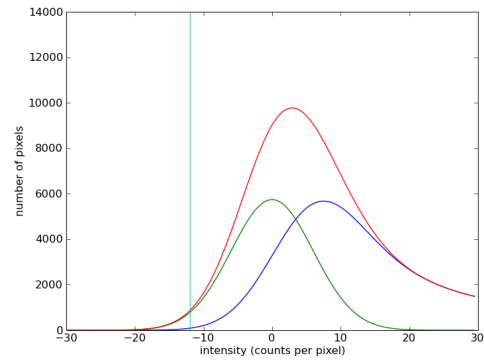


(d) Break at $I = 1.5\sigma$

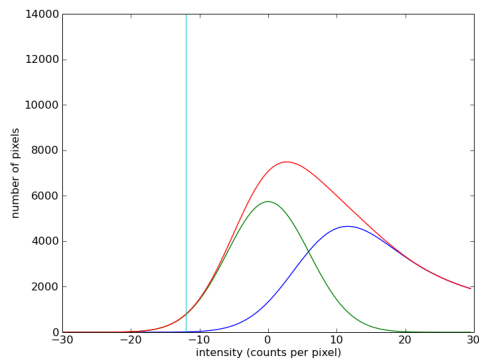
Figure 2.2: Equivalent profiles of 4 simulated galaxies



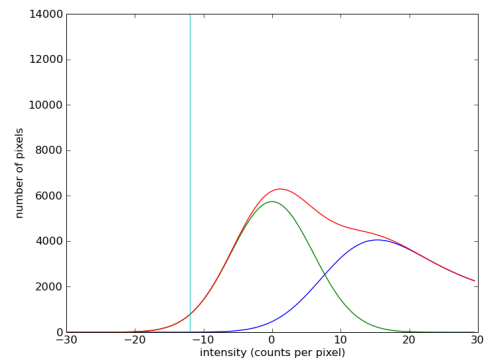
(a) Break at $I = 1$ count



(b) Break at $I = 3$ counts



(c) Break at $I = 6$ counts



(d) Break at $I = 9$ counts

Figure 2.3: Four different simulations. The green lines denote the total noise pixel distribution, the blue denote the total galaxy pixel distribution and the red denote the combined effect. The cyan vertical lines denote the -2σ (at -12 counts) point.

One obvious approach to counter this effect is to minimize the radius of the elliptical mask, so that it covers the least amount of background pixels as possible. In certain situations this proved to be insufficient due to the shape of the galaxy. To counter this effect a new approach dubbed *statistical background reduction* was developed. In an observation the background noise will always follow a Gaussian distribution with a central value μ and a standard deviation σ . This can easily be measured by placing boxes in areas of the observation devoid of any stars or galaxies. The intensities of the pixel in the box are then plotted in a single diagram per column. Possible sources clearly stand out in the plot, making it easy to remove such contaminations. When satisfied that the box will only contain noise the μ_{sky} and σ values can now be determined. On average a box will cover over 30.000 pixels.

Noise also affects the galaxies in observations with the same standard deviation σ . However, the central values of their distribution will not be equal to μ_{sky} but instead be centered around the true surface brightness of the galaxy in that area. For example, suppose one has an observation of a galaxy in which the true surface brightness of the galaxy at the very edge has an intensity of 3 counts, and the noise is defined by $\mu_{sky} = 0$ and $\sigma = 6$ counts. The intensity distributions of noise pixels and the (near) edge pixels will overlap in the 3 counts range as can be seen in figure 2.3. But from statistics it follows that almost all pixels in the distribution with values $< -2\sigma$ will be real background noise pixels.

Based on the amount of pixels found in this $< -2\sigma$ range, along with the μ_{sky} and σ_{sky} , one can then extrapolate how many background noise pixels should be at each count value. By simply removing this extrapolated distribution from the total observation, one almost perfectly recovers the original galaxy pixel distribution.

In figure 2.2 this effect is demonstrated by the red line. Note that the technique becomes strongest when the edge of the galaxy is above the 1.0σ (6 counts) level. But even with a break at 0.5σ (3 counts) the technique shows an improvement. Looking at 2.3 the reason for this becomes apparent. The -2.0σ range is, in all the cases with edge intensities ≤ 3 counts per pixel, almost completely dominated by the background noise. Even in a case of a break of almost absolute 0 it does not introduce very strange artifacts into the data, as can be seen in figure 2.3(a).

It is thus concluded that statistical background reduction is a valid noise reduction. Combined with the equivalent profiles technique it offers an inter-

esting new way to observe galaxies.

2.3 Principle Axis Summation

One of the problems that has always hindered the understanding of disk truncation, is the connection between face-on and edge-on galaxies. While both situations have been studied in great detail, there is no unifying technique allowing for a direct comparison between face-on and edge-on galaxies.

One of the most recent works to tackle this problem has been done by Pohlen et al. (2007). They have devised a new algorithm that, under simple axial symmetry assumptions, can project a two-dimensional edge-on galaxy into a three-dimensional galaxy. In their paper they then present a set of 10 edge-on galaxies with inclination i ranging between 80° and 90° . It is found that the typical scale-lengths match ones found in observations of face-on galaxies, as in Erwin et al. (2005) and Pohlen and Trujillo (2006). Eventhough the results of this technique are impressive, it still does not cover all possible inclinations. It also depends on the assumption of axial symmetry and a good understanding of the dust extinction in the galaxy.

The problem hampering comparisons of face-on and edge-on galaxies, has always been the unknown parameters. For face-on galaxies it will always be unclear what the height of the disk is. Likewise in edge-on galaxies it is always unknown what the exact inclination i is. A need thus exists for a single technique to unify both types of galaxies. Therefore a new technique dubbed *principle axis summation* is devised.

The premise of this technique is elegantly simple. By always summing the light in a galaxy onto a single axis, one effectively eliminates the inclination and height dependencies of the other techniques. The technique is equivalent to a line-of-sight integration along *both* the height and radius. Since the height will be of no significant impact in comparison to the data, this effectively results in a projection of any galaxy into an edge-on galaxy. The long axis of a galaxy is the logical choice for this summation as it is independent of inclination. As such, it will always be the same length in both edge-on and face-on galaxies. Note that this assumption will fail in the case of non-circular edge-on galaxies seen along the long axis. This will cause the short axis to appear the principle axis. Fortunatly this only occurs in a small amount of galaxies and as such will have little influence on the results of a large sample of galaxies.

In practice the principle axis of an image is first aligned with the horizontal axis of the image. In galaxies with known orientations this is done based on literature values, in others it has to be done by hand (or eye). The center of the galaxy is then selected. In cases where the galaxy center is already reported in literature, that value will be used. In cases where the exact center is still unknown, a summation onto both the horizontal and vertical axis is used to determine the brightest column and row. That position is taken as the center.

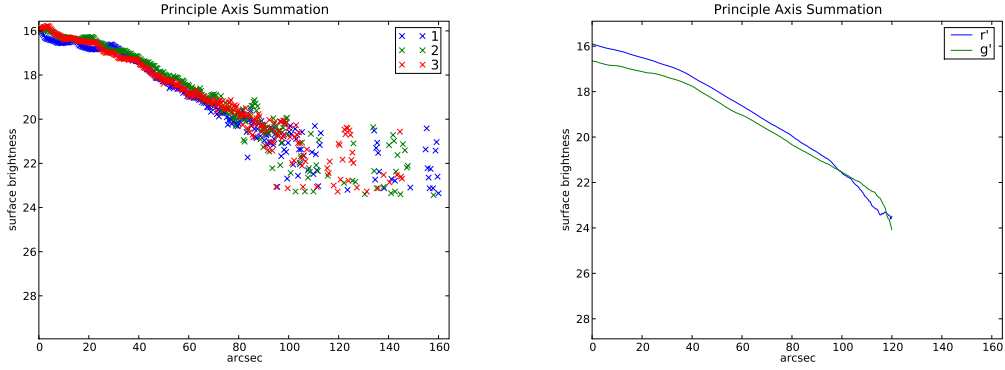
Each galaxy is then divided into four quadrants. The quadrants are created in such a way that they all share one pixel-column and pixel-row with their two neighbours. By sharing this row and column, it is ensured that each quadrant starts at the center of the galaxy. Each quadrant is then individually summed per pixel column onto the primary axis. Following the same system of magnitude calculations as in the previous section, this will lead to four sets of surface brightness profiles.

The size of the processed image has been selected as being large enough, that the summation will greatly extend beyond the edge of the galaxy. By calculating the median of the last group of columns the background noise level is found. Because uncertainty always goes down with increasing sample size, this measurement offers a reasonably good estimation of the background level below the 1σ threshold.

The variations between the four profiles give a convenient handle on the error and symmetry of the galaxy. In a perfectly symmetrical galaxy, all four profiles will be identical. But in non-symmetric galaxies they will have four different slopes. The main profile is constructed by taking the median of the four flux values at that radius. The median will filter out contaminations in a single quadrant. The system is set up in such a way that individual quadrants can be removed from the reduction if they are too contaminated. This may occur in the cases of strong stars, background galaxies or the edge of an observation.

A disadvantage of the method is the lack of treatment of dust extinction. Edge-on galaxies suffer from much extinction while face-on will have almost no problems with dust. The r' band is used to minimize this problem. Of all the possible SDSS bands, the r' -band typically suffers from the least dust absorption. In chapter 4 dust will be discussed in more detail, and this phenomena will actually be used map dust absorption in galaxies.

In figure 2.4 the profile derived for galaxy NGC 701, a typical untruncated



(a) Individual profiles of the 4 quadrants (g'-band)

(b) Main profile

Figure 2.4: Principle axis summation for the untruncated galaxy NGC 701

galaxy, is shown. Figure 2.5 shows the profile for a truncated galaxy, NGC 1084. The truncation in the second figure occurs at roughly 40 arcseconds, as can be seen by the sudden bend in the plot. See figures A.5 and A.9 for a more complete examination of these galaxies.

2.4 Profile fitting

2.4.1 Scalelengths

At various points in this report it was required to measure the scalelengths of galaxies. This was done by fitting a linear line of $y = a + bx$ to the data. The coefficients a and b can be determined by performing a least squares fit. These can be obtained through the following formulas.

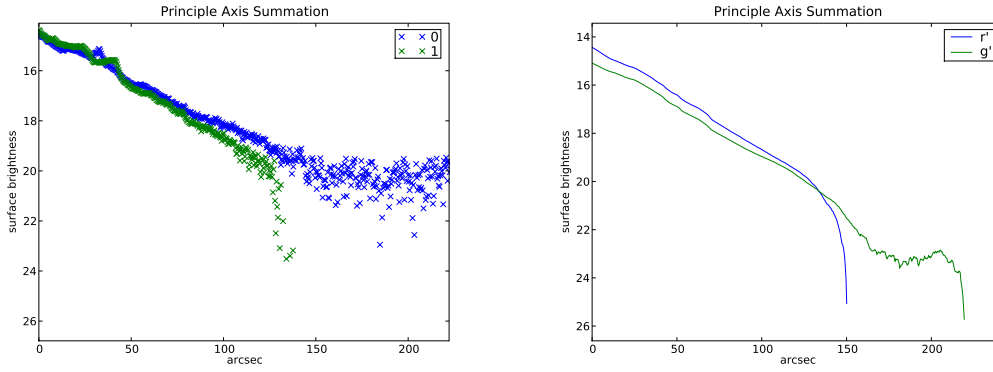
$$a = \frac{(\Sigma y)(\Sigma x^2) - (\Sigma x)(\Sigma xy)}{n\Sigma x^2 - (\Sigma x)^2} \quad (2.5)$$

$$b = \frac{n\Sigma xy - (\Sigma x)(\Sigma y)}{n\Sigma x^2 - (\Sigma x)^2} \quad (2.6)$$

$$error = \Sigma(y_{fit} - y_{data})^2 \quad (2.7)$$

Here Σ denotes the summation over all pixels.

From the coefficient b one can simply derive the scalelength h , since $h = 1/b$.



(a) Individual profiles of the 4 quadrants (g'-band)

(b) Main profile

Figure 2.5: Principle axis summation for truncated galaxy NGC 1084.

2.4.2 Break fitting

It will also be required to fit data to the break. An algorithm is therefore programmed wherein the user can provide the data over the desired range $[x_1, x_2]$. A separation point x_{break} is then defined. Two lines are fit to the data in ranges $[x_1, x_{break}]$ and $[x_{break}, x_2]$. The error is calculated using formula 2.7 and combined using $(error(x_{break}))^2 = (error_1(x_{break}))^2 + (error_2(x_{break}))^2$. $Error(x_{break})$ is calculated for each value for $x_{break} \in [x_1, x_2]$. The minimal value of $Error(x_{break})$ is the break distance x_{break} .

Chapter 3

Pohlen & Trujillo dataset

3.1 Description

In the previous chapter the valid workings of the equivalent profiles and principle axis summation profiles was established. The next step is to compare the technique to the preferred one in literature, the elliptical isophote fitting. This will allow for a deeper understanding of the similarities and differences between the various techniques.

In the Pohlen and Trujillo (2006) paper a sample of 85 face-on to intermediate inclined, nearby, late-type (Sb-Sdm) spiral galaxies is presented. This is based on elliptical isophote fitting. Using the second data release the authors analysed the quality of the SDSS observations in the r' and g' bands and compared them to deeper observations. They find that SDSS can indeed be used for the detection of disk truncations.

On each galaxy elliptical isophote fitting is performed. The sample is then classified according to the system of Erwin et al. (2005). In the remainder of this chapter a comparison of the new techniques against this well defined sample is performed. Micheal Pohlen graciously provided us with their original profile data.

In table A.2 all galaxies in the sample are listed. For each of these galaxies the appropriate r' and g' frame is retrieved from SDSS DR7 using the Catalog Archive Server (CAS) and Data Archive Server (DAS) services¹. For each frame, the overall median and standard deviation for the sky is analysed by measuring them in boxes placed at various places around the galaxy. The results can

¹CAS can be found at <http://das.sdss.org/> and DAS at <http://das.sdss.org/>

be found in table A.2

Using Vizier² the "II/294 The SDSS Photometric Catalog, Release 7" (Abazajian et al., 2009) is queried for all known stars brighter than 21 magnitudes in a large area around each galaxy. A mask is automatically constructed where-in every star is sufficiently covered. The masks are then inspected and corrected for possible errors. In certain cases the brighter core of a galaxy is identified as a group of stars. Because the new methods are both fairly invariant against fluctuations by small stars, these areas will not be masked. In addition clearly recognisable background galaxies are masked by hand. Using the *IRAF* package *fixpix* the frames are then corrected.

Based on the mean ellipticity M_e an elliptical mask is placed around each galaxy. This mean ellipticity is calculated from the dataset provides to us by Michael Pohlen. The area beyond the mask is believed to only contain background noise and is therefore set to 0. This ensures that it is of no further influence in the analysis.

This elliptical frame will only be used for the equivalent profiles and will on average be smaller than the regular frame used for the principal axis summations. This prevents the EP from suffering from too much background contamination. The sizes of the frames are roughly based on known dimensions of the galaxy. Afterwards they are adjusted for the best fit to the galaxy.

In a number of cases the elliptical mask is only partly covered by the frame. Pohlen and Trujillo (2006) make use of mosaicing to cover the entire galaxies. Mosaicing is however a tricky subject. In this paper it will not be used, as to avoid introducing possible ghost results. In some cases problems with the reduction software occurred. While attempts were made to fix these problems it has not always been succesful. In total 9 galaxies are removed from the sample for this reason. These have been marked in table A.2 by an asterix.

3.2 Results

The detailed data for each galaxy is presented in appendix A.3. Per galaxy six plots are presented along with a short discussion detailing the findings. The top-left plot gives an overview of the frame in the r' -band. The top-right plot is the same frame but has a different intensity scale so that the fainter regions

²Available at <http://vizier.u-strasbg.fr/viz-bin/VizieR>

are more discernable. The middle-left plot shows the equivalent profiles for the galaxy. Both the profiles with and without statistical background reduction are shown. The two horizontal lines are the 1σ levels as found from the background. The top line denotes the r' -band σ and the bottom line denotes the g' -band σ . The middle-right and bottom-left lines show the principal axis summations for the r' -band and g' -band. The various colours represent the various quadrants used. The correlation between the various lines is a clear test of the symmetry in the galaxy. The bottom-right plot is a combination of all three techniques. The r' and g' median profiles are shown by the red and green lines. The equivalent profiles are denoted by the purple and cyan lines. The elliptical isophote profile from Pohlen and Trujillo (2006) is shown by the blue line. In this plot there are also two vertical lines. The black line shows the maximal radius of the elliptical mask. The blue line denotes the derived edge of the galaxy.

A clear and direct problem, is the lack of depth of the equivalent profiles compared to both other techniques. While this is unfortunate its reason is well understood. The equivalent profiles rely on a direct count of the number of pixels per intensity level. Since the SDSS images are stored in an integer format the lowest measurable intensity will be at 1 count. In contrast, both other techniques rely on some form of averaging or binning. This allows for treatment of regions with average values below 1 count. By processing a smoothed version of a frame the resolution of the equivalent profiles can be improved. However, a smooth also removes any small substructure. From experiments with smoothing it is found that any sharp truncation will inevitably be blurred. As this is most undesirable, the equivalent profiles technique is performed on the original frames. Another striking feature is the correlation between the EP and the elliptically averaged profiles at low magnitudes. As long as the background noise is of no concern this is almost a one-on-one match.

The principle axis summation demonstrates a far deeper detection limit. In some cases this even goes as far out as the elliptical isophotes. It is hard to give a clear formulation of the maximal magnitude at which the data can still be trusted. The noisiness of the profile is used as an indication. In most cases a clear correlation in the shape of the profile is observed between the PAS and the elliptical isophotes. PAS therefore offers a good technique for deriving surface brightness profiles.

Next, a more detailed analysis of the galaxies is performed based on the PAS profiles. In the Erwin et al. (2005) classification system, the type III breaks represent a change of a steep intensity decline with radius to a less steep decline. In

comparison with the Pohlen et al. sample, type III breaks are confirmed in some galaxies like NGC 1299 and NGC 2701 (figures A.11 and A.15). Other galaxies, however, do not show them. Examples of this are NGC 853 and NGC 1084 (figures A.6 and A.9). In almost all of the galaxies marked by Pohlen et al. as a type III, asymmetries can be detected. As such, type III galaxies seem to correspond to galaxies at various phases of interaction.

The type II classification also raises questions. For example galaxy UGC 7700 (figure A.69). This galaxy has been classified by Pohlen et al. as a type II classical truncation. In this case the break is at a radius of 50 arcseconds. The first detections of truncations came from edge-on galaxies. In those galaxies a far sharper turnoff is found. The PAS profile between 60 and 70 arcseconds better represents these classical truncations far better than the profile around 50 arcseconds. In the original truncations publication by van der Kruit (1979), the truncation is defined as the radius at which the profile finally becomes 0. Following this classification, the detected break occurs at 70 arcseconds instead of 50 arcseconds.

The breaks as defined in the Erwin et al. system clearly exists. Here it is argued that the type II-CT's do not represent classical truncations. Instead they represent a separate group of features. To avoid any further confusion in the text, the Erwin et al. type II-CT's will from now on be referred to as 'breaks'.

Classical truncations are still an interest point of this report. Using the van der Kruit (1979) definition each galaxy is analysed. The only division made is between galaxies with and without truncations. In chapter A.1 the classification per galaxy is shown. The break radius r is defined as the radius at which the r' -band intensity goes to zero. When no truncation is found an underlimit to the break radius is provided. This is again based on the radius at which the intensity goes to zero. In some cases an unclear truncations is seen. These are marked by the break radius followed by a questionmark. Profiles are sometimes so bad that no valid statement can be made about them. These are therefore removed from the dataset.

For 66 galaxies valid profiles have been derived. Of these, 20 possess a clear truncation. Another 16 possess an unclear truncation. A total of 30 galaxies possess no truncation.

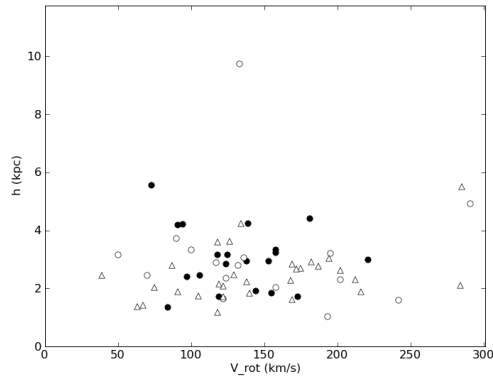
For each of the galaxies the scalelength h is derived. This follows the least squares line fitting as defined in chapter 2.4. Because the PAS profiles do not

provide a non regular profile system, it cannot be used for the derivation of a regular scalelength. In these cases equivalent profiles are used. In all galaxies the scalelength is derived from the area between 25% and 99% of the maximal radial range of the galaxy. The results are provided in table A.1.

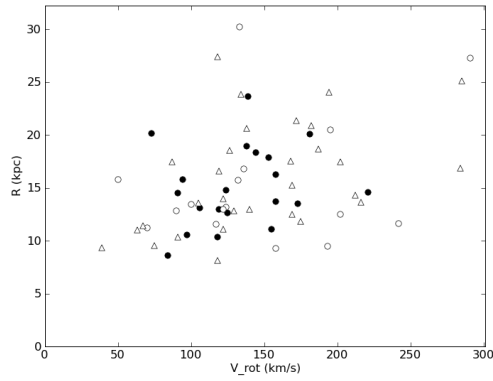
In figure 3.1 the truncation radius r and scalelength h for each galaxy has been plotted in various ways against the rotational speed v_{rot} of the galaxy. The used v_{rot} stems from Pohlen and Trujillo (2006). In each plot the black dots mark clear truncations, open dots mark unclear truncations and triangles mark underlimits.

In van der Kruit (2008) a review of all studies on truncations was performed. While most studies showed a clear relation between truncation radius r and v_{rot} , the Pohlen and Trujillo (2006) sample did not. The author speculated there may be a problem in the interpretation between edge-on and moderately inclined galaxies or that the sample has not been selected purely randomly.

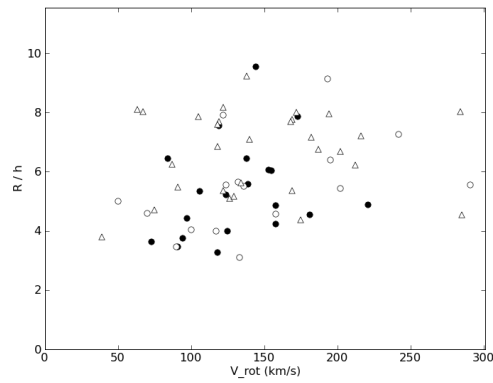
In this paper the Pohlen & Trujillo sample is re-analyzed using different techniques. In figure 3.1 a lack of correlation is again apparant. The findings of van der Kruit (2008) are therefore confirmed, and it is concluded that the sample of Pohlen & Trujillo may not be a random sample.



(a) v_{rot} vs r



(b) v_{rot} vs h



(c) v_{rot} vs r/h

Figure 3.1: Overview of the derived relations with v_{rot} . The black dots represent clear truncation detection. Open dot's represent unclear detections. The open triangles represent underlimits.

Chapter 4

Mapping dust

4.1 Introduction

In the previous chapter the power of the primary axis summation was shown using a known sample of moderately inclined galaxies. Truncations however, have been observed in both face-on and edge-on galaxies (e.g. van der Kruit (1979) and de Jong (1996)). Comparing these two has always been hard, due to the lack of a unifying technique.

One of the strong points of the PAS, is the independence of inclination. Because of this freedom, the technique offers an intriguing chance in comparing galaxies at *all* levels of inclination. Since the line of sight through an edge-on galaxy is far larger than the line of sight through a face-on galaxy, dust extinction will affect the first far more than the latter. The observed light intensity thus depends on inclination. By studying the relation between inclination i and brightness one can then derive the dust content of a galaxy.

Most galaxies come with two physical reference points. The first is the central surface brightness μ_0 , the central bright point in a galaxy. Disk breaks offer a second reference point. This is a tricky assumption as there appear to be several causes of disk breaks (Erwin et al., 2005). In the previous chapter the complications which can occur in classifying breaks were shown. The following chapter will therefore only treat type II breaks, from here-on simply called breaks. Even with this limitation the variety in break radii is still large. This can be used as an advantage. By assuming that the breaks detected at a fixed radius will almost all originate from a single physical cause, the breaks will *in general* all have the same brightness relation with the central brightness. By using a sufficiently large number of galaxies, statistics should reveal any relation with inclination.

At various levels of inclination the dust extinction will be different.

By analysing the inclination-extinction relation at various radii it should therefore be possible to map the general dust distribution in galaxies. In the remainder of this chapter such an analysis will be performed.

4.2 NYU value-added catalog

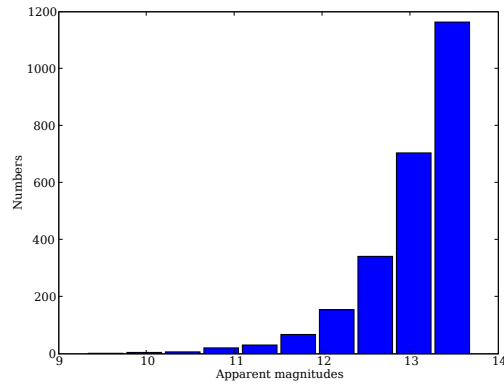
For any results to be statistically significant a large sample of galaxies at different levels of inclination is required. The NYU Value-Added Galaxy Catalog is chosen as the starting point for the creation of this sample. The NYU-VAGC is a catalog of local galaxies found in the SDSS catalog extended with galaxies crossmatched to various other surveys (Blanton et al., 2005).

From the NYU-VAGC the low-redshift catalog is selected. This comprises of a list of galaxies within the range of $10 < d < 150$ Mpc/h. The selection criterion that all galaxies should have a Sersic index lower than 2, is applied. This criterion selects for disk dominated galaxies. The subset of all galaxies is then sorted by relative k-band magnitude. The brightest 2500 galaxies are selected.

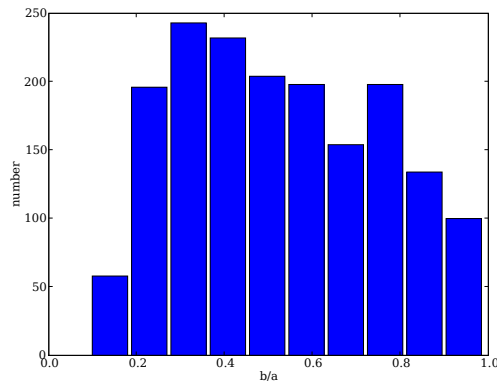
For each of these galaxies the g' , r' and i' -band observations from SDSS (data release 5) are obtained. The *sExtractor* tool (as described in Bertin and Arnouts (1996)) is used to detect all foreground and background sources in the images. An elliptical mask is then created covering each source. Each image and mask is then inspected and if needed adjusted. Using the IRAF package *fixpix* the background contaminations are then removed. A final inspection is performed in where-in all galaxies showing clear signs of interactions are removed from the sample. Galaxies in close proximity to the edge of the image are also removed.

The end result is a very nice sample of 1733 galaxies. In figure 4.1 an overview of the distribution of inclinations, apparent magnitudes and petrosian radii of the sample is shown. From figure 4.1(c) it becomes obvious that the typical angular size of the galaxies in the sample is smaller than the sample used in the previous chapter. A very likely scenario is thus the inability to detect truncations in this sample. Breaks, however, can almost always be detected.

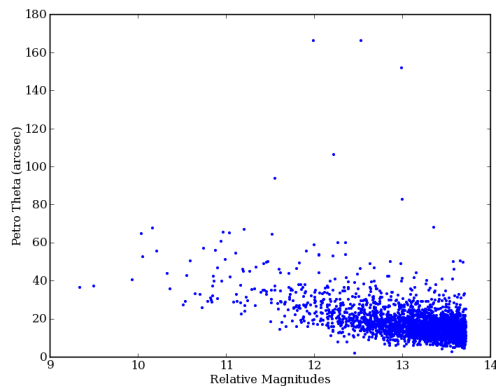
The background noise is determined. First by placing boxes in each corner of the galaxy and measuring the median pixel noise. Afterwards, finetuning is performed by demanding that the axial summations at the largest radii will hold an average of zero counts.



(a) Distribution of magnitudes in the full dataset



(b) Histogram of the distribution of the factor of short axis over long axis in the full dataset



(c) Petrosian theta radius of the galaxies in relation to their relative k-band magnitude

Figure 4.1: Overview of the brightness and angular distribution of the full 1733 galaxies sample.

Principal axis summation is then applied. Each of the 1733 profiles is inspected in both their median and individual quadrants. It is found that 479 of the galaxies exhibit clearly distinguishable breaks in their profiles. Using the technique described in chapter 2.4, the location and local surface brightness at the break is measured. In cases where multiple breaks appear the most outer break shall be used.

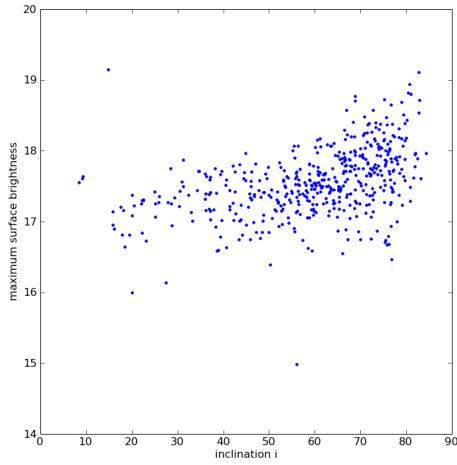
4.3 Results

In figure 4.2 the results for the r' -band reductions of 479 galaxies are demonstrated. The sample suffers from a lack of full face-on or edge-on galaxies as can be seen in figure 4.2(d). Most galaxies lie in the range between 55 and 80 degrees inclination.

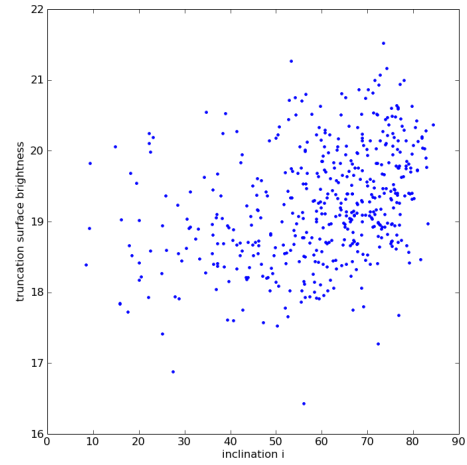
Figure 4.2(a) already reveals the presence of dust extinction. At low to medium levels of inclination, galaxies do not exhibit any strong form of extinction. The central surface brightness is thus fairly constant. This is not unexpected as the line-of-sight integration only slowly increases in this range. Starting from an inclination of 65 degree a sharp decrease in the surface brightness appears. In this range, the line-of-sight path through the galaxy is increasing exponentially. Because of this longer pathlength, the dust extinction also increases and a lower surface brightness is observed.

In figure 4.2(b) the surface brightness at the various breaks is demonstrated as a function of inclination. As seen in the previous chapter, breaks occur at all kinds of radii. A larger scattering compared to the central surface brightness is thus not unexpected. The distribution of points still exhibits the same turnoff as seen in the central surface brightness profiles. Dust thus still plays a role at the various radii.

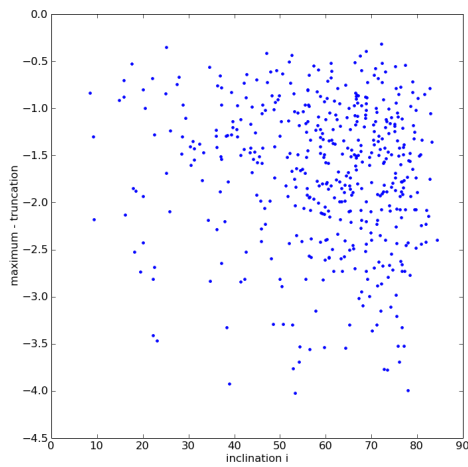
Figure 4.2(c) demonstrates the difference between central and break surface brightness as a function of inclination. As is clear from the plot, the scattering slowly increases with radius. This especially occurs in the last part of the inclination range, starting again at roughly 65 degrees. This can be explained as follows. The assumption is that the breaks are identified in a uniform way across inclinations. A single truncation will then always be detected at a fixed radius, independent of inclination. The increase of scattering with radius can then be interpreted as the impact of dust extinction. At small inclinations the pathlength through a galaxy for both the center and the break is about equal.



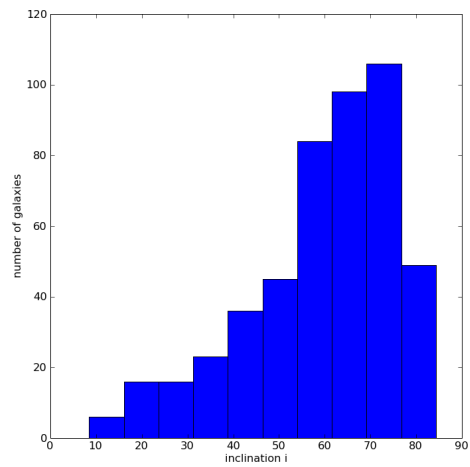
(a) Inclination against central surface brightness



(b) Inclination against truncation surface brightness



(c) Inclination against central surface brightness minus truncation surface brightness



(d) Histogram of the distribution of galaxies per inclination

Figure 4.2: Overview of the properties of the 479 galaxies that exhibit type II breaks.

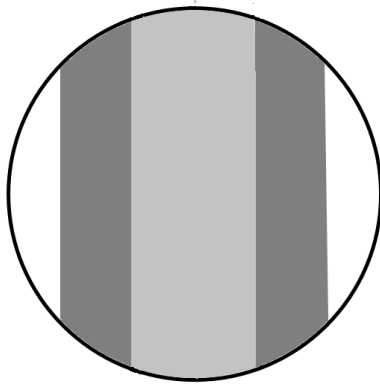


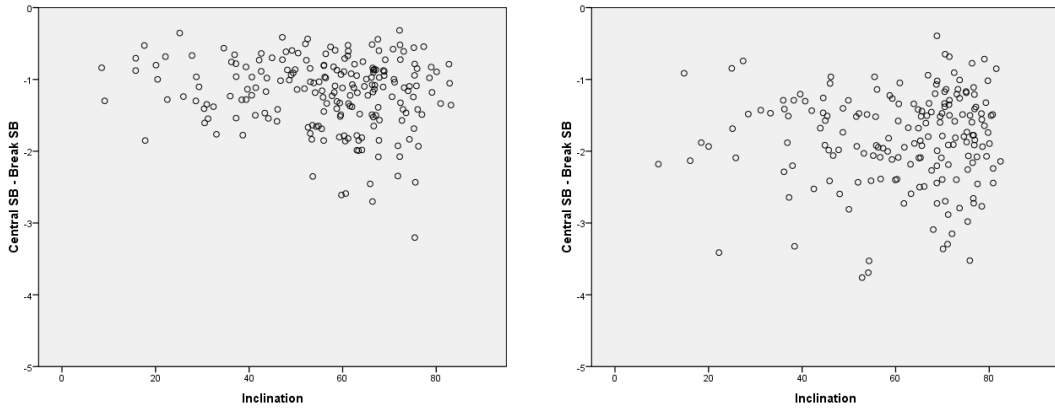
Figure 4.3: An artist sketch of the three bins and their relation in the galaxy. What becomes clear is the the differences in possible pathlengths, represented as the distance from top to bottom, in the central bin (bin 1) is far less than the other two bins.

As the inclination increases the difference in pathlengths also increases. The difference in brightness will, on average, thus be higher with higher inclination. The breaks occur at a range of radii. For different radii the ratios between pathlengths will depend differently on inclination. Edge-on (large inclination) galaxies with breaks at large radii will have a significantly larger difference in path-length ratios than edge-on galaxies with a break at a small radius. The increase of inclination will thus lead to an increase of scattering in the path-lengths, and thus lead to an increase of scattering in the magnitude - truncation surface brightness measurements. This is confirmed in the figure.

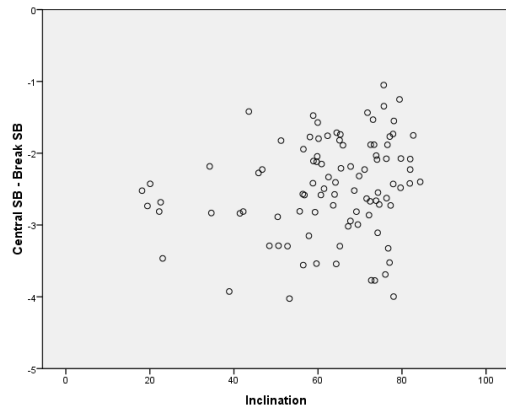
To demonstrate this effect further, in figure 4.4 the data has been split in various bins. Figure 4.4(a) contains all galaxy with $r_{break} > 0.36r_{max}$. Figure 4.4(b) contains all galaxies with break radius r_{break} between 0.36 and $0.55r_{max}$. Figure 4.4(c) contains all galaxies with break radius beyond $0.55r_{max}$. In figure 4.3 the division of the galaxy into various bins is demonstrated.

In the first bin the scattering is relatively small. Pathlength differences inside the bin, are relatively small. The same region of the galaxy is probed for all possible path-lengths. As such, the dust content distribution is of no large influence.

The differences in the individual path-lengths probed by the second bin (figure 4.4(b)) is larger. Possible non uniform dust content distributions will also affect this region more. This will amplify the path-length differences (inside the bin) and as such create an even larger scattering. With the same reasoning, the



(a) Inclination i plotted against central surface brightness (b) Inclination i plotted against truncation brightness



(c) Scattering of magnitudes with inclination for galaxies with $r_{break} \geq 0.55r_{max}$

Figure 4.4: Overview of the properties of the 479 galaxies that exhibit breaks

scattering in figure 4.4(c) is also explained.

The data seem to contradict the findings of Valentijn (1990). In that paper, evidence was found that galaxies might be opaque instead of the usual assumed transparency. As such only the outer layer of stars in a galaxy should be measured. It should therefore not be possible to detect profile breaks in the central regions of edge-on galaxies. The detection of breaks at all radii as done in this paper counters that statement. Figure 4.4(a) however demonstrates that breaks can indeed be found in the inner regions of galaxies at all levels of inclination. This suggests that galaxies are optically thin.

The results in this chapter should be considered a proof of concept. The 470 galaxies provide too few datapoints for any reliable model to be built. The various subfigures in figure 4.4 provide an interesting example of the technique. Based on these plots, it is thus believed that the galaxy dust content can indeed be mapped by using principle axis summation.

Chapter 5

Discussion & Conclusions

In this report, two new techniques have been developed for measuring the surface brightness profiles of galaxies. The first technique is the equivalent profiles. By assuming a perfectly circular distribution, with decline intensity with radius, the light in a galaxy can be reprojected. A problem that hinders this technique is the lack of averaging. As such the technique cannot dive deeper into the background noise than the absolute 1 count level.

Smoothing algorithms have been used in an effort to gain deeper resolutions. It was found that this leads to an unexceptable loss of resolution at higher intensities. A path that has not been explored, but might provide a way to dive deeper into the data, is the use of an adaptive smoothing algorithm. In such a system data will only be smoothed at ranges where the signal to noise level is high.

The second algorithm developed is the Principle Axis Summation. By summing all light onto the principle axis of a galaxy, the profiles are derived. In this system the derived profiles behave as if the galaxy was a perfect edge-on system.

In chapter 3 both systems are compared to the dataset of Pohlen and Trujillo (2006). From this it is found that the systems are indeed valid for surface brightness profile reduction. Furthermore it is concluded that the classification system of Erwin et al. (2005) does not seem to equal the disk truncations as found by van der Kruit (1979). Instead, they appear to model disk breaks instead of disk truncations. Disk truncations in the van der Kruit (1979) sense appear far further out in the galaxy. It is also found that almost all their type III galaxies exhibit indications non-symmetry, possibly signs of merging and interaction.

In chapter 4 the principle axis summation is used in relation to dust. Galaxies at all ranges of inclination are reprojected using PAS as if they were edge-on. In galaxies with no dust content, the PAS surface brightness profiles should be equal at all inclinations. With inclination the physical pathlength through a galaxy varies. A longer pathlength will suffer from more dust extinction. Galaxies with a dust content would then have a changing surface brightness dependence on inclination. This phenomena is indeed found. By using profile breaks as a measure of the brightness at certain points, the dust extinction at various radii can be mapped. While the sample was already large (479 galaxies), it still contained too few datapoints for any significant conclusions about the dust content to be drawn. As such the chapter provides a proof of concept of this system. Other interesting results can be expected from a comparison of the g' and i' bands to the r' bands in this report.

Chapter 6

Acknowledgements

In this final chapter I would like to take a minute to thank everyone that supported me throughout this project. First off, I would like to thank my supervisors Piet van der Kruit and Roelof de Jong. It has been a very interesting project, both in terms of the project itself as well as the experience of working at the STSci and Johns Hopkins University. I would also like to thank the various people at JHU that helped with my travelplans towards the USA, especially naming Ron Allen for his help.

Next I would like to thank my parents and sisters. My plan for a 6 month stay abroad was initially met with reluctance, but they saw the opportunities being offered and encouraged me throughout. Thanks for the support throughout the years! And to my grandparents: Thanks for worrying about me. I hope that my blogging helped you stay in touch.

My fellow students and roommates. Thanks for all the pointless lunch discussions to take mind of work. Especially thanks to Jonathan for helping me settle in Baltimore and a big thanks to Thijs van der Hulst for not being mad when I accidentally printed over 1800 pages of full-colour surface brightness diagrams.

My colleagues at work. Sorry to have to screw up all the schedules, but thanks for sticking with me and offering a fantastic chance to work on my presentation skills.

My friends for encouraging me to pursue this project. A big thanks to Arjan for visiting me in the US. I hope you saw what it was like to be a local. Another big thanks to Sjoukje and Roos for proofreading this report. It might not make a lot of sense to you, but at least it is a better sounding nonsense now.

Thanks to all the really cool people I met in the US. Rianne, Michelle, Keetie, Lars, Samantha, Pien, Theo, Francesco, Joris, Martijn, Timothy and all the other people I am forgetting. Thanks for making a fantastic time in Baltimore! Especially I would like to thank Sjoukje, for being crazy enough to fly back to the US and spend a crazy but awesome 4-week vacation with someone she barely knew. Thanks hon!

A final big thanks to the guys behind the internet. Yes, this may be a strange thing to write but thanks to you I was able to keep in touch with everyone *and*, make new friends and waste precious time in ways I could not even imagine 10 years ago.

Thanks all!

Bibliography

- Abazajian, K. N., Adelman-McCarthy, J. K., and Agüeros, M. A. e. a. (2009). The Seventh Data Release of the Sloan Digital Sky Survey. *APJS*, 182:543–558.
- Bertin, E. and Arnouts, S. (1996). SExtractor: Software for source extraction. *aaps*, 117:393–404.
- Blanton, M. R., Schlegel, D. J., Strauss, M. A., Brinkmann, J., Finkbeiner, D., Fukugita, M., Gunn, J. E., Hogg, D. W., Ivezić, Ž., Knapp, G. R., Lupton, R. H., Munn, J. A., Schneider, D. P., Tegmark, M., and Zehavi, I. (2005). New York University Value-Added Galaxy Catalog: A Galaxy Catalog Based on New Public Surveys. *aj*, 129:2562–2578.
- de Jong, R. S. (1996). B, V, R, I, H and K images of 86 face-on spiral galaxies. *Journal of Astronomical Data*, 2:1–+.
- de Vaucouleurs, G. (1959). Photometry, kinematics and dynamics of the Magellanic-type barred spiral galaxy NGC 4027. *Handbuch der Physik*, 53:311.
- de Vaucouleurs, G. and Davoust, E. (1980). Southern galaxies. VIII - Surface photometry of the SD spiral NGC 7793. *APJ*, 239:783–802.
- de Vaucouleurs, G., de Vaucouleurs, A., and Freeman, K. C. (1968). Photometry, kinematics and dynamics of the Magellanic-type barred spiral galaxy NGC 4027. *MNRAS*, 139:425–+.
- Erwin, P., Beckman, J. E., and Pohlen, M. (2005). Antitruncation of Disks in Early-Type Barred Galaxies. *APJL*, 626:L81–L84.
- Florido, E., Battaner, E., Zurita, A., and Guijarro, A. (2007). The truncation of the stellar disc of NGC 6504. *AAP*, 472:L39–L42.
- Freeman, K. C. (1970). On the Disks of Spiral and so Galaxies. *APJ*, 160:811–+.
- Janssens, A. (2009). Parameters of the gratama telescope and the dust distribution in spiral galaxies. *Bachelor Thesis*.

- Lupton, R. H., Gunn, J. E., and Szalay, A. S. (1999). A Modified Magnitude System that Produces Well-Behaved Magnitudes, Colors, and Errors Even for Low Signal-to-Noise Ratio Measurements. *AJ*, 118:1406–1410.
- Pohlen, M. and Trujillo, I. (2006). The structure of galactic disks. Studying late-type spiral galaxies using SDSS. *AAP*, 454:759–772.
- Pohlen, M., Zaroubi, S., Peletier, R. F., and Dettmar, R.-J. (2007). On the three-dimensional structure of edge-on disc galaxies. *MNRAS*, 378:594–616.
- Sánchez-Blázquez, P., Courty, S., Gibson, B. K., and Brook, C. B. (2009). The origin of the light distribution in spiral galaxies. *MNRAS*, 398:591–606.
- Schaye, J. (2004). Star Formation Thresholds and Galaxy Edges: Why and Where. *APJ*, 609:667–682.
- Valentijn, E. A. (1990). Opaque spiral galaxies. *Nature*, 346:153–155.
- van der Kruit, P. C. (1979). Optical surface photometry of eight spiral galaxies studied in Westerbork. *AAPS*, 38:15–38.
- van der Kruit, P. C. (1987). The radial distribution of surface brightness in galactic disks. *AAP*, 173:59–80.
- van der Kruit, P. C. (2008). The Stars and Gas in Outer Parts of Galaxy Disks: Extended or Truncated, Flat or Warped? In J. G. Funes & E. M. Corsini, editor, *Astronomical Society of the Pacific Conference Series*, volume 396 of *Astronomical Society of the Pacific Conference Series*, pages 173–+.

Appendix A

The Pohlen & Trujillo dataset

A.1 Derived Parameters

Table A.1: P&T dataset derived parameters

name	$v_{rot}(km/s)$	$h(kpc)$	$r(kpc)$	name	$v_{rot}(km/s)$	$h(kpc)$	$r(kpc)$
IC 1067	158	2.0	9.3?	NGC 4480	169	2.8	9.3?
IC 1125	106	2.5	13.1	NGC 4517A	73	5.6	13.1
IC 1158	125	3.2	12.6	NGC 4545	136	3.1	12.6
NGC 0450	118	3.2	10.4	NGC 4653	181	4.4	10.4
NGC 0701	140	1.8	> 13.0	NGC 4668	63	1.4	> 13.0
NGC 0853	?	1.4	> 9.8	NGC 4904	122	1.6	> 9.8
NGC 0941	91	1.9	> 10.4	NGC 5147	118	1.2	> 10.4
NGC 1042	50	3.2	15.8?	NGC 5300	124	2.8	15.8?
NGC 1068	310	?	?	NGC 5334	145	?	?
NGC 1084	173	1.7	13.5	NGC 5376	216	1.9	13.5
NGC 1087	125	2.4	?	NGC 5430	195	3.2	?
NGC 1299	?	1.0	> 10.5	NGC 5480	138	2.2	> 10.5
NGC 2541	97	2.4	10.6	NGC 5584	136	?	10.6
NGC 2543	158	3.3	16.2	NGC 5624	67	1.4	16.2
NGC 2684	99	1.5	?	NGC 5660	138	2.9	?
NGC 2701	168	2.3	> 17.5	NGC 5667	119	1.7	> 17.5
NGC 2776	118	3.6	> 27.4	NGC 5668	87	2.8	> 27.4
NGC 2967	172	2.7	> 21.4	NGC 5693	39	2.5	> 21.4
NGC 3055	155	1.8	11.1	NGC 5713	135	?	11.1
NGC 3246	117	2.9	11.5?	NGC 5768	122	1.7	11.5?
NGC 3259	119	2.2	> 16.6	NGC 5774	91	4.2	> 16.6
NGC 3310	280	1.6	?	NGC 5806	182	2.9	?
NGC 3359	139	4.2	23.6	NGC 5850	133	9.7	23.6
NGC 3423	122	2.1	> 11.1	NGC 5937	202	2.6	> 11.1
NGC 3488	132	2.8	15.7?	NGC 6070	215	?	15.7?
NGC 3583	194	3.0	> 24.1	NGC 6155	105	1.7	> 24.1
NGC 3589	75	2.0	> 9.5	NGC 7437	175	2.7	> 9.5
NGC 3631	82	?	?	NGC 7606	291	4.9	?
NGC 3642	45	?	?	PGC 006667	129	2.5	?
NGC 3756	153	2.9	17.8	UGC 02081	100	3.3	17.8
NGC 3888	191	1.7	?	UGC 04393	70	2.4	?
NGC 3893	175	2.4	?	UGC 06309	124	2.4	?
NGC 3982	193	1.0	9.4?	UGC 06518	84	1.3	9.4?
NGC 3992	285	5.5	> 25.1	UGC 06903	158	3.2	> 25.1
NGC 4030	231	?	?	UGC 07700	94	4.2	?
NGC 4041	284	2.1	> 16.9	UGC 08041	93	?	> 16.9
NGC 4102	169	1.6	> 12.5	UGC 08084	90	3.7	> 12.5
NGC 4108B	212	2.3	> 14.3	UGC 08237	?	1.8	> 14.3
NGC 4108	242	1.6	11.6?	UGC 08658	126	3.6	11.6?
NGC 4123	134	4.2	> 23.8	UGC 09741	?	1.0	> 23.8
NGC 4210	202	2.3	12.5?	UGC 09837	221	3.0	12.5?
NGC 4273	187	2.8	> 18.7	UGC 10721	144	1.9	> 18.7
NGC 4480	169	2.8	> 15.2	UGC 12709	70	4.9	> 15.2

A.2 Main parameters

Table A.2: Overview of the galaxies used in the P&T sample and their most important parameters

name	ra	dec	R_{ell}	M_e	μ_g	σ_g	N_g	μ_r	σ_r	N	Note
IC 1067	14:53:05.24	+03:19:54.4	98	0.26	1069.0	3.0	33473	1122.8	3.6	33473	
IC 1125	15:33:05.61	-01:37:41.6	76	0.44	1074.0	3.1	42800	1112.6	3.4	42800	
IC 1158	16:01:34.07	+01:42:28.1	98	0.44	1112.3	4.8	33304	1164.0	4.1	33304	
NGC 0450	01:15:30.44	-00:51:39.5	120	0.36	1099.1	4.7	80080	1164.5	4.1	80080	
NGC 0701	01:51:03.83	-09:42:09.3	130	0.49	1068.4	3.0	48888	1157.1	3.9	48888	
NGC 0853	02:11:41.18	-09:18:21.5	100	0.36	1075.0	3.1	68352	1144.2	3.8	68352	
NGC 0941	02:28:27.85	-01:09:05.5	120	0.3	1068.0	4.2	22490	1099.0	3.3	22490	
NGC 1042	02:40:23.96	-08:26:00.7	220	0.2	1074.7	3.0	81366	1175.9	4.2	81366	
NGC 1068	02:42:40.71	-00:00:47.8	362	0.09	1095.7	3.5	50025	1188.6	4.5	50025	*
NGC 1084	02:45:59.90	-07:34:42.4	179	0.39	1069.8	2.9	57680	1171.5	4.2	57680	
NGC 1087	02:46:25.16	-00:29:55.1	239	0.39	1091.4	3.4	40040	1175.5	4.2	40040	
NGC 1299	03:20:09.68	-06:15:43.2	75	0.45	1081.6	3.1	64935	1190.1	4.3	64935	
NGC 2541	08:14:40.11	+49:03:42.1	213	0.52	1091.1	3.3	27664	1180.3	4.3	27664	
NGC 2543	08:12:57.92	+36:15:16.6	106	0.5	1078.4	3.1	27420	1129.0	3.7	27420	
NGC 2684	08:54:54.04	+49:09:37.4	44	0.18	1069.6	3.0	91238	1121.2	3.5	91238	
NGC 2701	08:59:05.74	+53:46:18.0	93	0.32	1086.0	3.1	23856	1162.0	4.0	23856	
NGC 2776	09:12:14.51	+44:57:17.4	149	0.05	1067.4	2.8	76260	1156.0	3.8	76260	
NGC 2967	09:42:03.29	+00:20:11.1	156	0.07	1105.8	3.7	37935	1149.7	3.9	37935	
NGC 3055	09:55:18.06	+04:16:12.0	87	0.42	1072.8	3.2	55560	1117.0	3.5	55560	
NGC 3246	10:26:41.80	+03:51:42.9	96	0.48	1071.8	3.0	37148	1124.6	3.5	37148	
NGC 3259	10:32:34.85	+65:02:27.9	122	0.43	1069.9	3.0	57792	1157.7	4.0	57792	

Continued on next page

Table A.2 – continued from previous page

name	ra	dec	Re	Me	mu	sigma	N	mu	sigma	N	Note
NGC 3310	10:38:45.85	+53:30:12.1	171	0.05	1069.6	3.5	42588	1133.4	3.6	42588	
NGC 3359	10:46:36.86	+63:13:27.2	257	0.48	1083.8	3.3	47040	1150.1	3.9	47040	
NGC 3423	10:51:14.33	+05:50:24.1	175	0.19	1075.4	4.3	43056	1103.1	3.4	43056	
NGC 3488	11:01:23.61	+57:40:39.6	70	0.34	1070.1	3.0	69120	1119.3	3.4	74752	
NGC 3583	11:14:10.89	+48:19:06.6	150	0.32	1058.2	2.8	62408	1103.6	3.3	62408	
NGC 3589	11:15:13.33	+60:41:59.7	72	0.5	1059.9	2.8	60192	1138.5	3.9	60192	*
NGC 3631	11:21:02.87	+53:10:10.4	232	0.16	1076.7	4.3	83398	1140.1	3.9	83398	*
NGC 3642	11:22:17.89	+59:04:28.2	239	0.05	1053.4	2.6	33488	1093.7	3.1	33488	
NGC 3756	11:36:48.01	+54:17:36.8	154	0.5	1066.3	2.8	53890	1135.1	3.7	53890	
NGC 3888	11:47:34.36	+55:58:01.9	81	0.26	1064.6	4.4	26702	1133.0	3.6	26702	
NGC 3893	11:48:38.18	+48:42:38.9	250	0.41	1066.1	4.2	55480	1106.5	3.5	55480	
NGC 3982	11:56:28.12	+55:07:30.8	91	0.11	1068.0	2.9	86984	1132.5	3.7	60900	
NGC 3992	11:57:35.98	+53:22:28.3	322	0.42	1059.2	4.1	71004	1112.8	3.3	57246	
NGC 4030	12:00:23.62	-01:06:00.3	265	0.2	1095.8	4.6	50400	1137.5	3.8	50400	*
NGC 4041	12:02:12.20	+62:08:13.9	190	0.05	1062.1	2.8	44415	1151.7	3.9	43210	
NGC 4102	12:06:23.00	+52:42:39.7	162	0.43	1067.7	2.9	58740	1123.0	3.5	58740	
NGC 4108B	12:07:11.61	+67:14:06.5	67	0.23	1092.0	3.3	52510	1173.2	4.2	52510	
NGC 4108	12:06:44.57	+67:09:47.1	66	0.22	1092.1	3.3	47488	1173.2	4.2	47488	
NGC 4123	12:08:11.11	+02:52:41.8	220	0.33	1090.1	3.4	33453	1161.1	4.0	33453	
NGC 4210	12:15:15.83	+65:59:07.2	76	0.24	1061.9	2.9	30800	1120.1	3.5	30800	
NGC 4273	12:19:56.07	+05:20:35.9	119	0.39	1072.9	3.1	31875	1130.1	3.6	31875	
NGC 4480	12:30:26.78	+04:14:47.6	90	0.5	1076.8	3.1	99275	1143.5	3.8	99275	
NGC 4517A	12:32:28.15	+00:23:22.8	190	0.43	1078.0	3.1	29841	1135.9	3.7	29841	
NGC 4545	12:34:34.15	+63:31:30.2	97	0.42	1054.1	2.7	41420	1114.4	3.3	41420	
NGC 4653	12:43:50.90	-00:33:40.4	142	0.17	1075.0	3.2	45333	1134.8	3.7	45333	
NGC 4668	12:45:31.99	-00:32:08.6	110	0.48	1074.9	3.1	32899	1134.6	3.7	41031	

Continued on next page

Table A.2 – continued from previous page

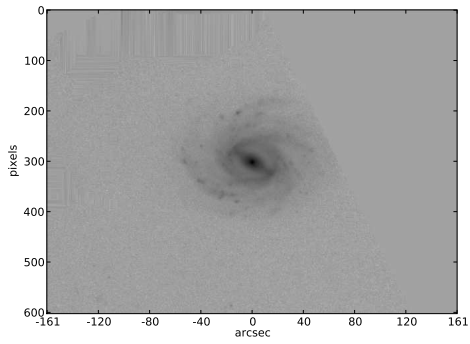
name	ra	dec	Re	Me	mu	sigma	N	mu	sigma	N	Note
NGC 4904	13:00:58.66	-00:01:39.4	120	0.29	1074.9	3.0	56270	1142.1	3.9	56270	
NGC 5147	13:26:19.73	+02:06:03.0	120	0.21	1092.0	3.3	39611	1179.0	4.3	34944	
NGC 5300	13:48:16.03	+03:57:03.0	155	0.33	1081.2	3.2	31320	1145.9	3.8	31320	
NGC 5334	13:52:54.45	-01:06:52.6	150	0.23	1086.0	4.4	48692	1125.0	3.6	48692	*
NGC 5376	13:55:16.06	+59:30:23.8	92	0.39	1055.9	2.6	53350	1108.5	3.4	53350	
NGC 5430	14:00:45.74	+59:19:41.8	110	0.35	1055.4	2.7	50778	1108.1	3.5	50778	
NGC 5480	14:06:21.57	+50:43:30.3	130	0.15	1069.3	4.3	56916	1149.5	4.0	40640	
NGC 5584	14:22:23.76	-00:23:15.6	162	0.26	1073.5	3.1	59364	1134.8	3.7	59364	*
NGC 5624	14:26:35.20	+51:35:07.2	92	0.34	1062.9	3.3	50007	1147.5	3.8	50007	
NGC 5660	14:29:49.81	+49:37:21.6	100	0.05	1064.0	2.8	44421	1122.4	3.5	44421	
NGC 5667	14:30:22.90	+59:28:11.1	96	0.47	1055.2	2.7	21735	1099.0	3.2	21735	
NGC 5668	14:33:24.33	+04:27:01.6	178	0.15	1070.0	3.1	24674	1116.9	3.4	24674	
NGC 5693	14:36:11.18	+48:35:06.1	71	0.05	1074.3	4.3	38236	1151.2	4.0	38236	
NGC 5713	14:40:11.50	-00:17:20.3	161	0.13	1073.3	3.1	29458	1133.6	3.7	29458	*
NGC 5768	14:52:07.95	-02:31:47.0	90	0.11	1075.7	3.1	34810	1128.3	3.6	34810	
NGC 5774	14:53:42.46	+03:34:56.9	181	0.22	1085.0	3.2	31740	1173.4	4.1	31740	
NGC 5806	15:00:00.40	+01:53:28.7	240	0.46	1082.2	3.1	33660	1179.2	4.3	33660	
NGC 5850	15:07:07.68	+01:32:39.2	232	0.22	1094.4	3.4	68853	1194.6	4.5	68853	
NGC 5937	15:30:46.12	-02:49:46.1	116	0.44	1083.9	4.4	15950	1121.4	3.7	15950	
NGC 6070	16:09:58.69	+00:42:33.5	161	0.57	1062.1	2.7	25821	1148.7	3.9	25821	*
NGC 6155	16:26:08.33	+48:22:00.5	71	0.28	1062.9	2.8	34239	1125.1	3.5	34239	
NGC 7437	22:58:10.06	+14:18:30.5	91	0.1	1086.3	3.3	24192	1153.5	3.9	24192	
NGC 7606	23:19:04.77	-08:29:06.3	195	0.62	1088.6	3.3	28860	1224.8	4.7	28860	
PGC 006667	01:49:10.36	-10:03:40.3	106	0.19	1073.6	3.1	31493	1175.8	4.2	31493	
UGC 02081	02:36:00.96	+00:25:12.7	90	0.42	1055.6	2.6	22820	1099.4	3.1	22820	
UGC 04393	08:26:04.38	+45:58:03.5	125	0.45	1065.9	2.8	30710	1115.9	3.4	30710	

Continued on next page

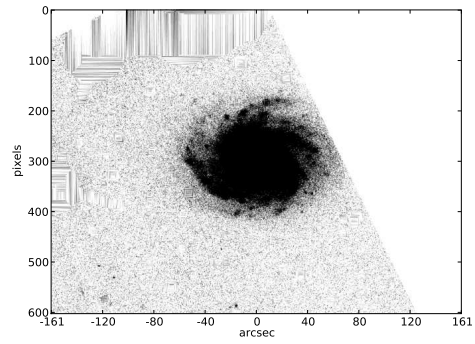
Table A.2 – continued from previous page

name	ra	dec	Re	Me	mu	sigma	N	mu	sigma	N	Note
UGC 06309	11:17:46.47	+51:28:35.7	74	0.31	1058.6	2.7	25788	1108.8	3.2	25788	
UGC 06518	11:32:20.35	+53:54:16.0	45	0.39	1064.7	2.9	36632	1136.9	3.8	36632	
UGC 06903	11:55:36.94	+01:14:13.8	95	0.12	1076.6	3.1	17000	1135.9	3.8	17000	
UGC 07700	12:32:33.55	+63:52:39.3	94	0.24	1071.1	4.3	35206	1123.7	3.7	35206	
UGC 08041	12:55:12.65	+00:06:59.9	143	0.48	1077.7	3.2	21855	1127.1	3.6	21855	*
UGC 08084	12:58:22.06	+02:47:32.3	71	0.18	1085.3	3.3	26260	1156.9	3.9	26260	
UGC 08237	13:08:54.47	+62:18:22.9	50	0.22	1055.5	2.7	23171	1103.0	3.2	23171	
UGC 08658	13:40:39.85	+54:19:58.2	102	0.39	1066.2	3.7	32231	1122.3	3.5	32231	
UGC 09741	15:08:33.50	+52:17:46.1	62	0.11	1057.7	2.9	41230	1128.8	4.0	41230	
UGC 09837	15:23:51.67	+58:03:10.5	69	0.05	1062.0	3.9	50380	1114.9	3.5	50380	
UGC 10721	17:08:25.54	+25:31:02.6	80	0.33	1055.3	3.6	31486	1118.2	3.4	31486	
UGC 12709	23:37:24.00	+00:23:30.0	102	0.39	1080.0	3.2	20898	1154.3	3.9	20898	

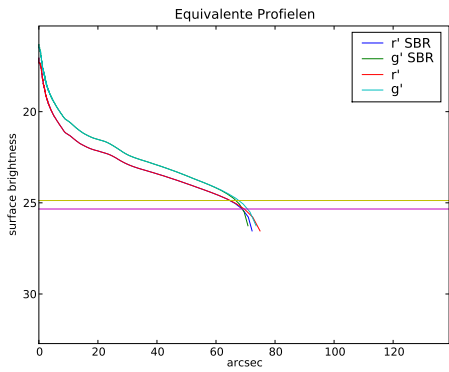
A.3 Plots for each galaxy



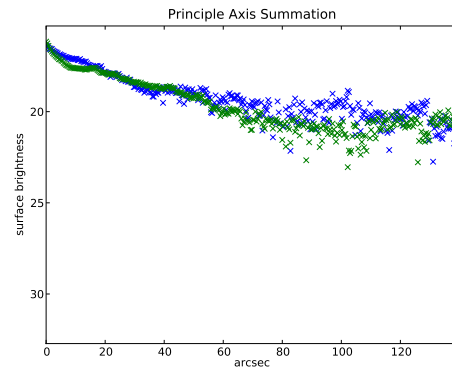
(a) r' band image



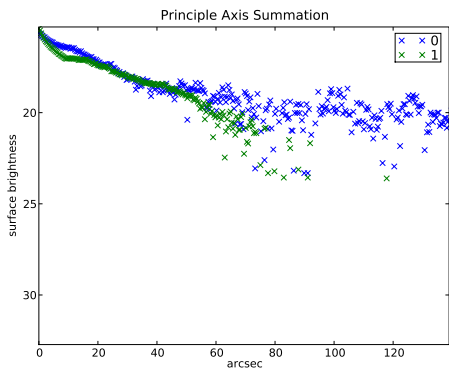
(b) low luminosity r' band image



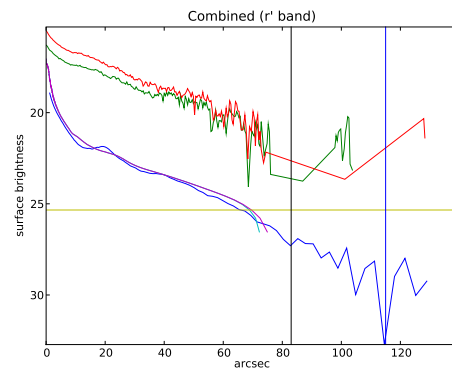
(c) Equivalent Profiles



(d) Axial Summation of 4 Quadrants

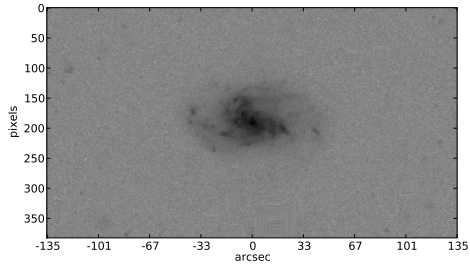


(e) Axial Summation of 4 Quadrants

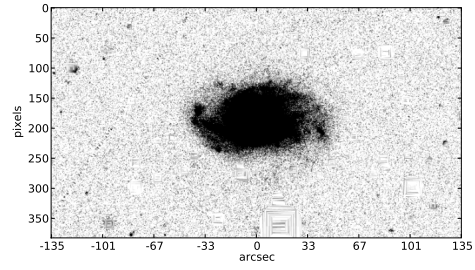


(f) Combined

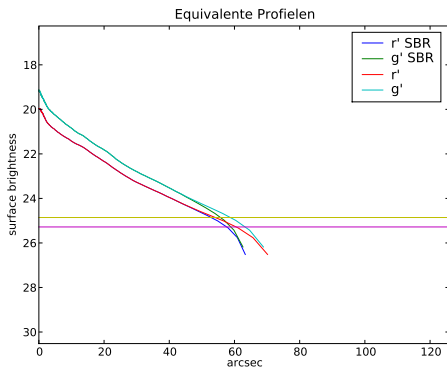
Figure A.1: *Galaxy IC 1067* - Pohlen en Trujillo have classified this galaxy as II.o-OLR (possible Type I). A sign of truncation at 70 arcseconds is seen.



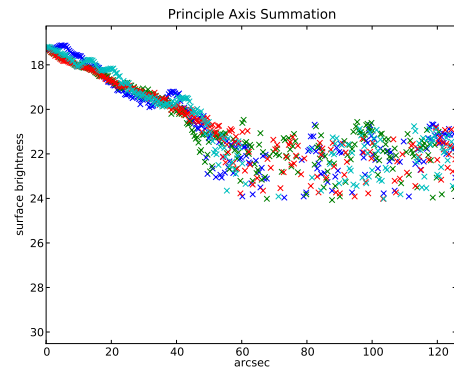
(a) r' band image



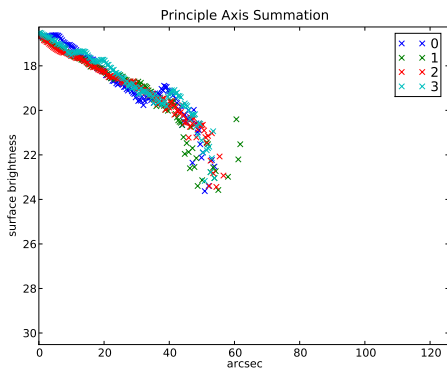
(b) low luminosity r' band image



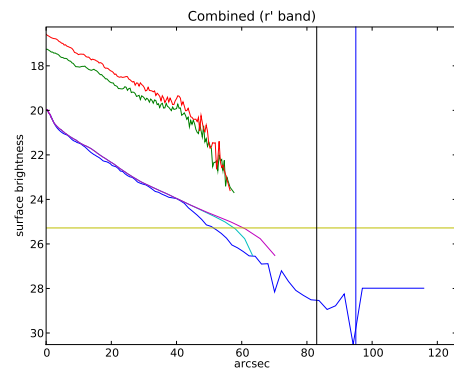
(c) Equivalent Profiles



(d) Axial Summation of 4 Quadrants

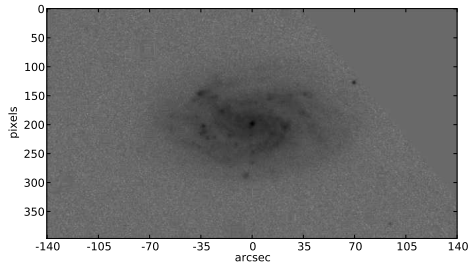


(e) Axial Summation of 4 Quadrants

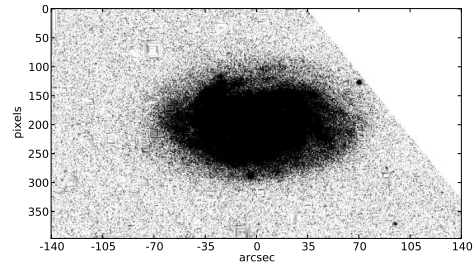


(f) Combined

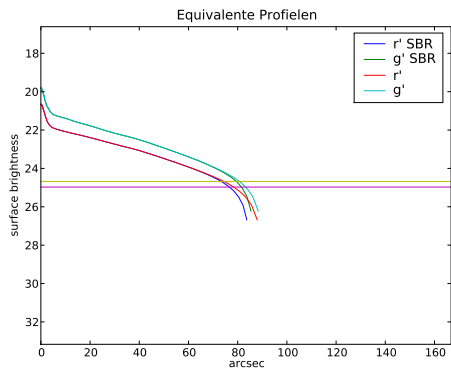
Figure A.2: *Galaxy IC 1125* - Pohlen en Trujillo have classified this galaxy as Type I. A clear truncation is seen at 60 arcseconds.



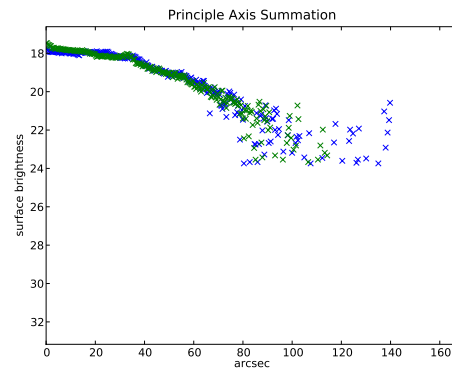
(a) r' band image



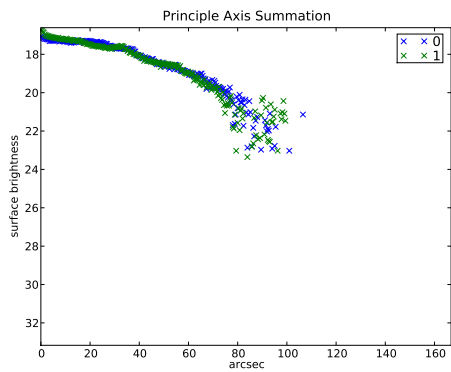
(b) low luminosity r' band image



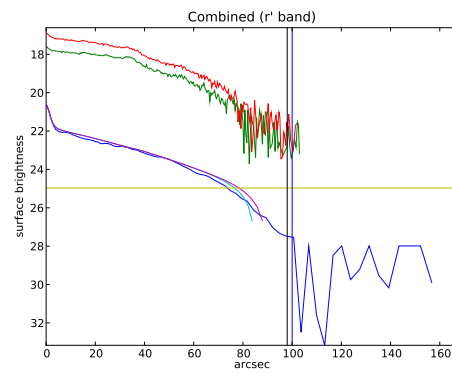
(c) Equivalent Profiles



(d) Axial Summation of 4 Quadrants

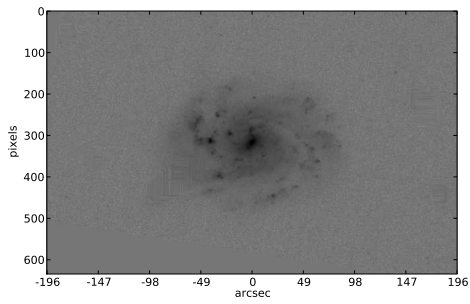


(e) Axial Summation of 4 Quadrants

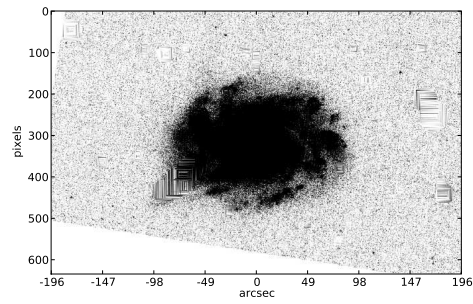


(f) Combined

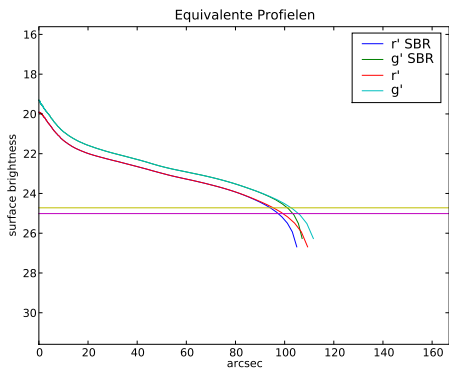
Figure A.3: *Galaxy IC 1158* - Pohlen en Trujillo have classified this galaxy as Type II.o-CT. A clear truncation is seen at 80 arcseconds. Even in the Erwin et al. (2005) this galaxy appears as a type II galaxy.



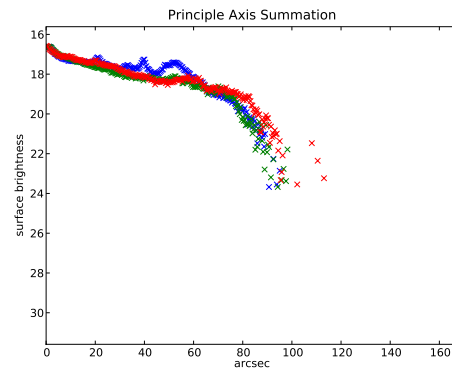
(a) r' band image



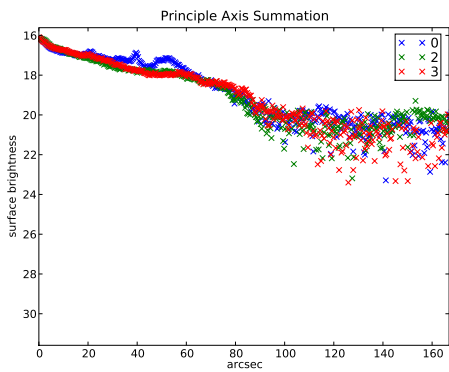
(b) low luminosity r' band image



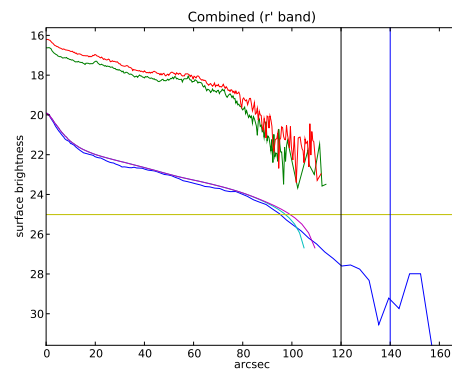
(c) Equivalent Profiles



(d) Axial Summation of 4 Quadrants

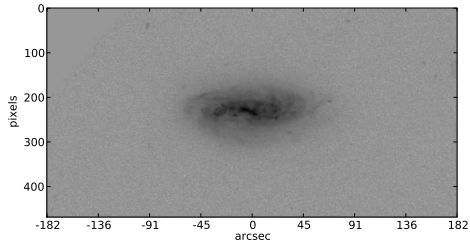


(e) Axial Summation of 4 Quadrants

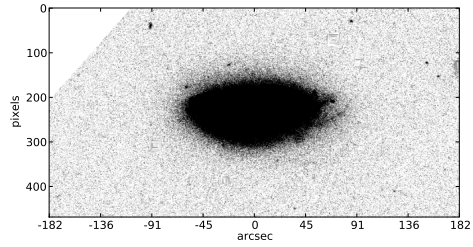


(f) Combined

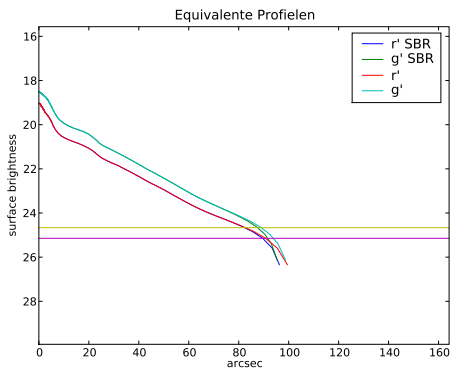
Figure A.4: *Galaxy NGC 0450* - Pohlen en Trujillo have classified this galaxy as Type II.o-CT. A severe problem hampering this image is the background galaxy that is seen through the galaxy. A truncation is seen at 90 arcseconds.



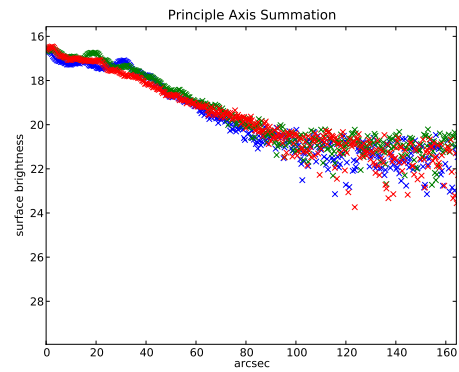
(a) r' band image



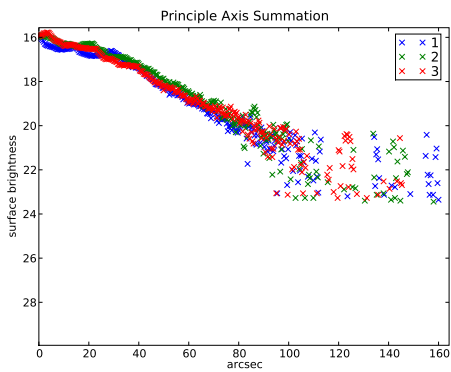
(b) low luminosity r' band image



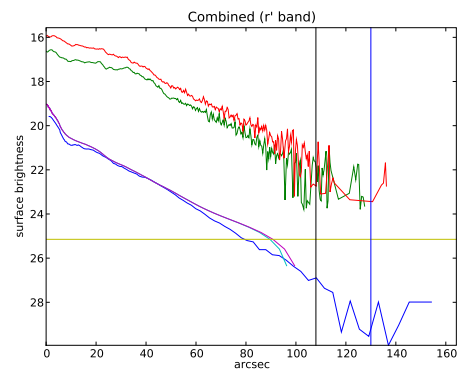
(c) Equivalent Profiles



(d) Axial Summation of 4 Quadrants

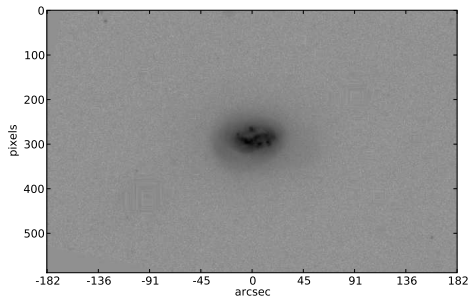


(e) Axial Summation of 4 Quadrants

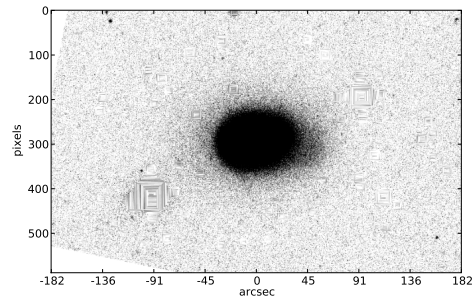


(f) Combined

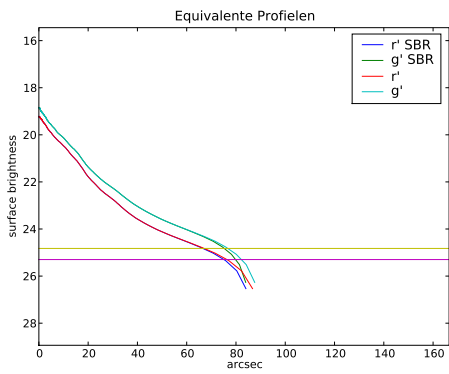
Figure A.5: *Galaxy NGC 0701* - Pohlen en Trujillo have classified this galaxy as Type II.i (possible Type 1). No signs of truncation is seen. The truncation has an upper range of $\lesssim 110$ arcseconds.



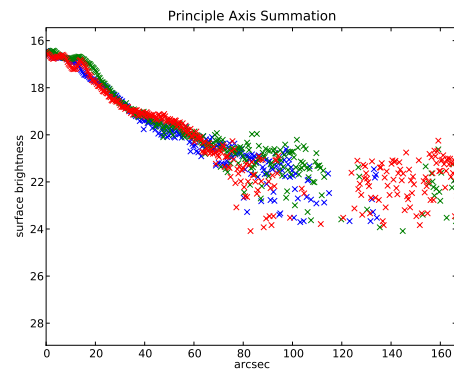
(a) r' band image



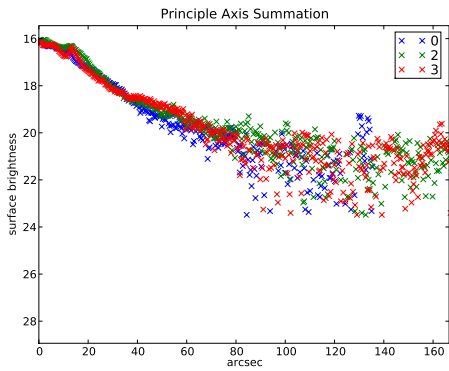
(b) low luminosity r' band image



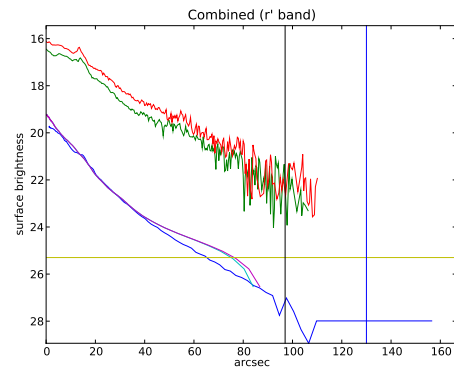
(c) Equivalent Profiles



(d) Axial Summation of 4 Quadrants

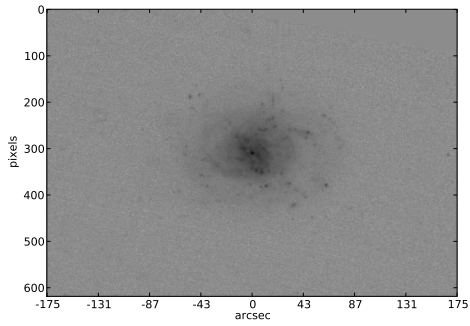


(e) Axial Summation of 4 Quadrants

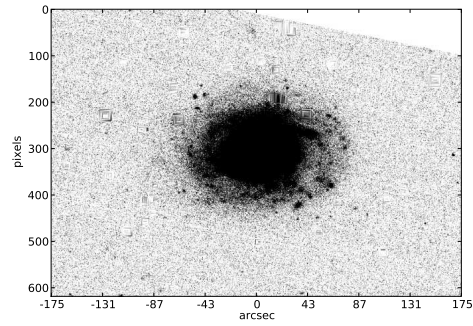


(f) Combined

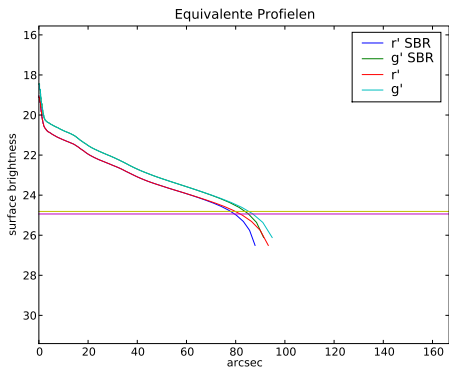
Figure A.6: *Galaxy NGC 0853* - Pohlen en Trujillo have classified this galaxy as Type III. There is an upward bent explaining the Type III classification. Plot *b* shows that the galaxy is not symmetric. No signs of a truncation is seen and an underlimit of 100 arcseconds is set.



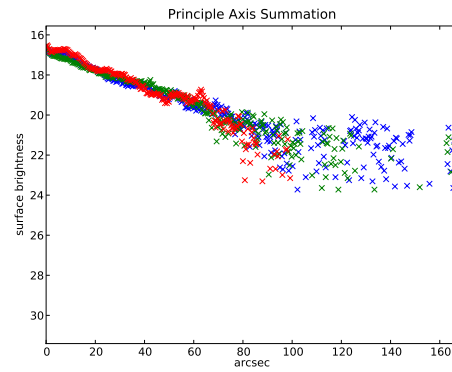
(a) r' band image



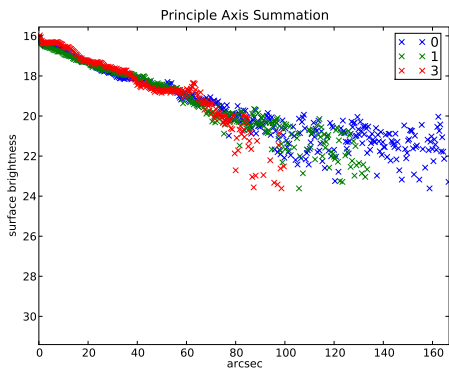
(b) low luminosity r' band image



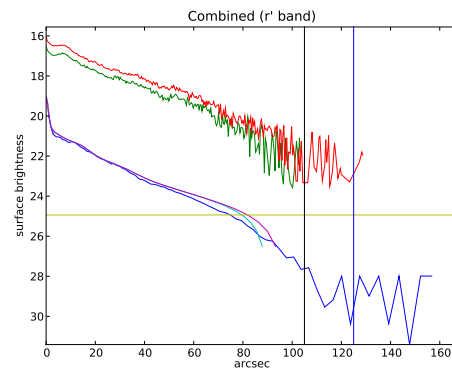
(c) Equivalent Profiles



(d) Axial Summation of 4 Quadrants

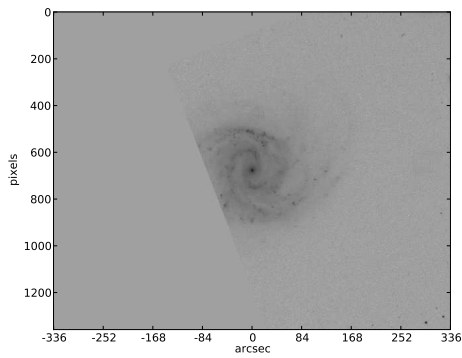


(e) Axial Summation of 4 Quadrants

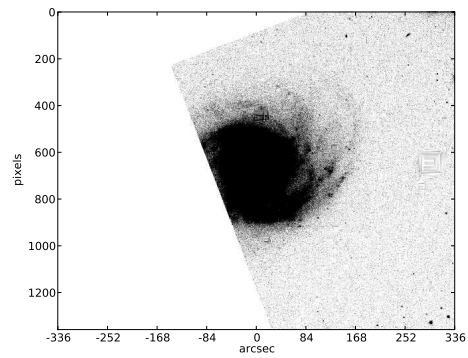


(f) Combined

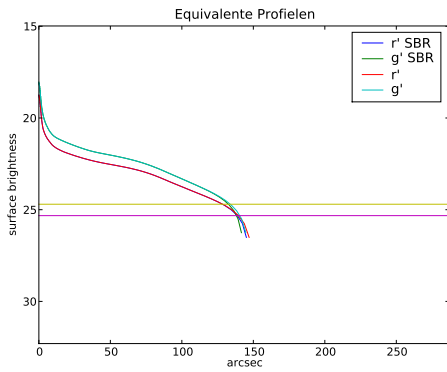
Figure A.7: *Galaxy NGC 0941* - Pohlen en Trujillo have classified this galaxy as Type II-CT. No truncation is seen below 100 arcseconds.



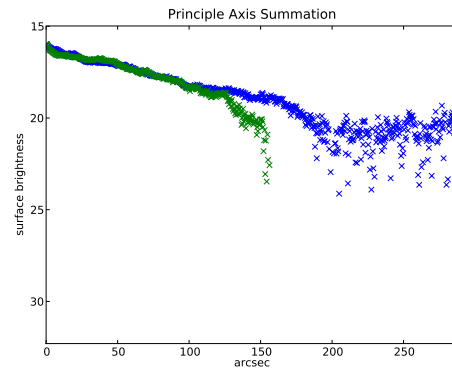
(a) r' band image



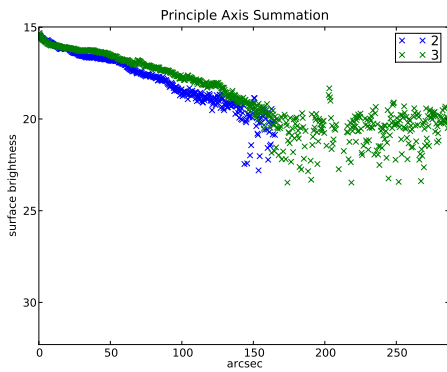
(b) low luminosity r' band image



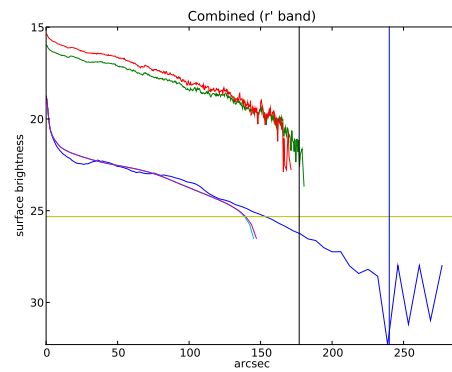
(c) Equivalent Profiles



(d) Axial Summation of 4 Quadrants

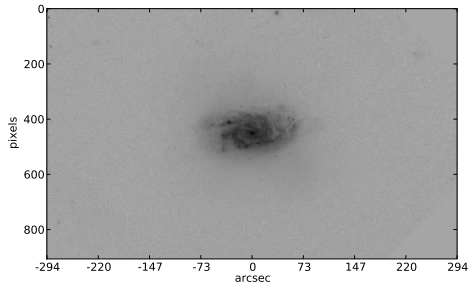


(e) Axial Summation of 4 Quadrants

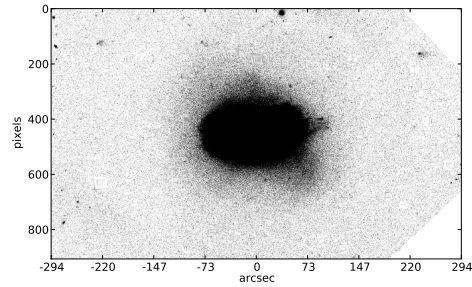


(f) Combined

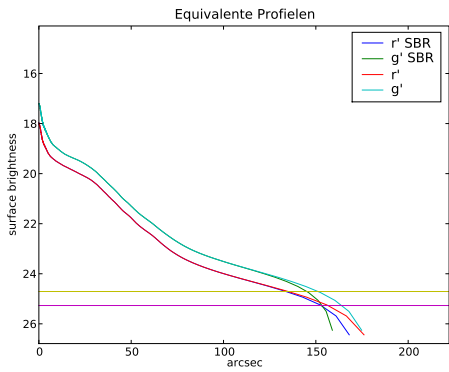
Figure A.8: *Galaxy NGC 1042* - Pohlen en Trujillo have classified this galaxy as Type II-AB. An indication of truncation is present at 180 arcseconds.



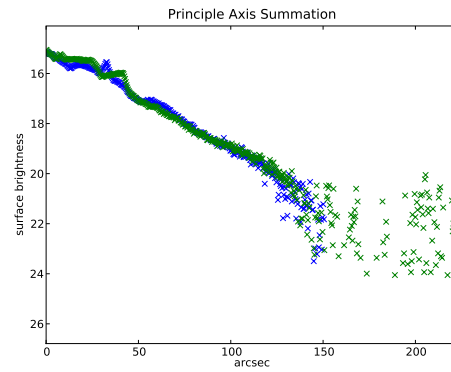
(a) r' band image



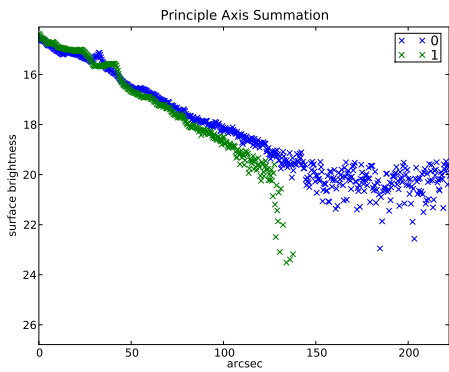
(b) low luminosity r' band image



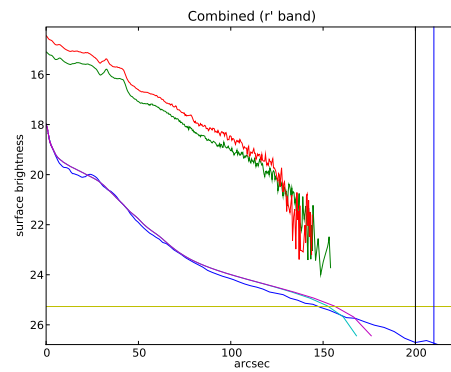
(c) Equivalent Profiles



(d) Axial Summation of 4 Quadrants

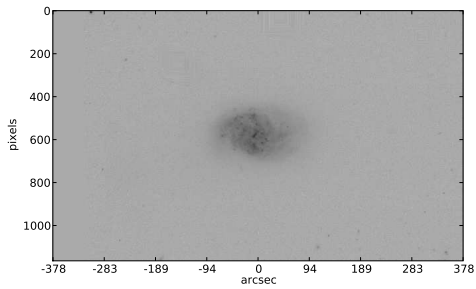


(e) Axial Summation of 4 Quadrants

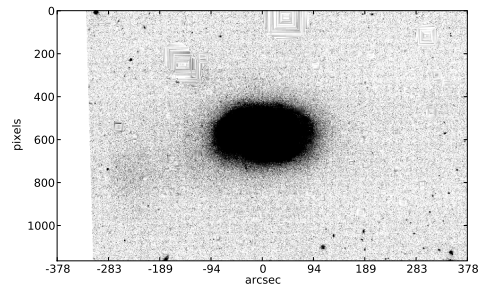


(f) Combined

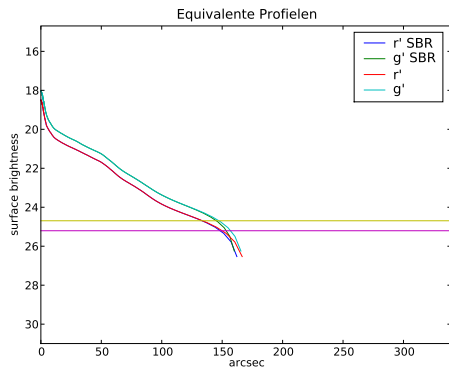
Figure A.9: *Galaxy NGC 1084* - Pohlen en Trujillo have classified this galaxy as Type III. Heavily disturbed galaxy. Truncation present at 150 arcseconds.



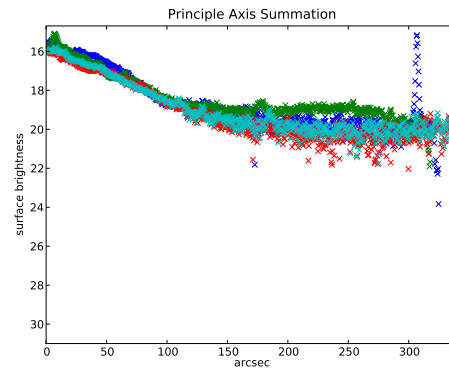
(a) r' band image



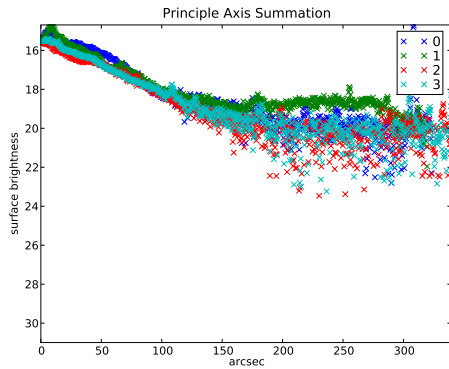
(b) low luminosity r' band image



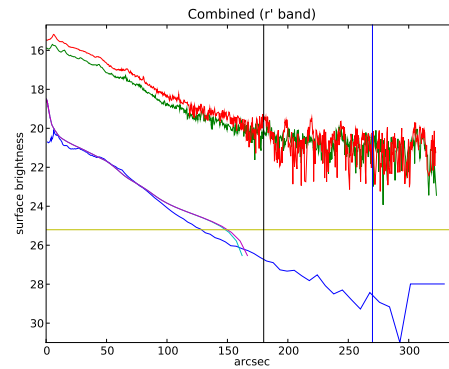
(c) Equivalent Profiles



(d) Axial Summation of 4 Quadrants

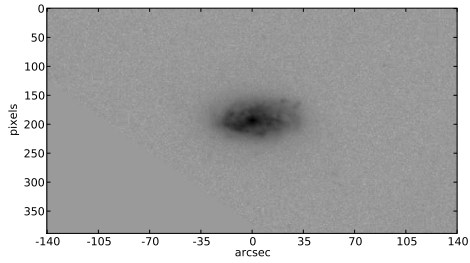


(e) Axial Summation of 4 Quadrants

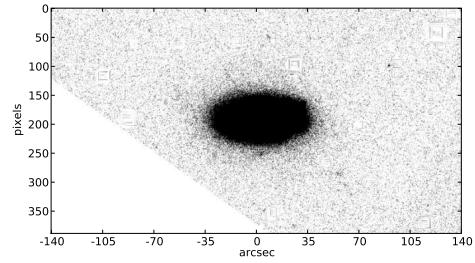


(f) Combined

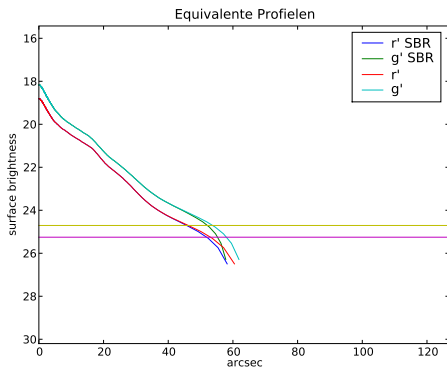
Figure A.10: *Galaxy NGC 1087* - Pohlen en Trujillo have classified this galaxy as Type III. From *b* it is clear that this galaxy is disturbed and will not be used any further.



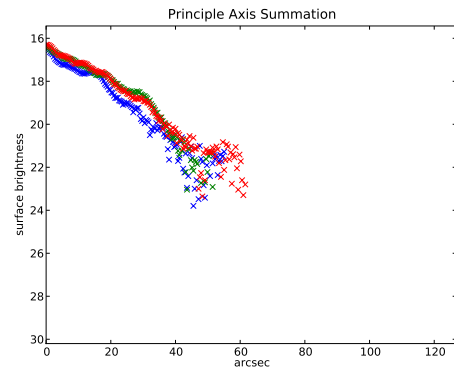
(a) r' band image



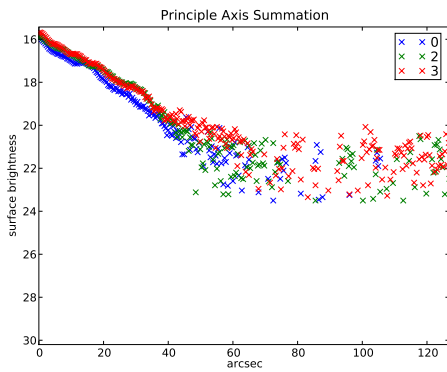
(b) low luminosity r' band image



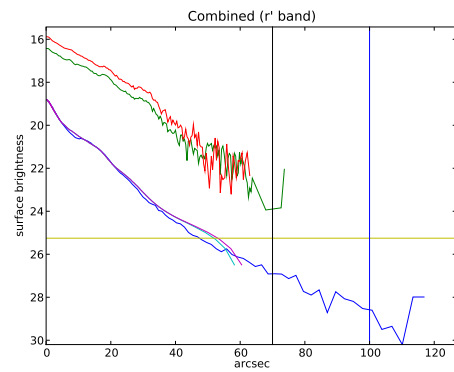
(c) Equivalent Profiles



(d) Axial Summation of 4 Quadrants

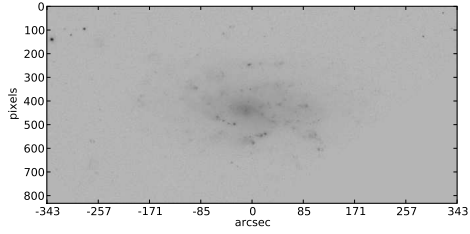


(e) Axial Summation of 4 Quadrants

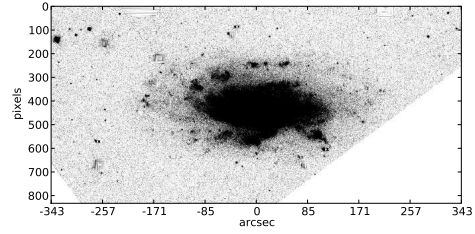


(f) Combined

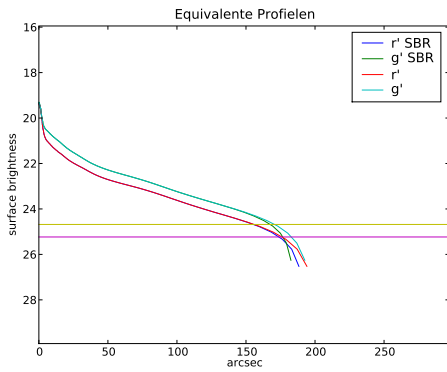
Figure A.11: *Galaxy NGC 1299* - Pohlen en Trujillo have classified this galaxy as Type III. No truncation is seen. Underlimit is set at 70 arcseconds.



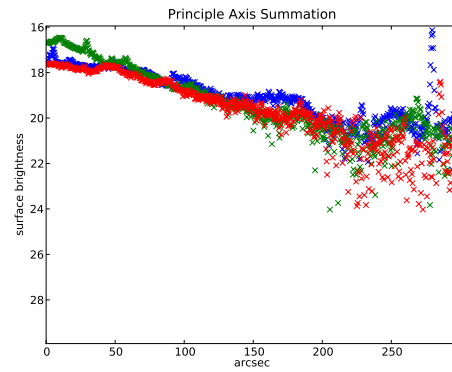
(a) r' band image



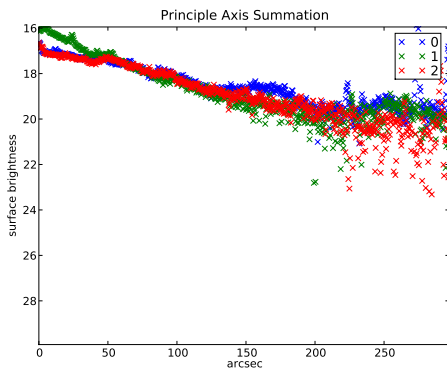
(b) low luminosity r' band image



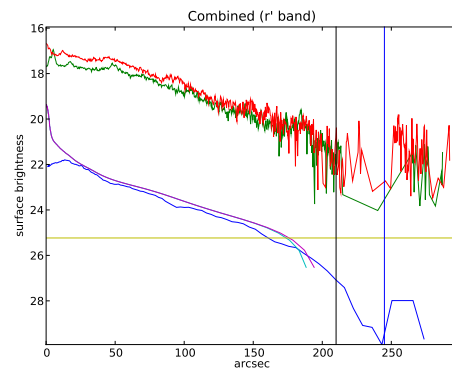
(c) Equivalent Profiles



(d) Axial Summation of 4 Quadrants

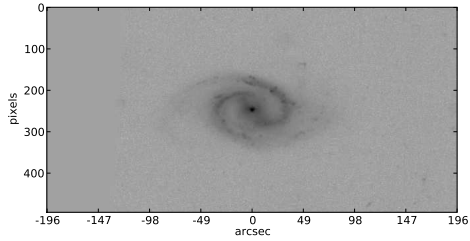


(e) Axial Summation of 4 Quadrants

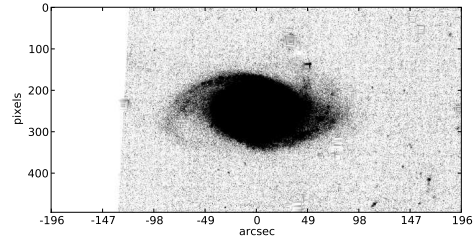


(f) Combined

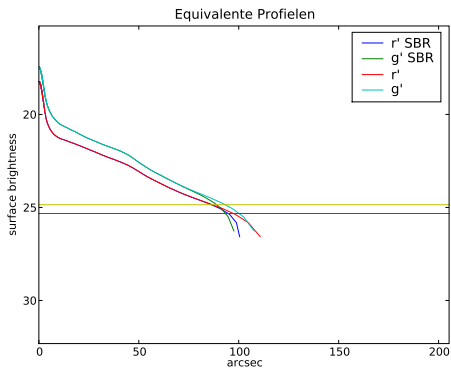
Figure A.12: *Galaxy NGC 2541* - Pohlen en Trujillo have classified this galaxy as Type II-CT. A truncation is present at 210 arcseconds.



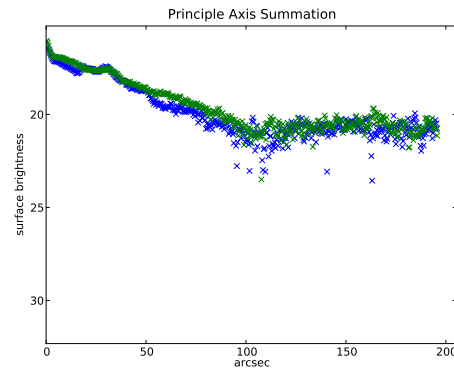
(a) r' band image



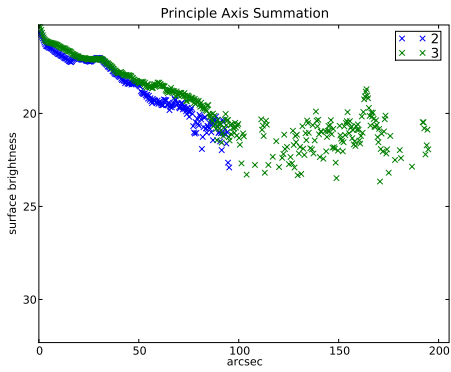
(b) low luminosity r' band image



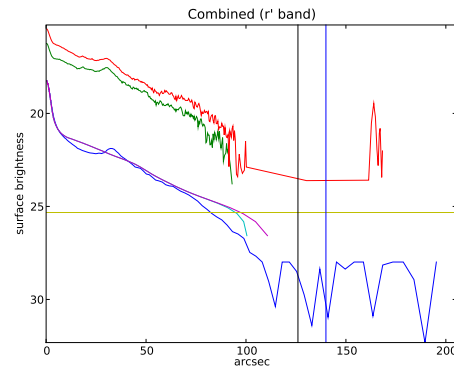
(c) Equivalent Profiles



(d) Axial Summation of 4 Quadrants

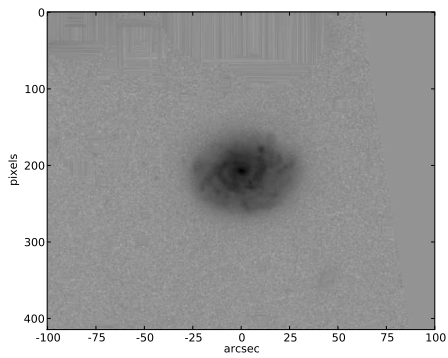


(e) Axial Summation of 4 Quadrants

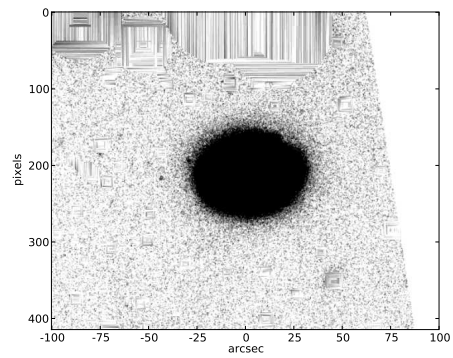


(f) Combined

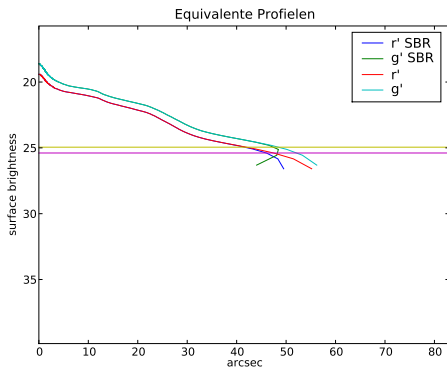
Figure A.13: *Galaxy NGC 2543* - Pohlen en Trujillo have classified this galaxy as Type II.i. A truncation is present at 90 arcseconds.



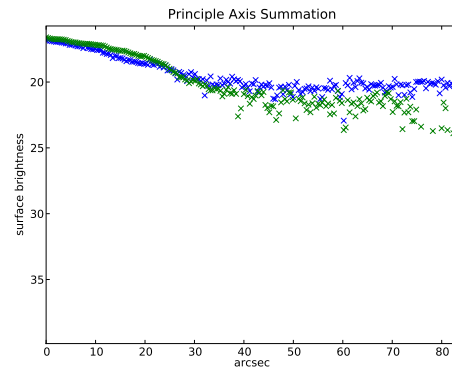
(a) r' band image



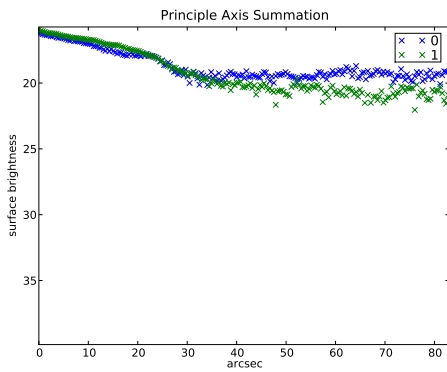
(b) low luminosity r' band image



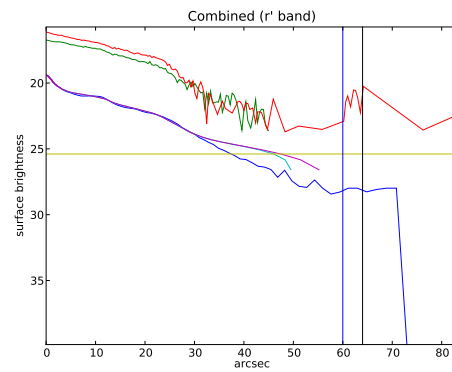
(c) Equivalent Profiles



(d) Axial Summation of 4 Quadrants

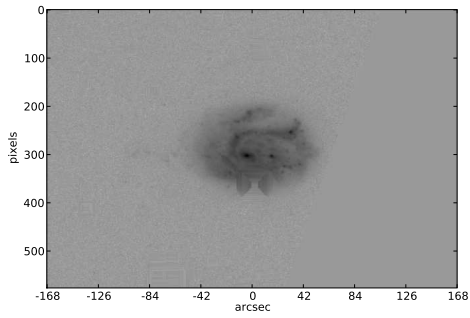


(e) Axial Summation of 4 Quadrants

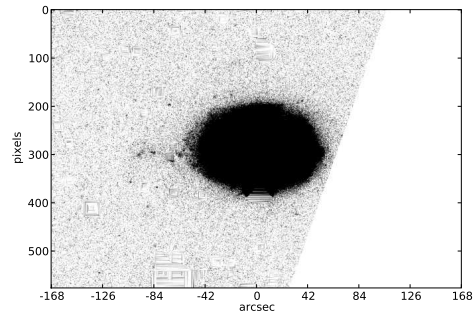


(f) Combined

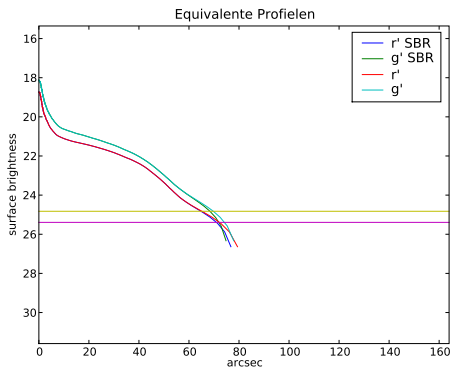
Figure A.14: *Galaxy NGC 2684* - Pohlen en Trujillo have classified this galaxy as Type II-CT. Horribly masked galaxy, will not be used further.



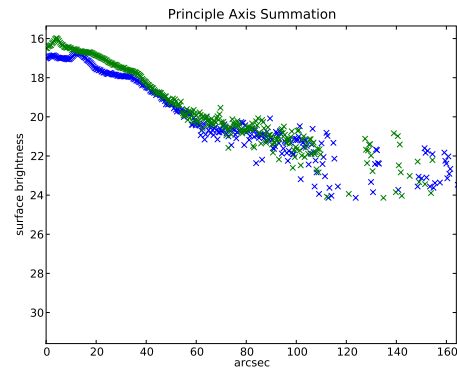
(a) r' band image



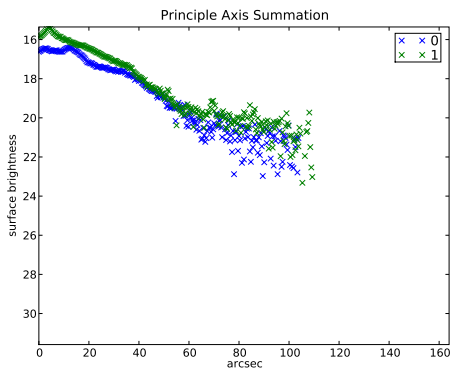
(b) low luminosity r' band image



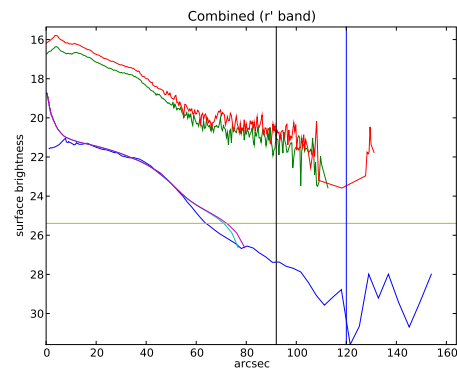
(c) Equivalent Profiles



(d) Axial Summation of 4 Quadrants

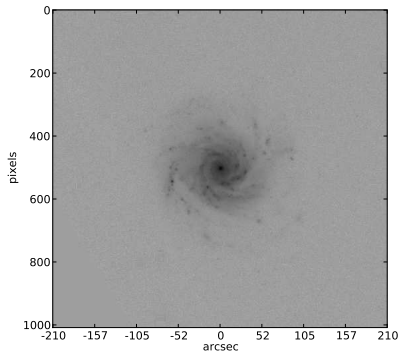


(e) Axial Summation of 4 Quadrants

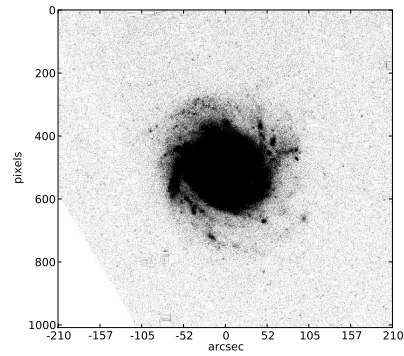


(f) Combined

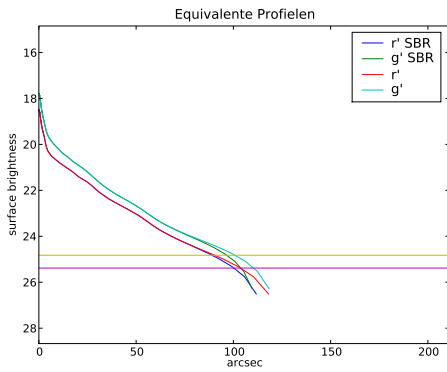
Figure A.15: *Galaxy NGC 2701* - Pohlen en Trujillo have classified this galaxy as Type II-AB + III. No truncation is seen below 100 arcseconds.



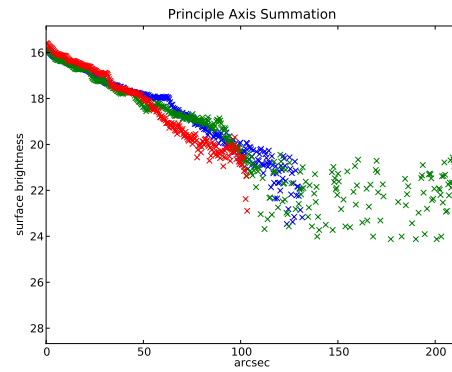
(a) r' band image



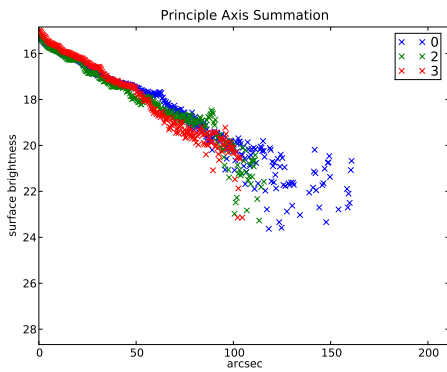
(b) low luminosity r' band image



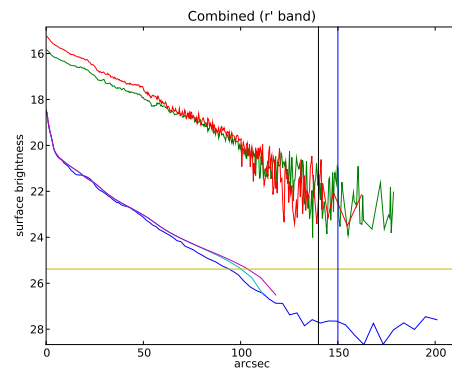
(c) Equivalent Profiles



(d) Axial Summation of 4 Quadrants

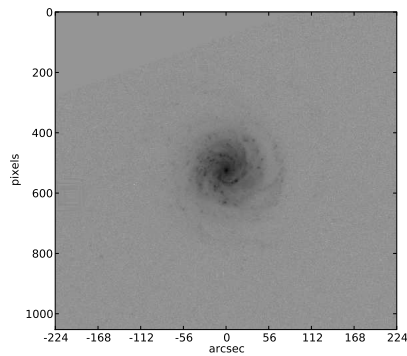


(e) Axial Summation of 4 Quadrants

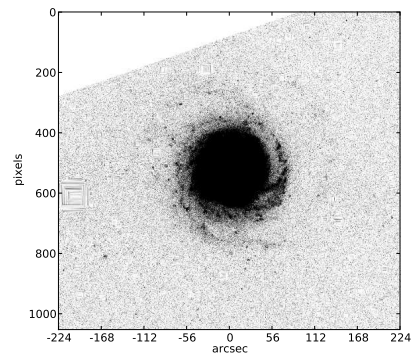


(f) Combined

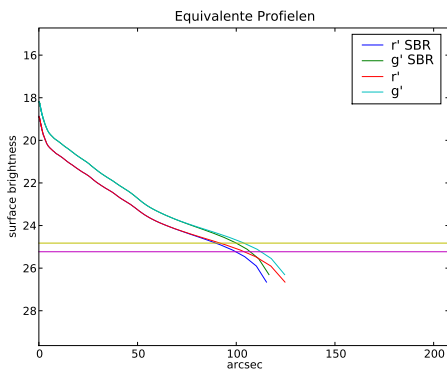
Figure A.16: *Galaxy NGC 2776* - Pohlen en Trujillo have classified this galaxy as Type I. No truncation is seen and the underlimit is set at 140 arcseconds.



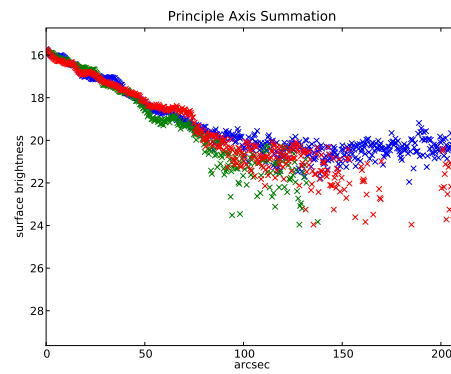
(a) r' band image



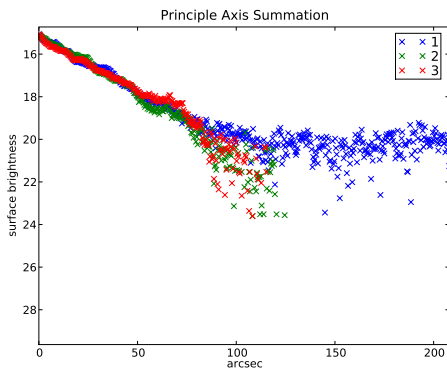
(b) low luminosity r' band image



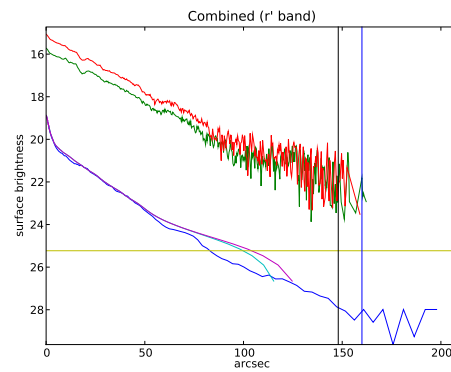
(c) Equivalent Profiles



(d) Axial Summation of 4 Quadrants

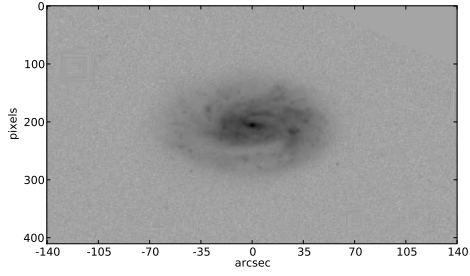


(e) Axial Summation of 4 Quadrants

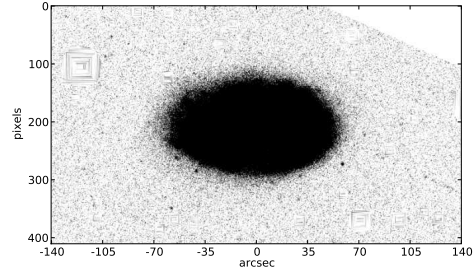


(f) Combined

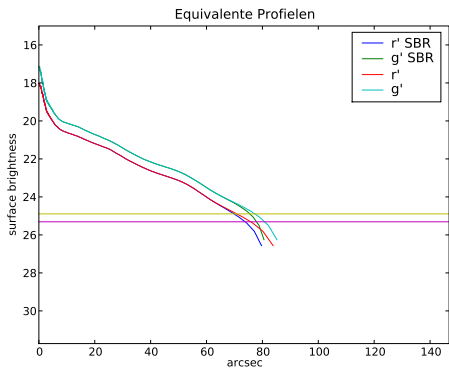
Figure A.17: *Galaxy NGC 2967* - Pohlen en Trujillo have classified this galaxy as Type III-d. No truncation is seen. The underlimit is set at 150 arcseconds.



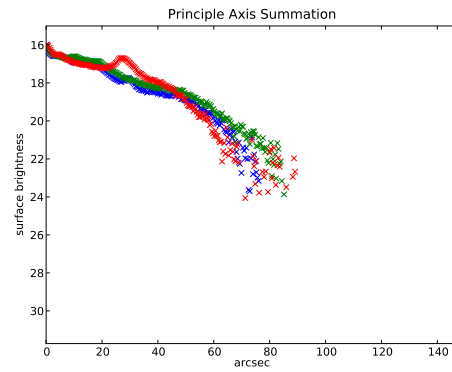
(a) r' band image



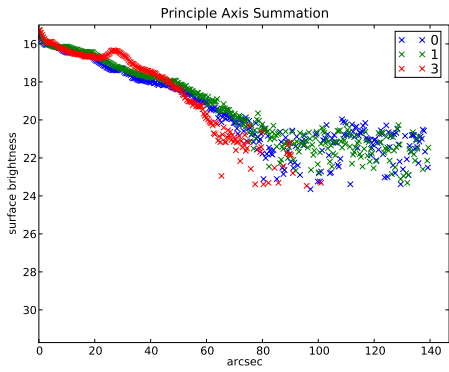
(b) low luminosity r' band image



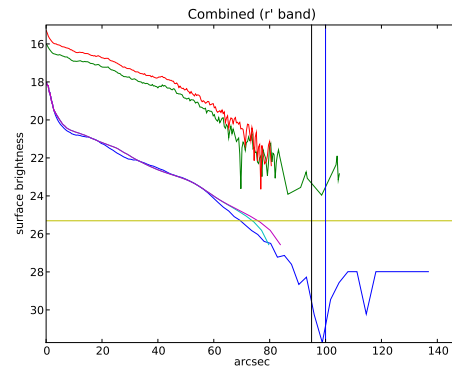
(c) Equivalent Profiles



(d) Axial Summation of 4 Quadrants

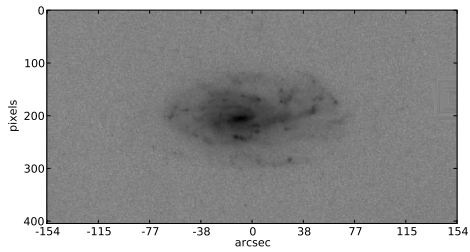


(e) Axial Summation of 4 Quadrants

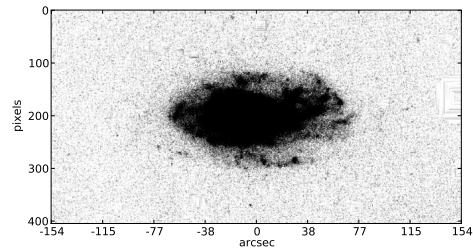


(f) Combined

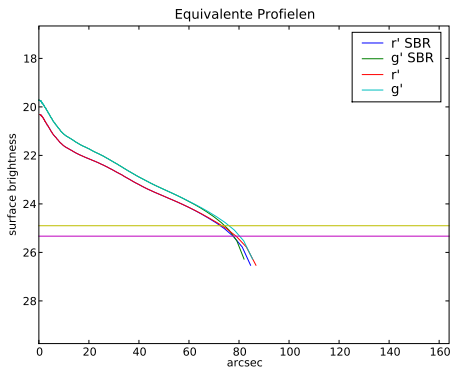
Figure A.18: *Galaxy NGC 3055* - Pohlen en Trujillo have classified this galaxy as Type II.o-CT. A truncation is seen at 80 arcseconds.



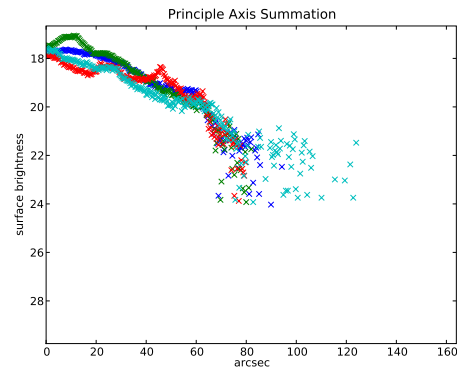
(a) r' band image



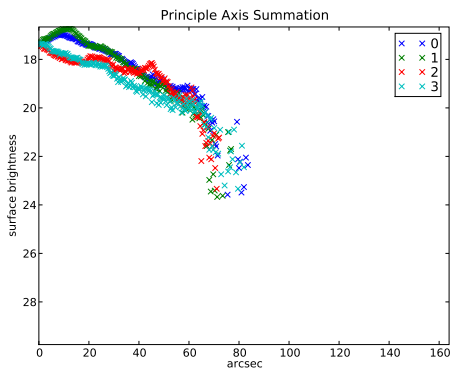
(b) low luminosity r' band image



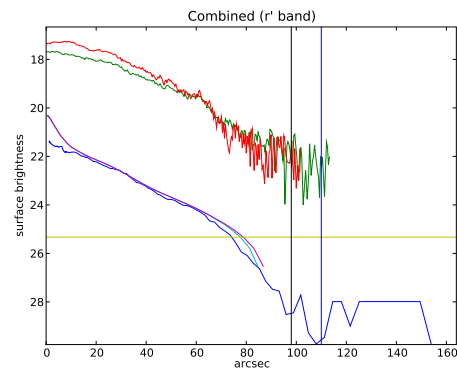
(c) Equivalent Profiles



(d) Axial Summation of 4 Quadrants

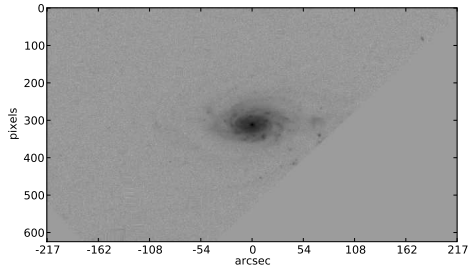


(e) Axial Summation of 4 Quadrants

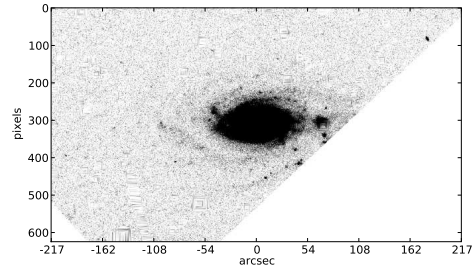


(f) Combined

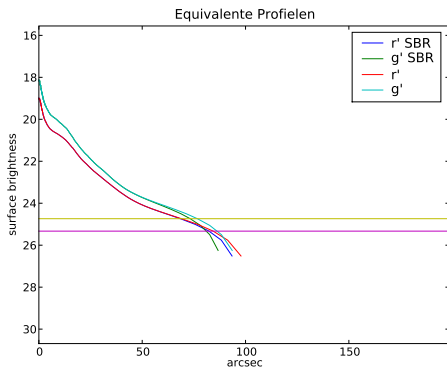
Figure A.19: *Galaxy NGC 3246* - Pohlen en Trujillo have classified this galaxy as Type II-AB. A possible truncation is seen at 70 arcseconds.



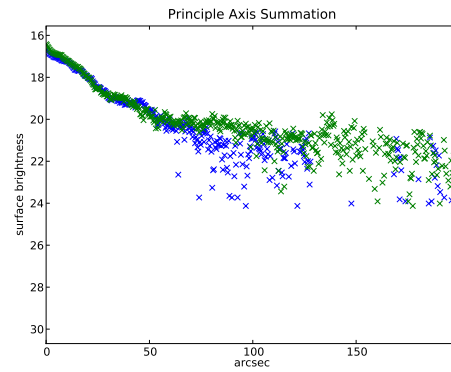
(a) r' band image



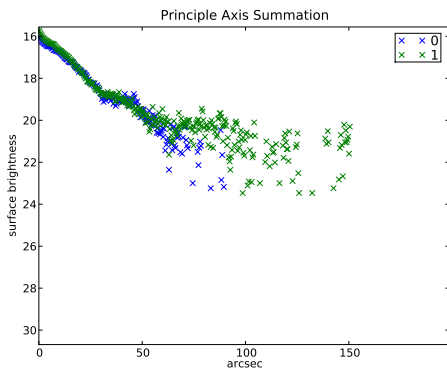
(b) low luminosity r' band image



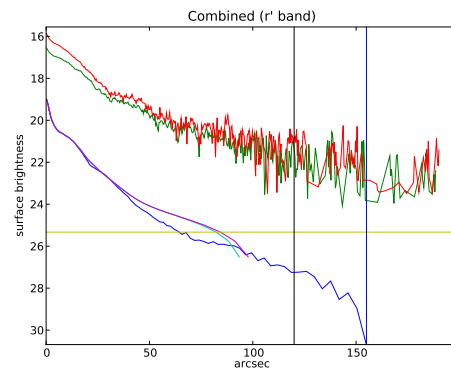
(c) Equivalent Profiles



(d) Axial Summation of 4 Quadrants

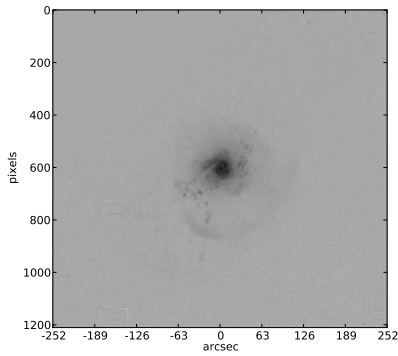


(e) Axial Summation of 4 Quadrants

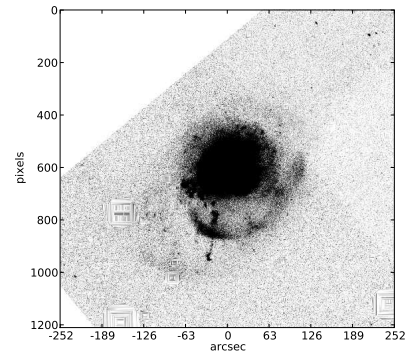


(f) Combined

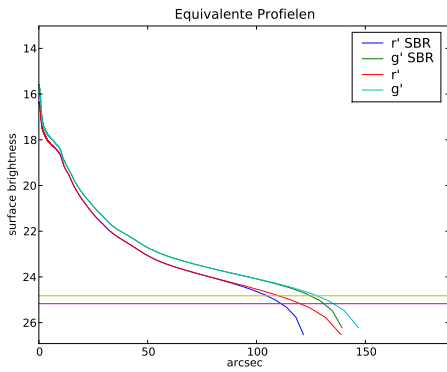
Figure A.20: *Galaxy NGC 3259* - Pohlen en Trujillo have classified this galaxy as Type III-d. No signs of truncation is seen below 120 arcseconds.



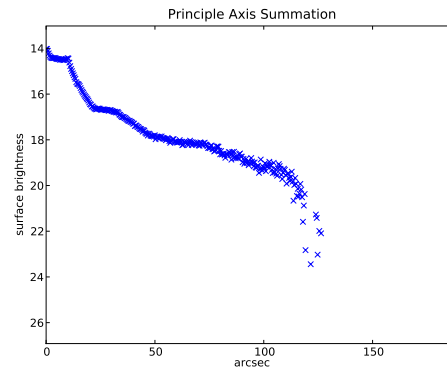
(a) r' band image



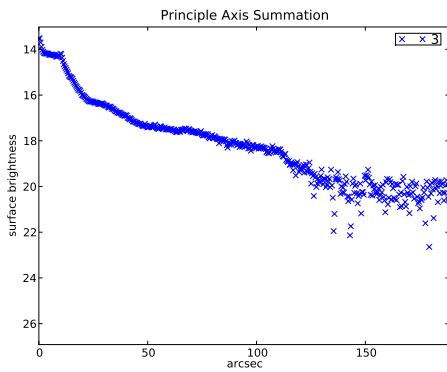
(b) low luminosity r' band image



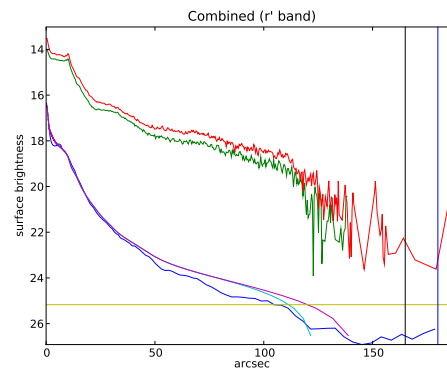
(c) Equivalent Profiles



(d) Axial Summation of 4 Quadrants

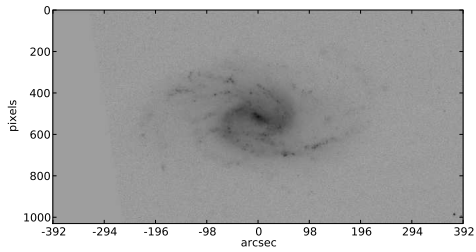


(e) Axial Summation of 4 Quadrants

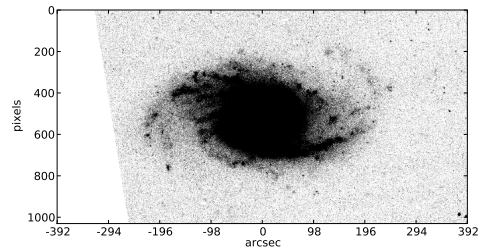


(f) Combined

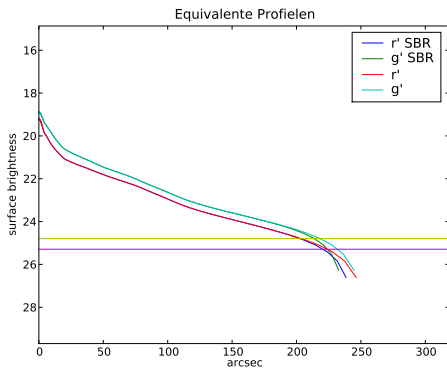
Figure A.21: *Galaxy NGC 3310* - Pohlen en Trujillo have classified this galaxy as Type III. It is clearly disturbed. The galaxy is not used in the sample.



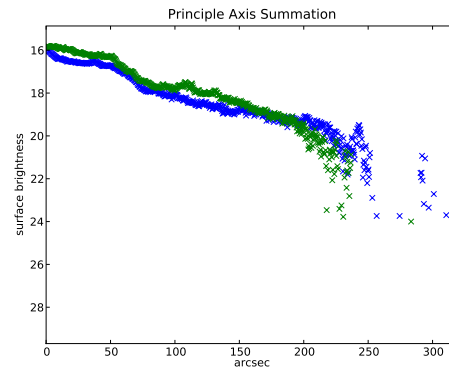
(a) r' band image



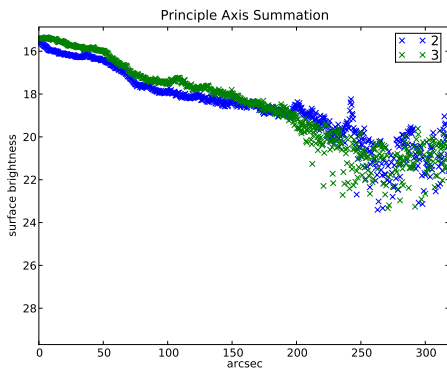
(b) low luminosity r' band image



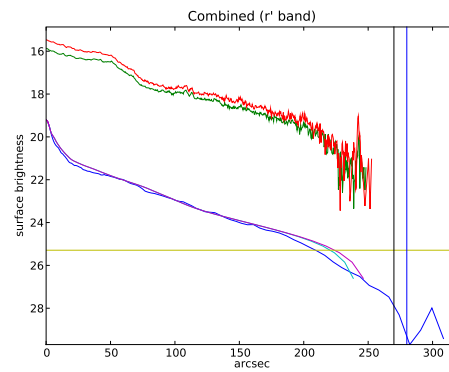
(c) Equivalent Profiles



(d) Axial Summation of 4 Quadrants

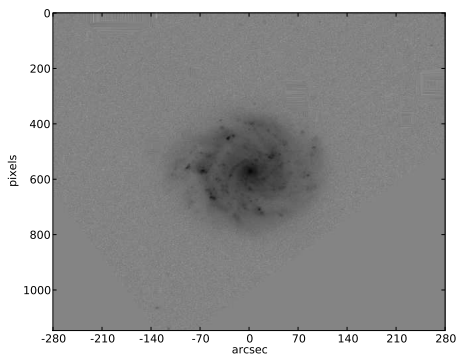


(e) Axial Summation of 4 Quadrants

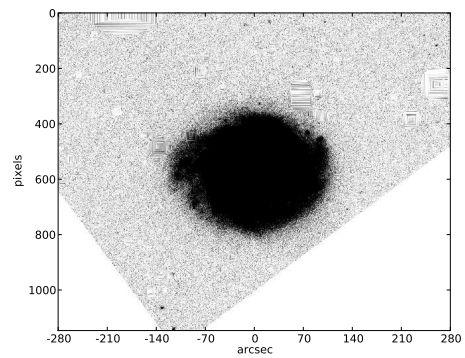


(f) Combined

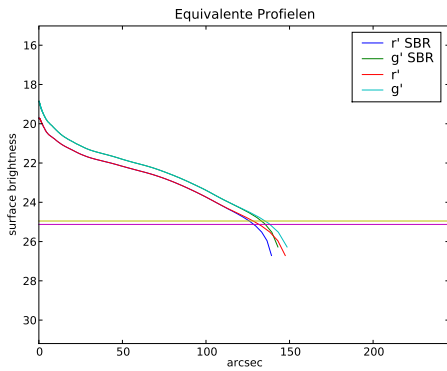
Figure A.22: *Galaxy NGC 3359* - Pohlen en Trujillo have classified this galaxy as Type II-AB. A truncation is present at 250 arcseconds.



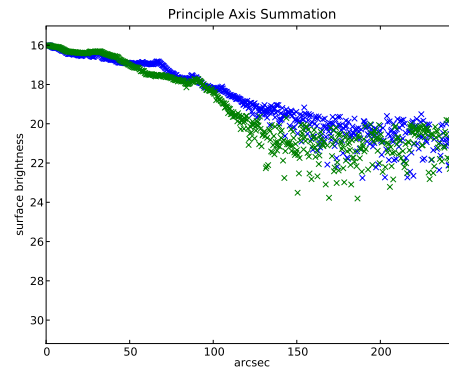
(a) r' band image



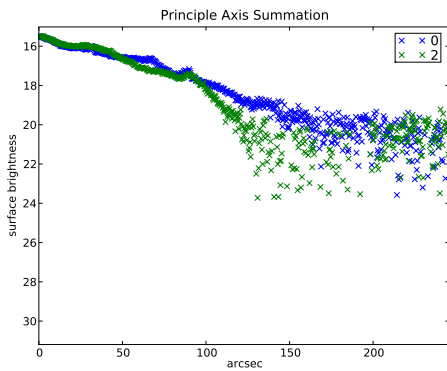
(b) low luminosity r' band image



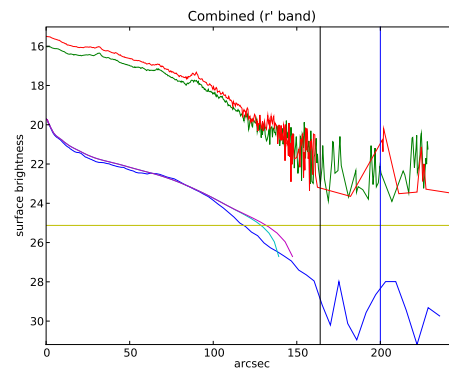
(c) Equivalent Profiles



(d) Axial Summation of 4 Quadrants

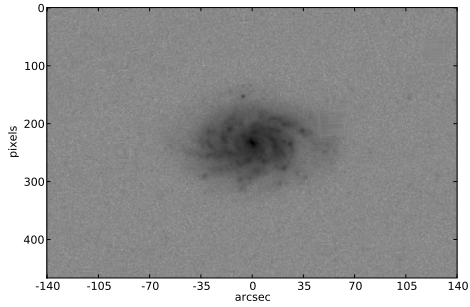


(e) Axial Summation of 4 Quadrants

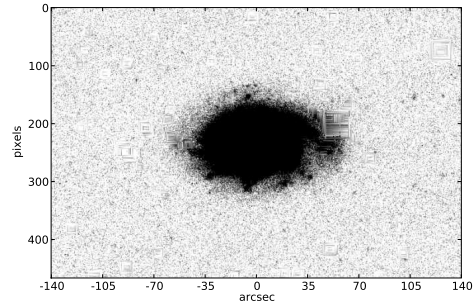


(f) Combined

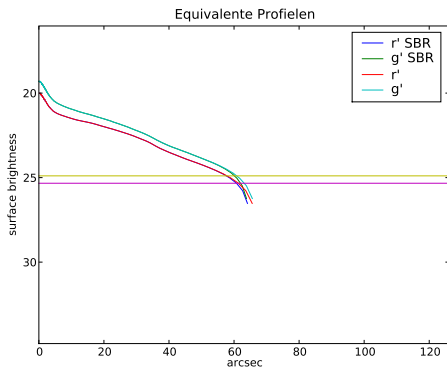
Figure A.23: *Galaxy NGC 3423* - Pohlen en Trujillo have classified this galaxy as Type II-CT. No strong indications of truncation are seen. The underlimit is set at 160 arcseconds.



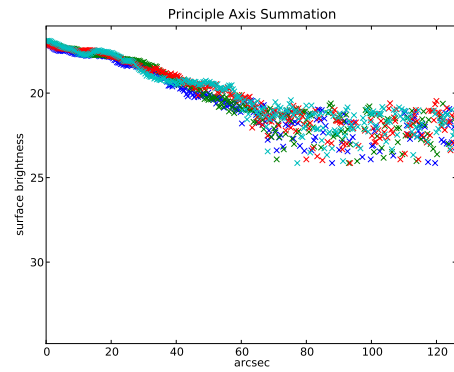
(a) r' band image



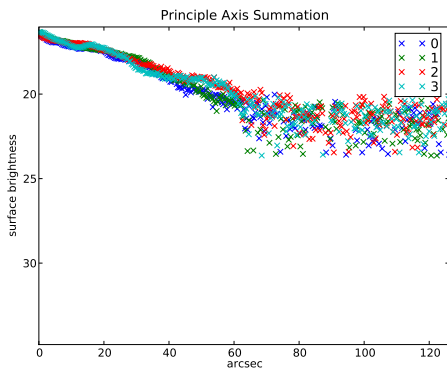
(b) low luminosity r' band image



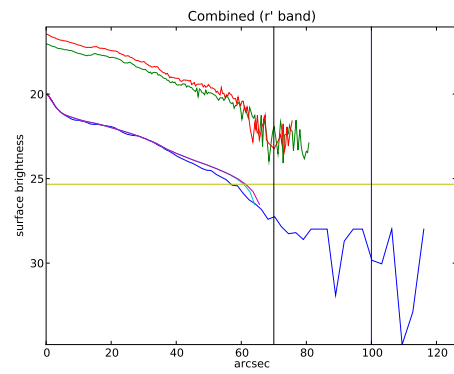
(c) Equivalent Profiles



(d) Axial Summation of 4 Quadrants

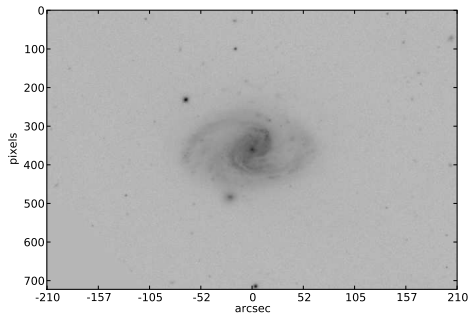


(e) Axial Summation of 4 Quadrants

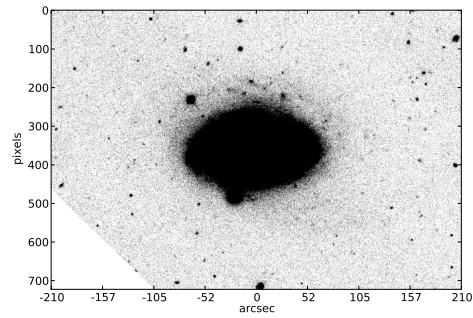


(f) Combined

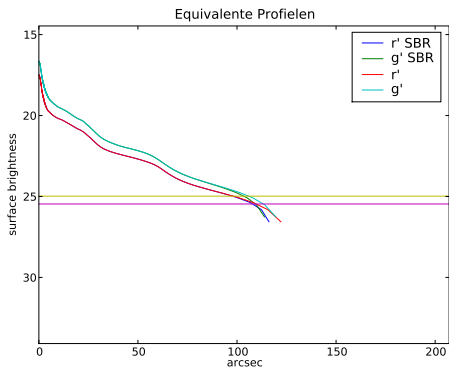
Figure A.24: *Galaxy NGC 3488* - Pohlen en Trujillo have classified this galaxy as Type II.o-CT. A not so confining break is seen at 70 arcseconds.



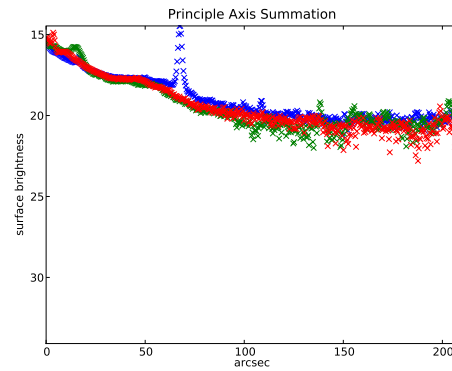
(a) r' band image



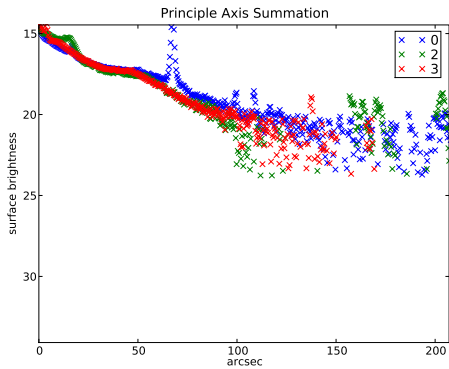
(b) low luminosity r' band image



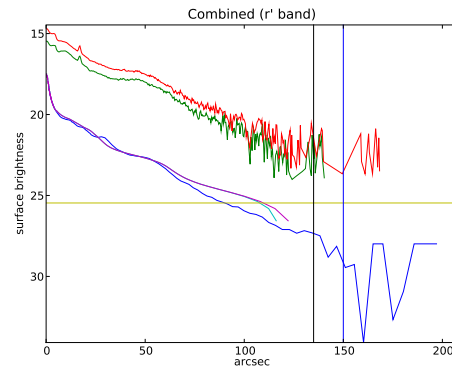
(c) Equivalent Profiles



(d) Axial Summation of 4 Quadrants

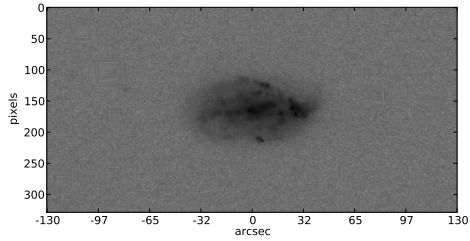


(e) Axial Summation of 4 Quadrants

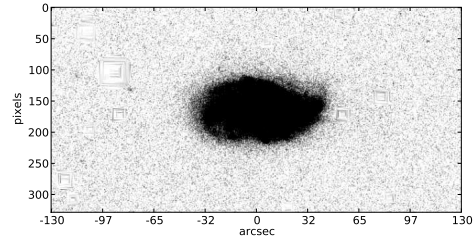


(f) Combined

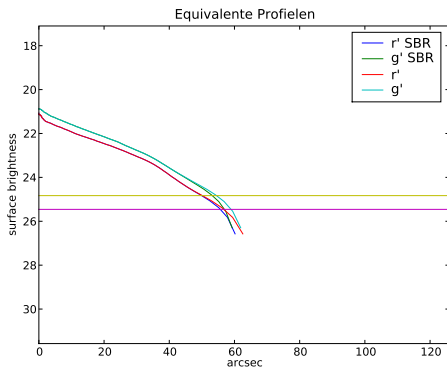
Figure A.25: *Galaxy NGC 3583* - Pohlen en Trujillo have classified this galaxy as Type III-d. Masking failed in this image. No signs of truncations are seen below 140 arcseconds.



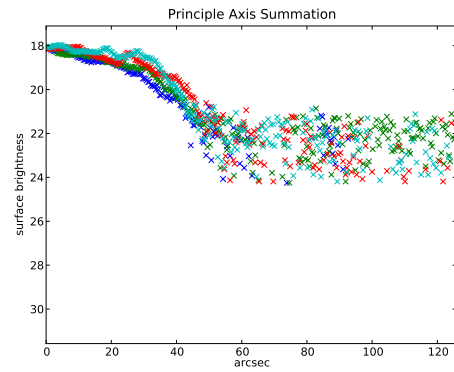
(a) r' band image



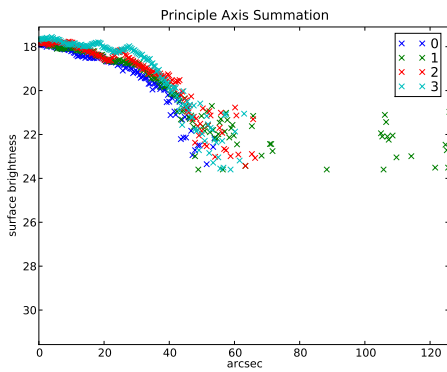
(b) low luminosity r' band image



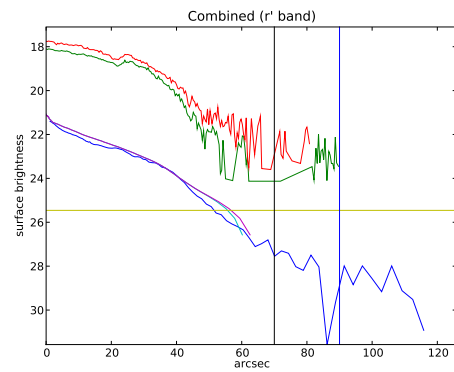
(c) Equivalent Profiles



(d) Axial Summation of 4 Quadrants

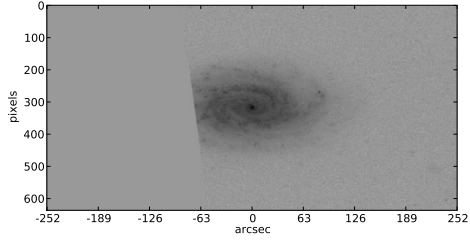


(e) Axial Summation of 4 Quadrants

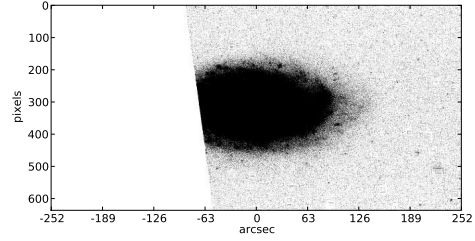


(f) Combined

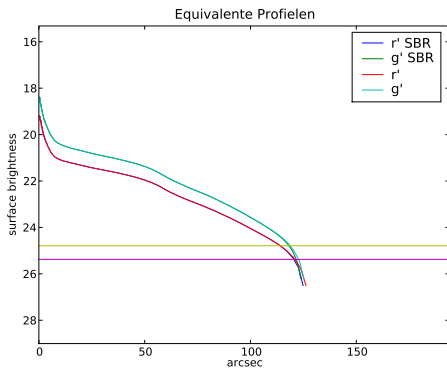
Figure A.26: *Galaxy NGC 3589* - Pohlen en Trujillo have classified this galaxy as Type II-CT. No truncation is seen below 60 arcseconds.



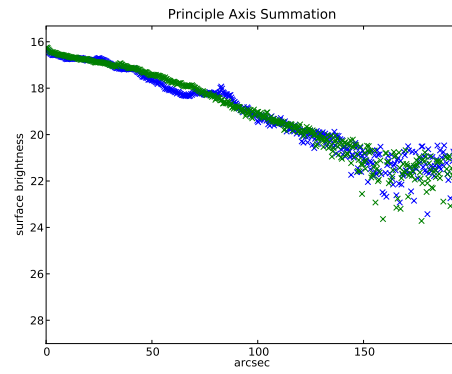
(a) r' band image



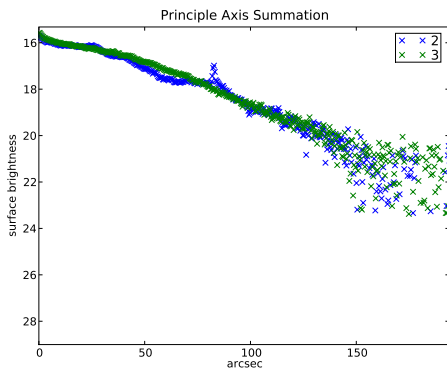
(b) low luminosity r' band image



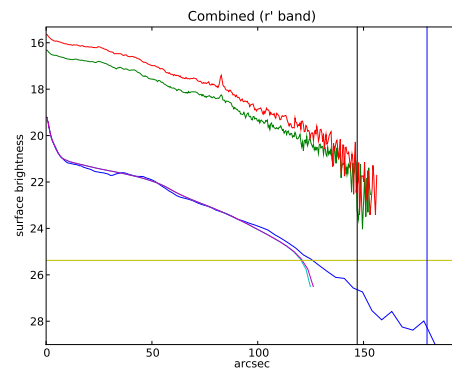
(c) Equivalent Profiles



(d) Axial Summation of 4 Quadrants

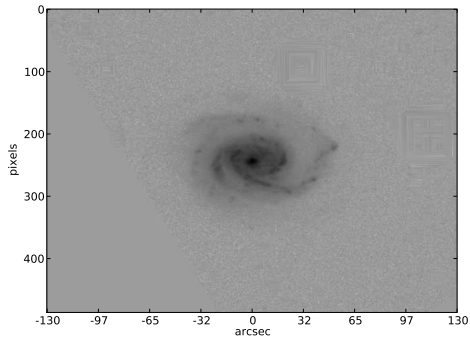


(e) Axial Summation of 4 Quadrants

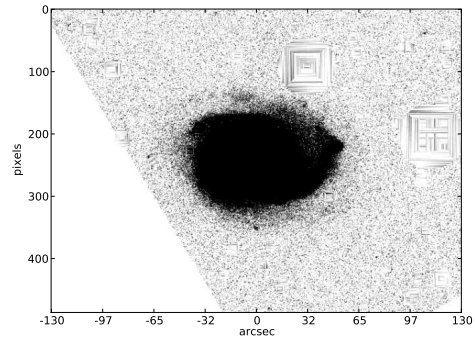


(f) Combined

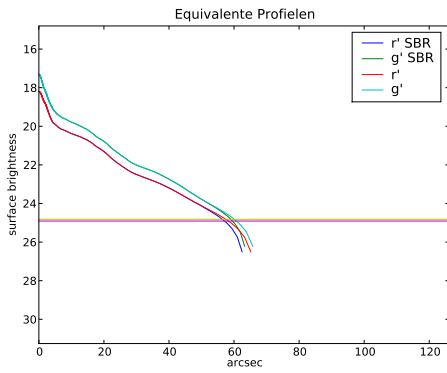
Figure A.27: *Galaxy NGC 3756* - Pohlen en Trujillo have classified this galaxy as Type II.o-CT. A truncation is seen at 150 arcseconds.



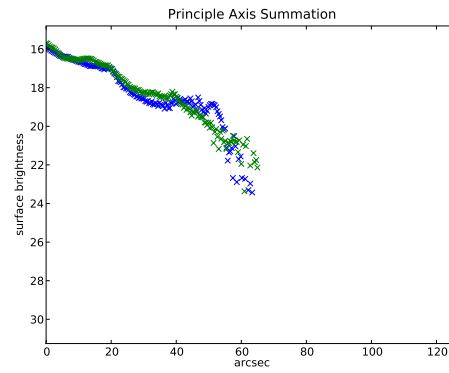
(a) r' band image



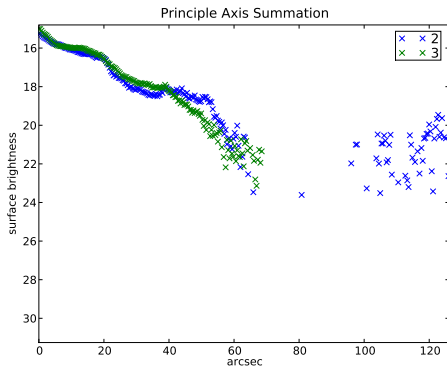
(b) low luminosity r' band image



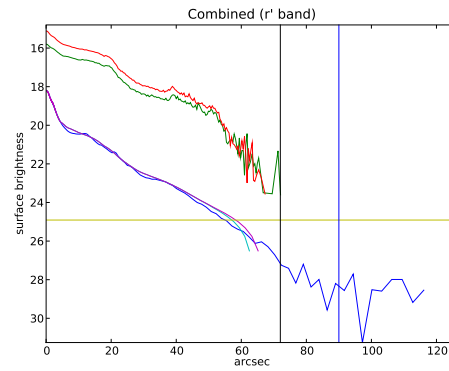
(c) Equivalent Profiles



(d) Axial Summation of 4 Quadrants

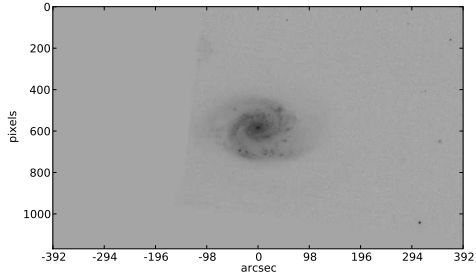


(e) Axial Summation of 4 Quadrants

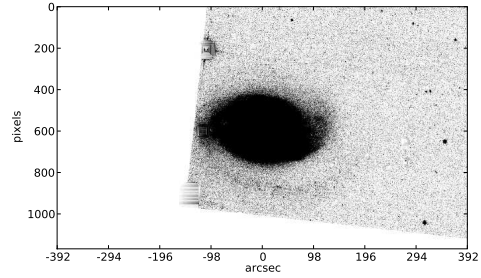


(f) Combined

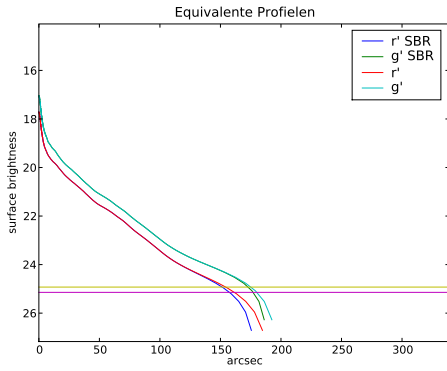
Figure A.28: *Galaxy NGC 3888* - Pohlen en Trujillo have classified this galaxy as Type I. A horrible profile due to the large masks. The galaxy is not used any further.



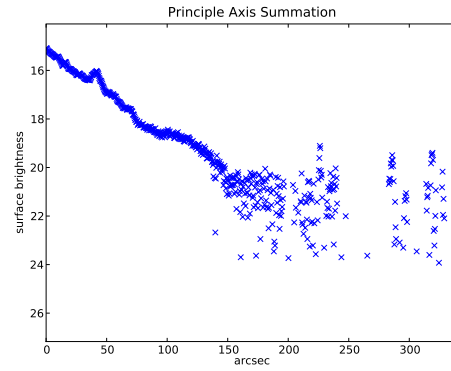
(a) r' band image



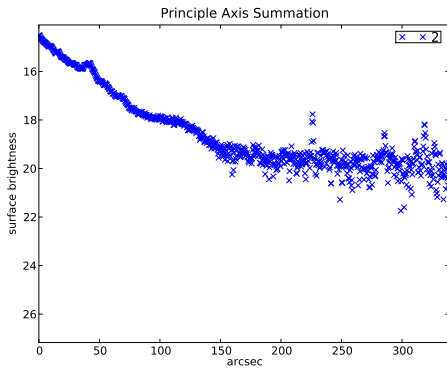
(b) low luminosity r' band image



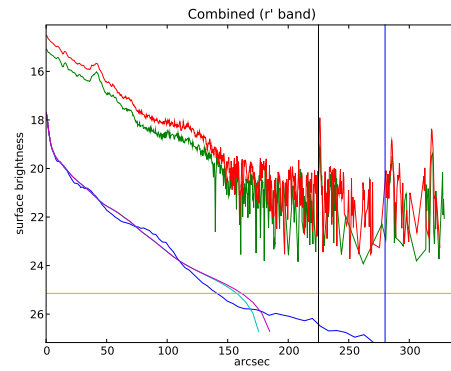
(c) Equivalent Profiles



(d) Axial Summation of 4 Quadrants

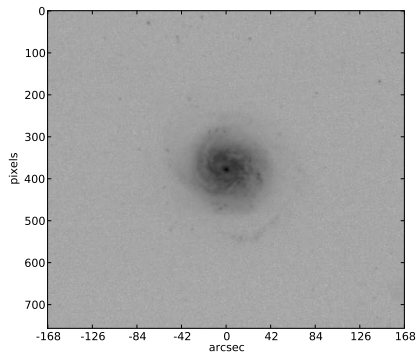


(e) Axial Summation of 4 Quadrants

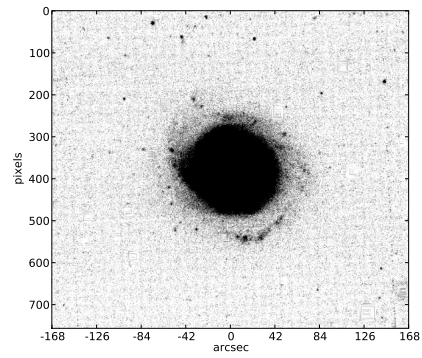


(f) Combined

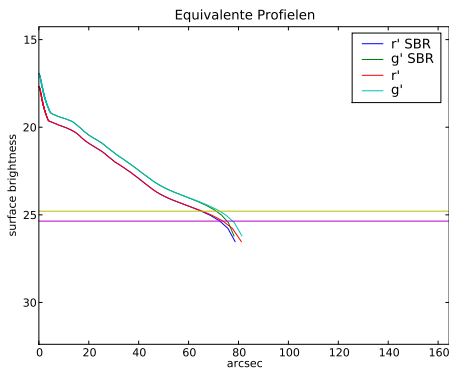
Figure A.29: *Galaxy NGC 3893* - Pohlen en Trujillo have classified this galaxy as Type III-d. A lot of signs of interaction are presented. This galaxy is not used further.



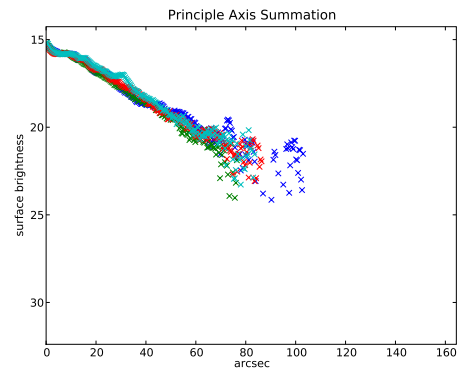
(a) r' band image



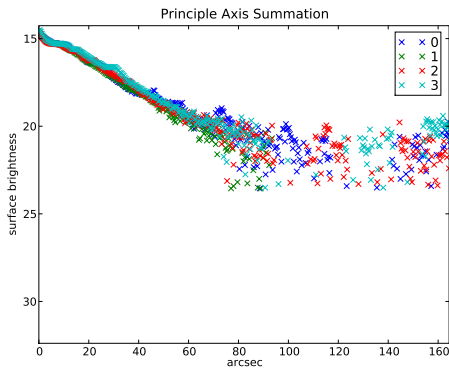
(b) low luminosity r' band image



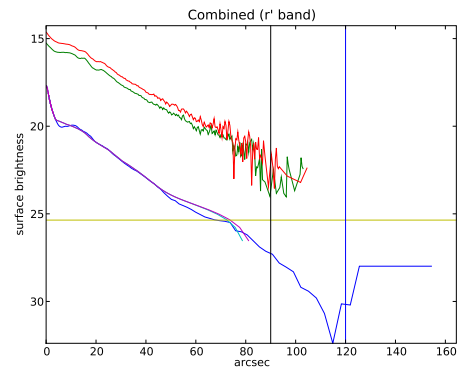
(c) Equivalent Profiles



(d) Axial Summation of 4 Quadrants

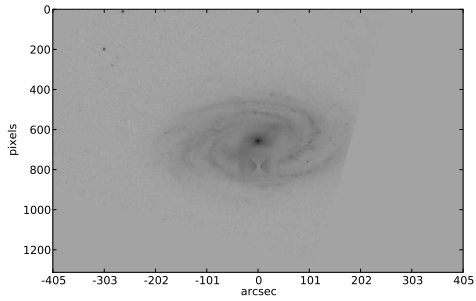


(e) Axial Summation of 4 Quadrants

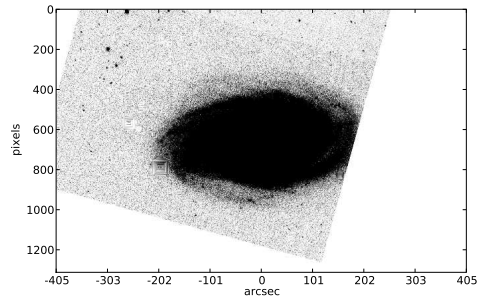


(f) Combined

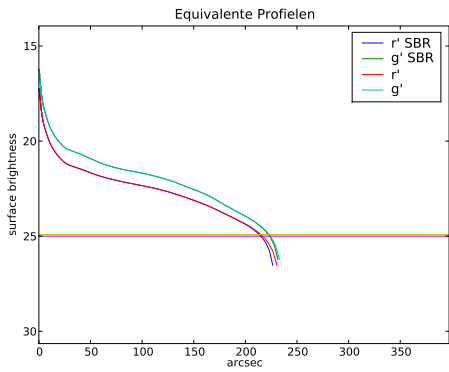
Figure A.30: *Galaxy NGC 3982* - Pohlen en Trujillo have classified this galaxy as Type III. A possible truncation is seen at 90 arcseconds. Plot *b* again reveals the disturbance leading to the type III classification.



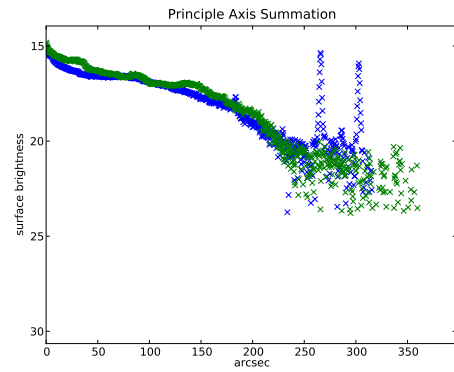
(a) r' band image



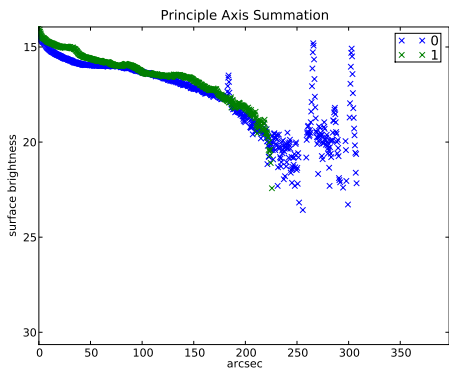
(b) low luminosity r' band image



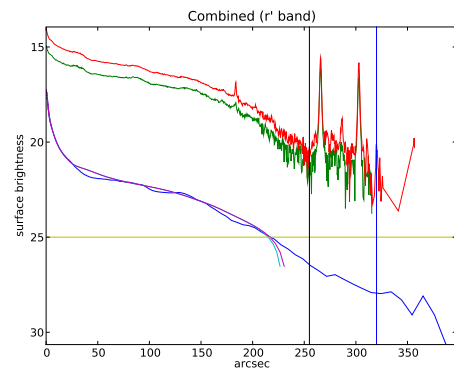
(c) Equivalent Profiles



(d) Axial Summation of 4 Quadrants

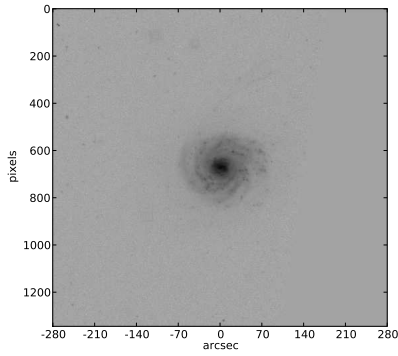


(e) Axial Summation of 4 Quadrants

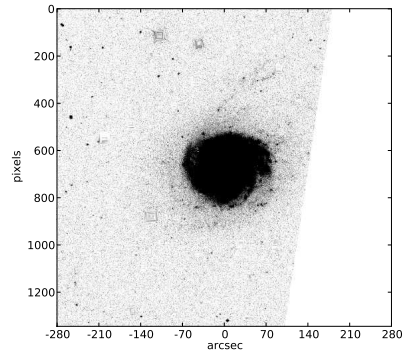


(f) Combined

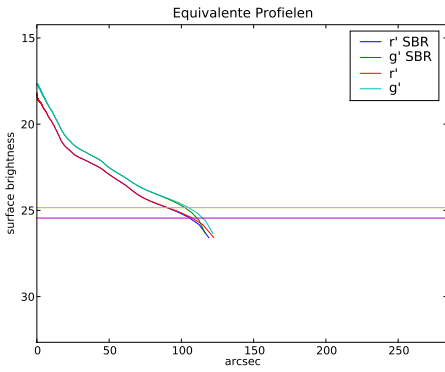
Figure A.31: *Galaxy NGC 3992* - Pohlen en Trujillo have classified this galaxy as Type II.o-OLR. No truncation below 250 arcseconds.



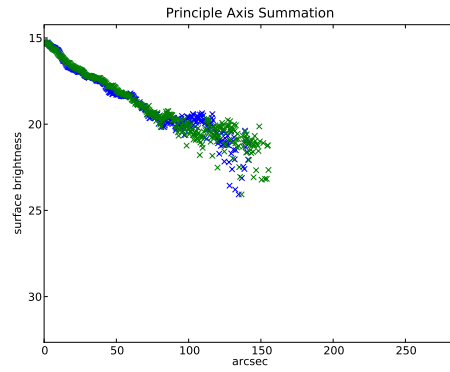
(a) r' band image



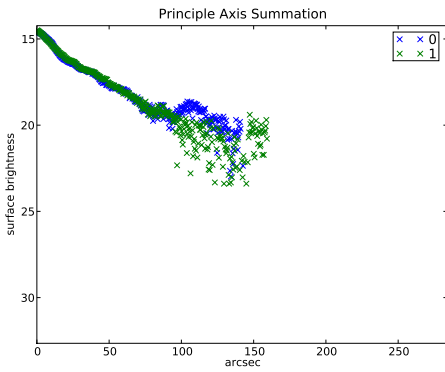
(b) low luminosity r' band image



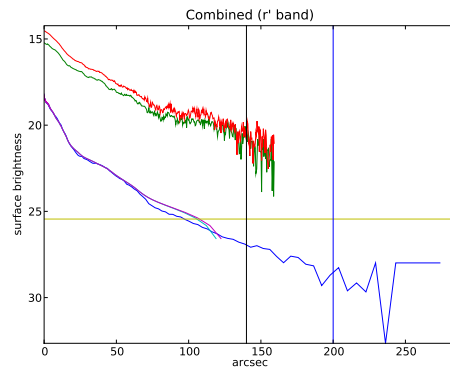
(c) Equivalent Profiles



(d) Axial Summation of 4 Quadrants

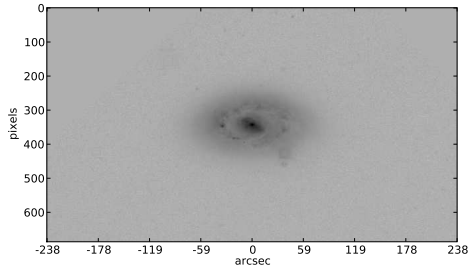


(e) Axial Summation of 4 Quadrants

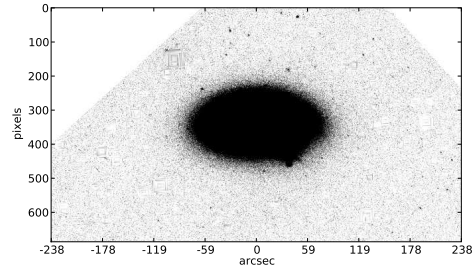


(f) Combined

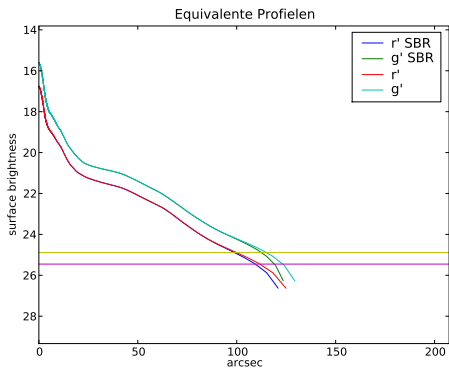
Figure A.32: *Galaxy NGC 4041* - Pohlen en Trujillo have classified this galaxy as Type III-d. This clearly a disturbed galaxy as seen in figure *b*. It is removed from the sample.



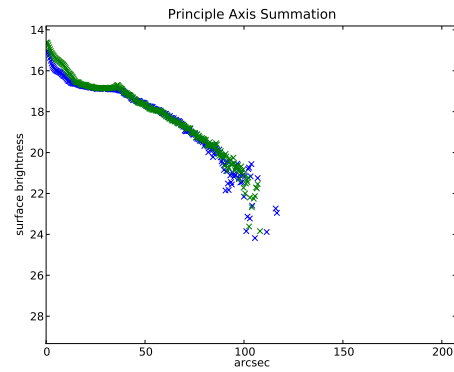
(a) r' band image



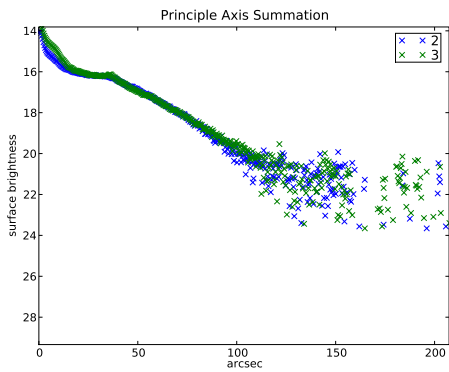
(b) low luminosity r' band image



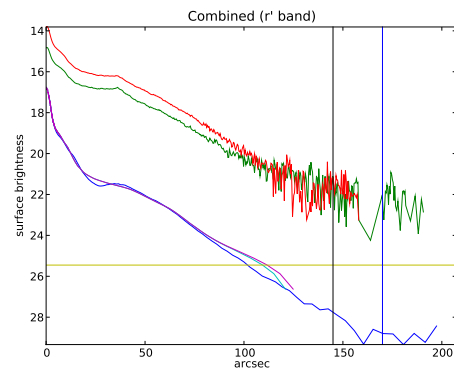
(c) Equivalent Profiles



(d) Axial Summation of 4 Quadrants

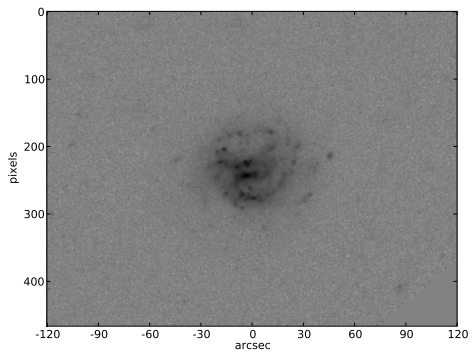


(e) Axial Summation of 4 Quadrants

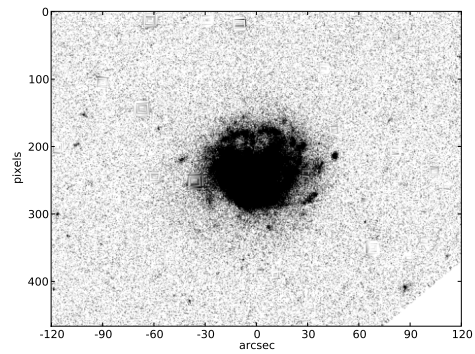


(f) Combined

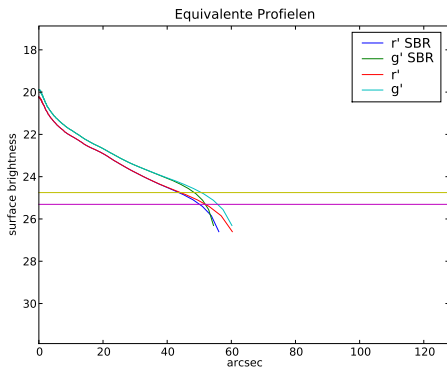
Figure A.33: *Galaxy NGC 4102* - Pohlen en Trujillo have classified this galaxy as Type II.o-OLR + III. No truncation is seen below 150 arcseconds.



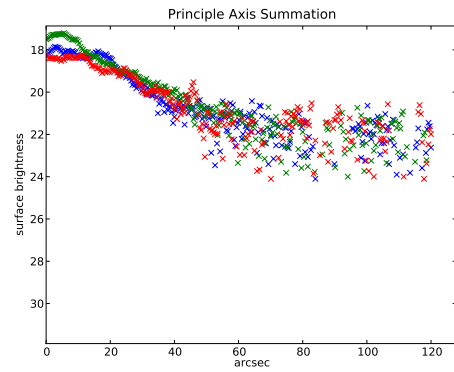
(a) r' band image



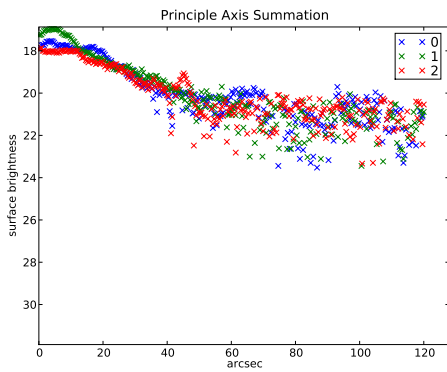
(b) low luminosity r' band image



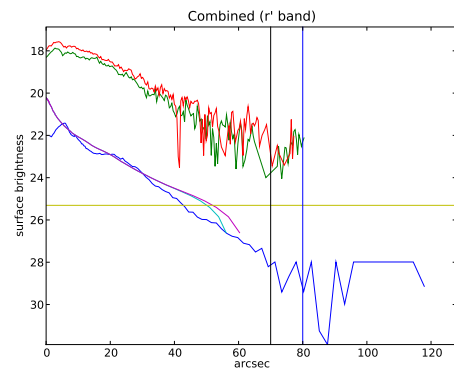
(c) Equivalent Profiles



(d) Axial Summation of 4 Quadrants

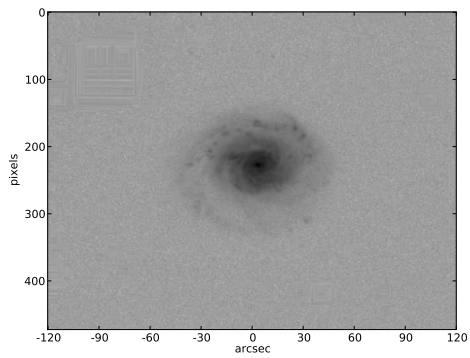


(e) Axial Summation of 4 Quadrants

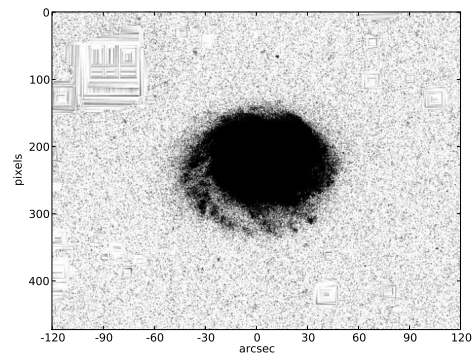


(f) Combined

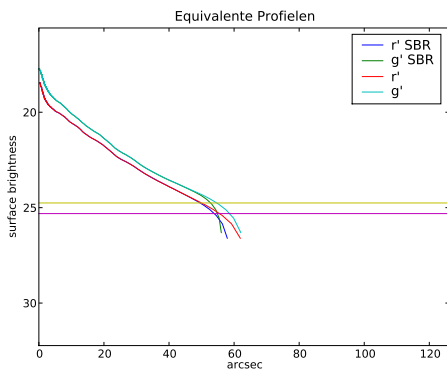
Figure A.34: *Galaxy NGC 4108B* - Pohlen en Trujillo have classified this galaxy as Type I. No truncation is seen below 70 arcseconds.



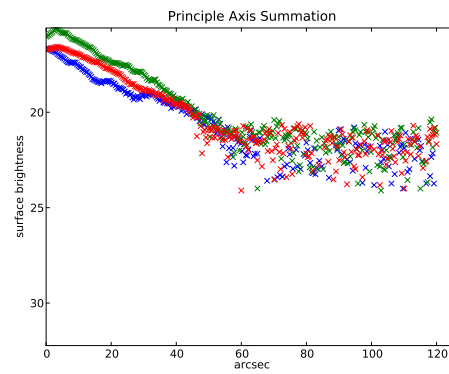
(a) r' band image



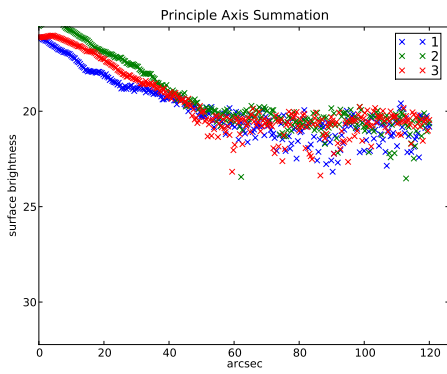
(b) low luminosity r' band image



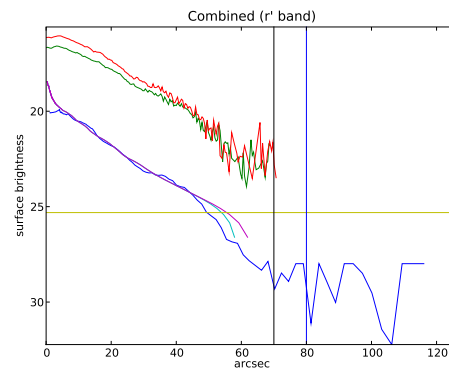
(c) Equivalent Profiles



(d) Axial Summation of 4 Quadrants

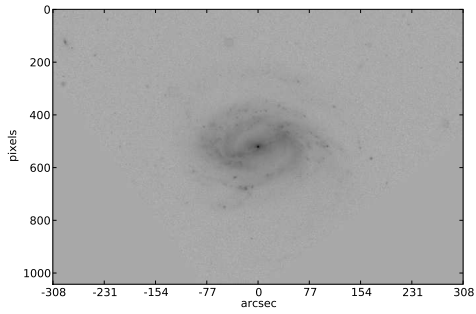


(e) Axial Summation of 4 Quadrants

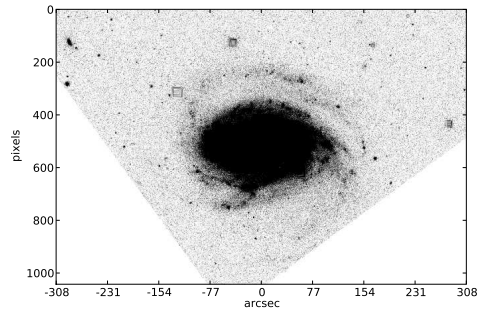


(f) Combined

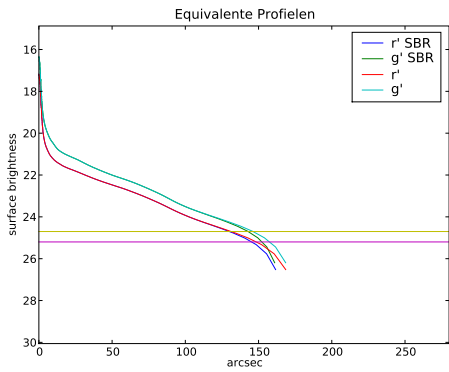
Figure A.35: *Galaxy NGC 4108* - Pohlen en Trujillo have classified this galaxy as Type II-AB. A possible truncation is visible at 60 arcseconds.



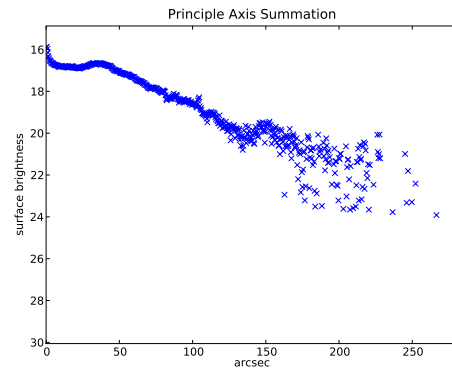
(a) r' band image



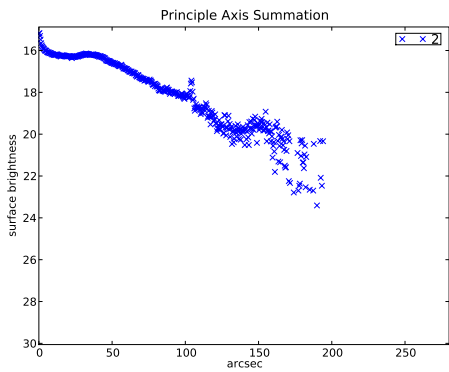
(b) low luminosity r' band image



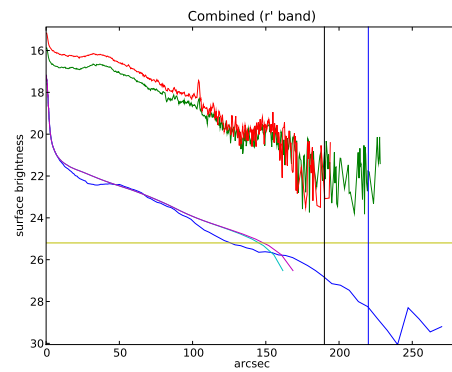
(c) Equivalent Profiles



(d) Axial Summation of 4 Quadrants

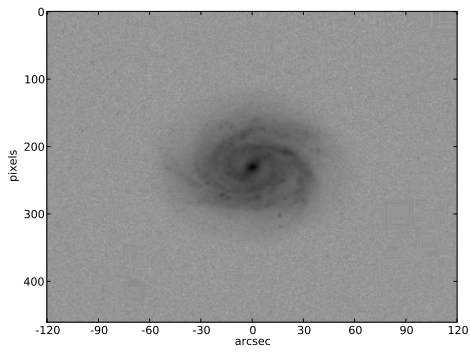


(e) Axial Summation of 4 Quadrants

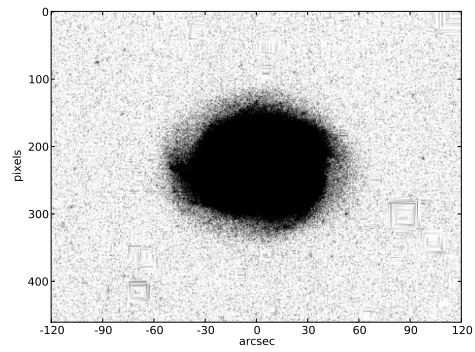


(f) Combined

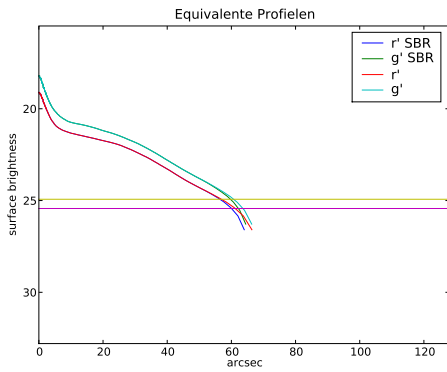
Figure A.36: *Galaxy NGC 4123* - Pohlen en Trujillo have classified this galaxy as Type I. No truncation is indeed seen below 180 arcseconds.



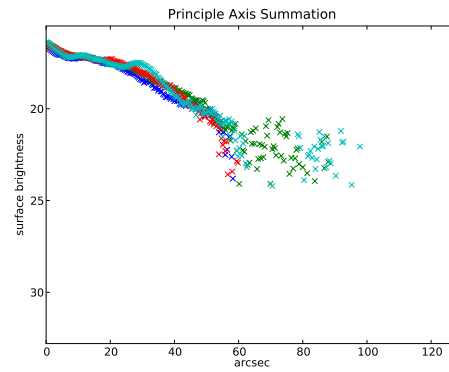
(a) r' band image



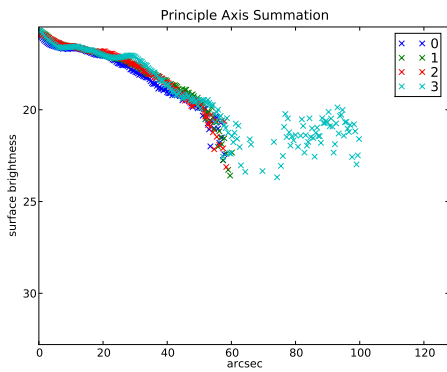
(b) low luminosity r' band image



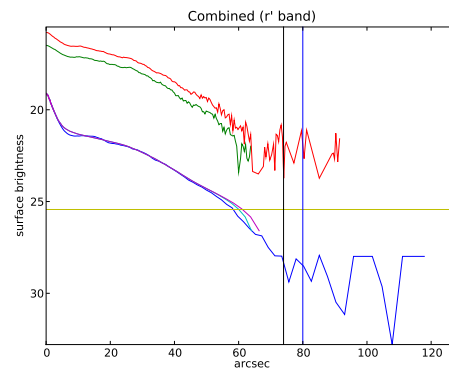
(c) Equivalent Profiles



(d) Axial Summation of 4 Quadrants

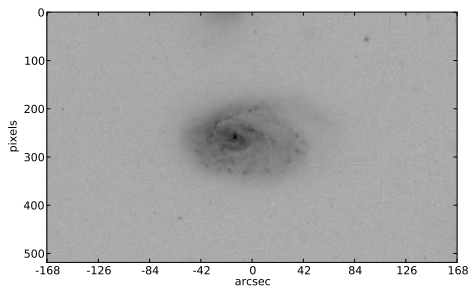


(e) Axial Summation of 4 Quadrants

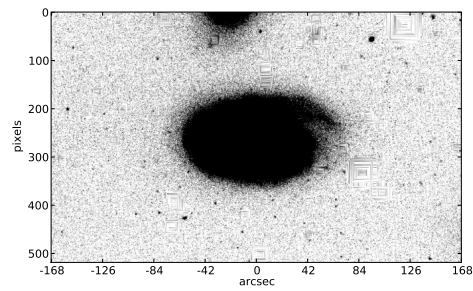


(f) Combined

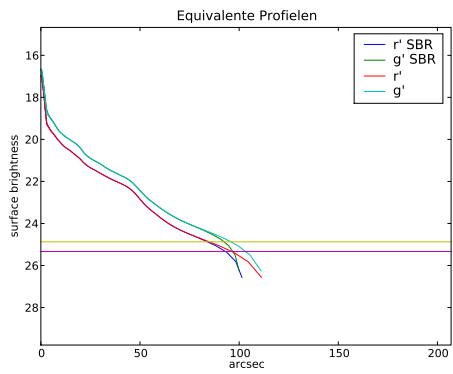
Figure A.37: *Galaxy NGC 4210* - Pohlen en Trujillo have classified this galaxy as Type II.o-OLR + II.o-CT. A possible truncation is seen at 60 arcseconds.



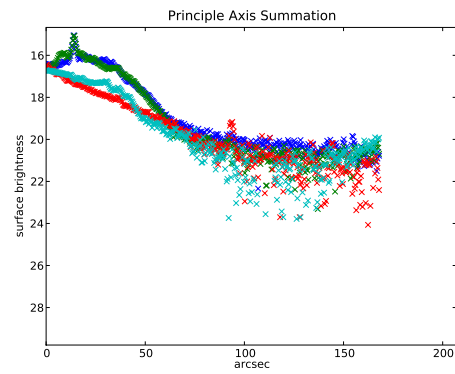
(a) r' band image



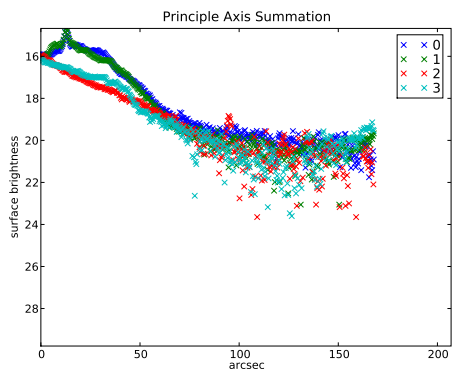
(b) low luminosity r' band image



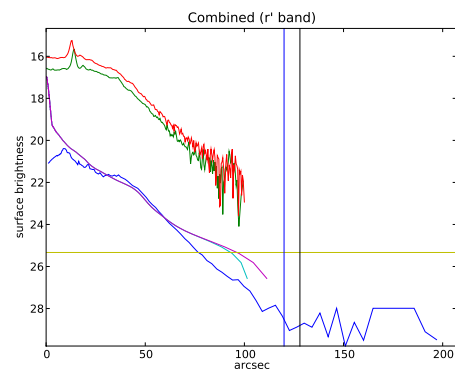
(c) Equivalent Profiles



(d) Axial Summation of 4 Quadrants

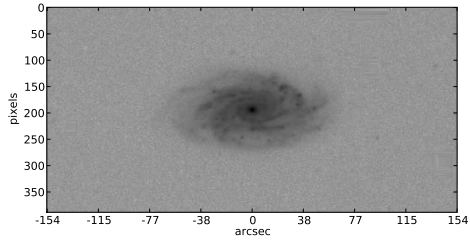


(e) Axial Summation of 4 Quadrants

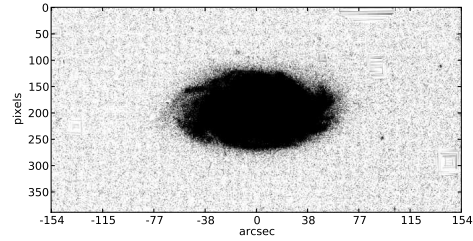


(f) Combined

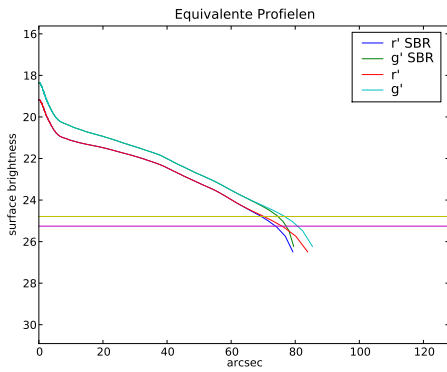
Figure A.38: *Galaxy NGC 4273* - Pohlen en Trujillo have classified this galaxy as Type II-AB + III. The underlimit is set at 100 arcseconds as no truncation is seen. In figure *a* a large spiral arm far from the galaxy is seen, this may be the source of the type III classification.



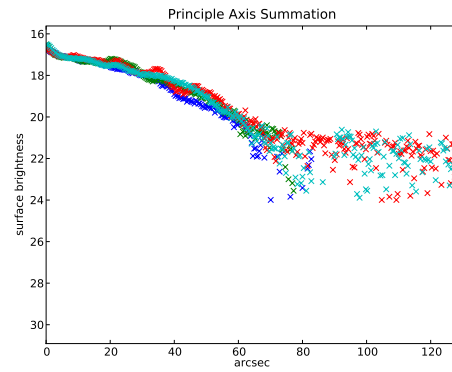
(a) r' band image



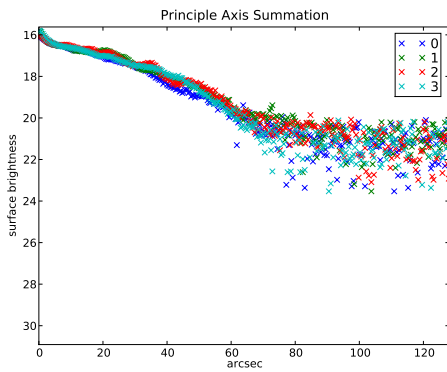
(b) low luminosity r' band image



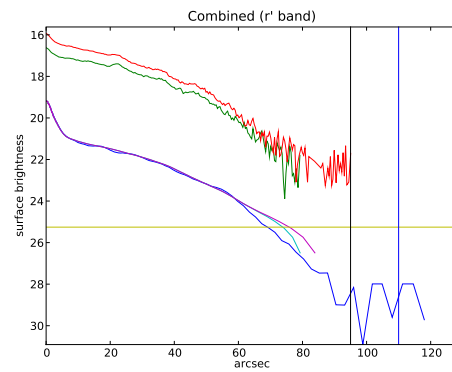
(c) Equivalent Profiles



(d) Axial Summation of 4 Quadrants

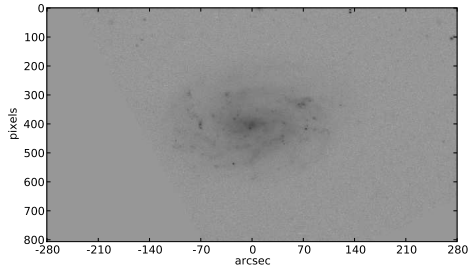


(e) Axial Summation of 4 Quadrants

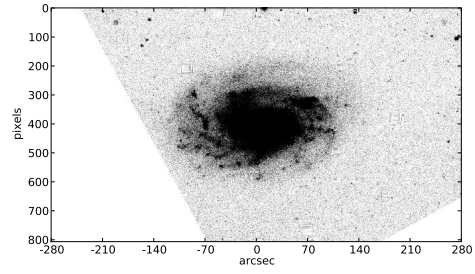


(f) Combined

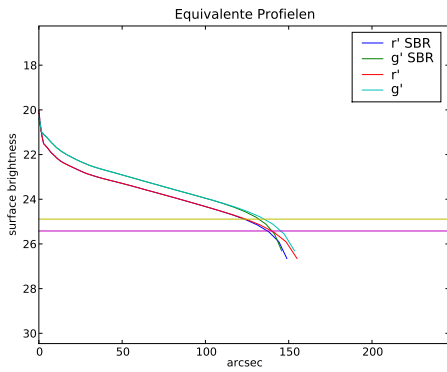
Figure A.39: *Galaxy NGC 4480* - Pohlen en Trujillo have classified this galaxy as Type II.o-CT. No truncation is seen below 80 arcseconds.



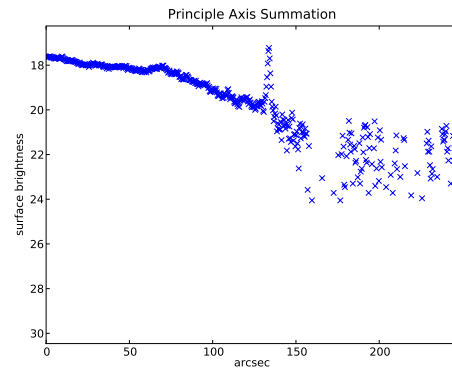
(a) r' band image



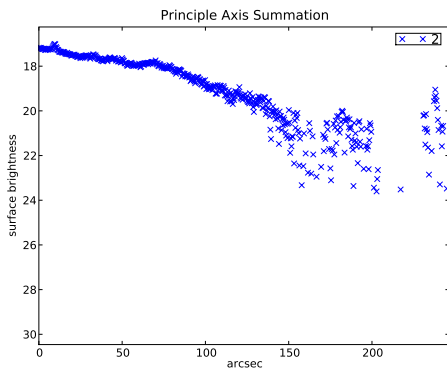
(b) low luminosity r' band image



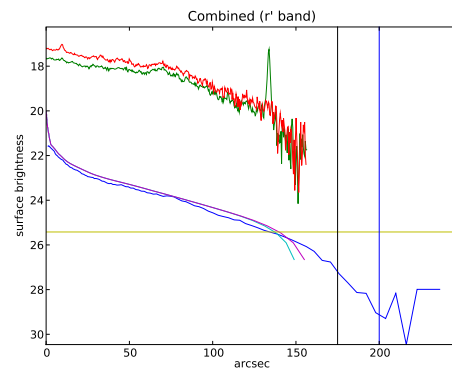
(c) Equivalent Profiles



(d) Axial Summation of 4 Quadrants

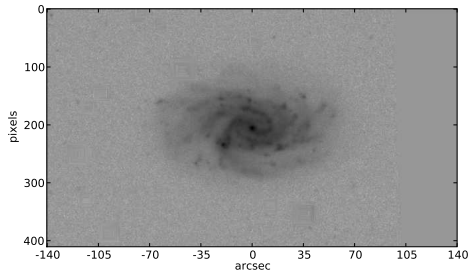


(e) Axial Summation of 4 Quadrants

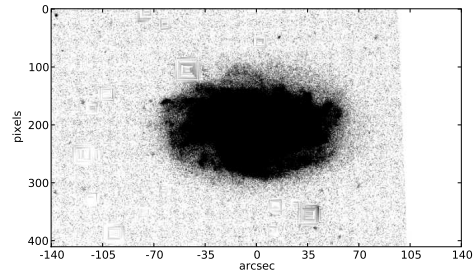


(f) Combined

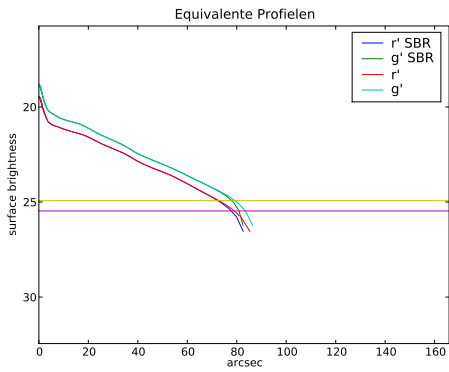
Figure A.40: *Galaxy NGC 4517A* - Pohlen en Trujillo have classified this galaxy as Type II.o-CT + II.o-AB. A truncation is seen at 150 arcseconds.



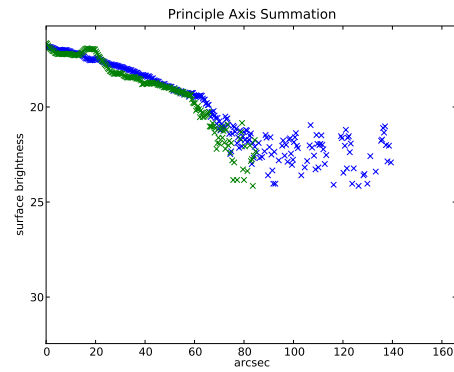
(a) r' band image



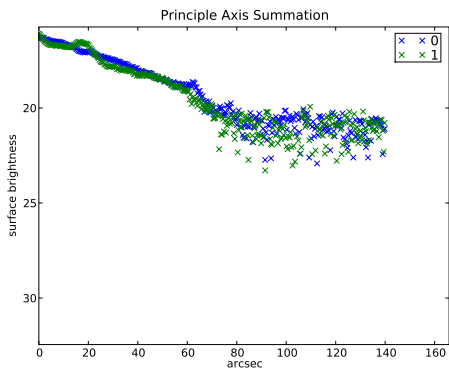
(b) low luminosity r' band image



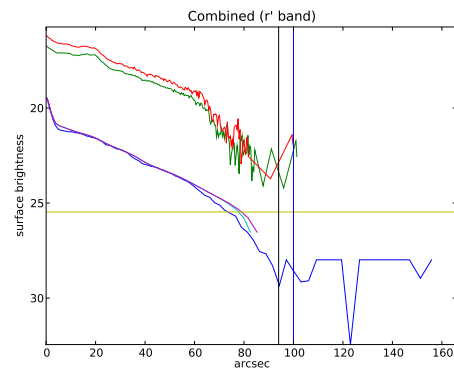
(c) Equivalent Profiles



(d) Axial Summation of 4 Quadrants

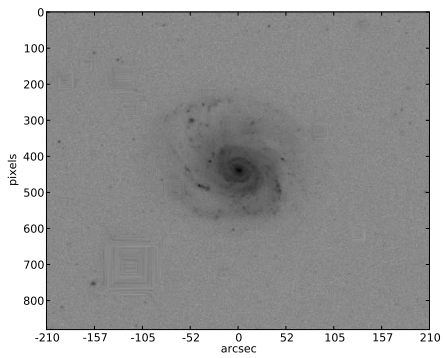


(e) Axial Summation of 4 Quadrants

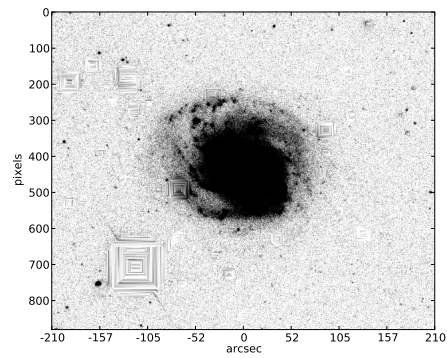


(f) Combined

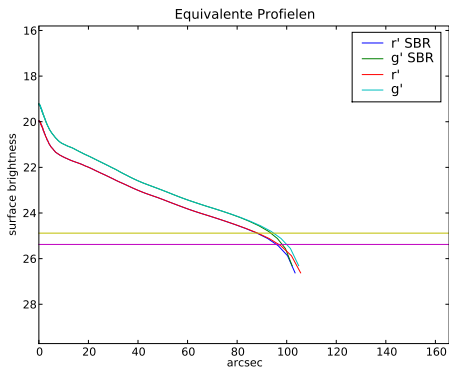
Figure A.41: *Galaxy NGC 4545* - Pohlen en Trujillo have classified this galaxy as Type II.o-CT. A possible truncation is seen at 80 arcseconds.



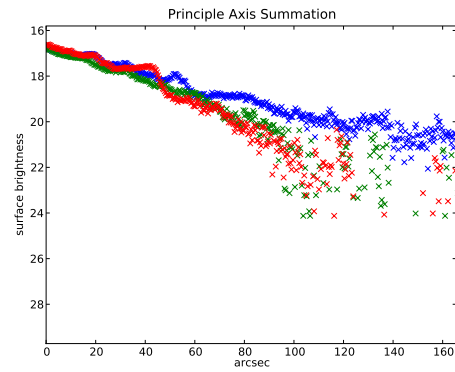
(a) r' band image



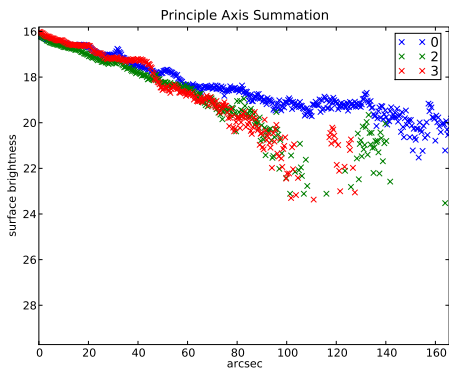
(b) low luminosity r' band image



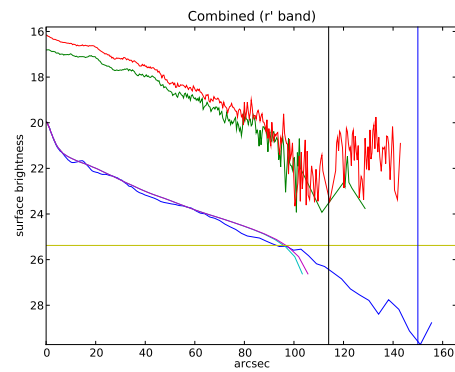
(c) Equivalent Profiles



(d) Axial Summation of 4 Quadrants

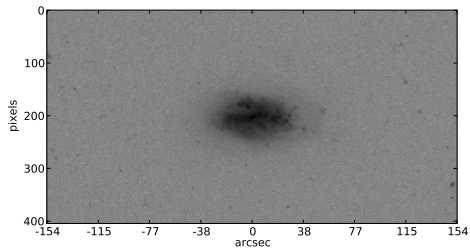


(e) Axial Summation of 4 Quadrants

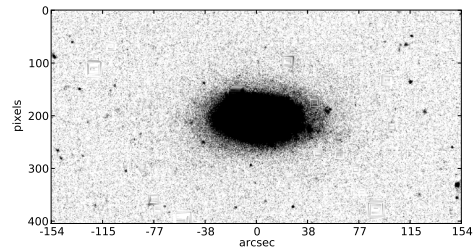


(f) Combined

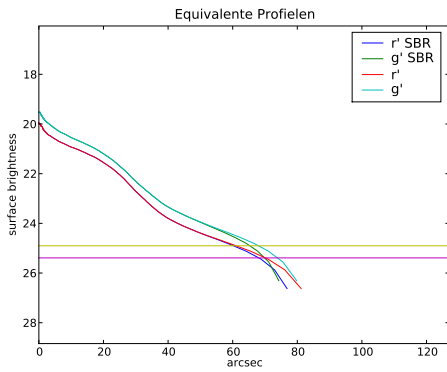
Figure A.42: *Galaxy NGC 4653* - Pohlen en Trujillo have classified this galaxy as Type II-AB. A truncation is seen at 100 arcseconds.



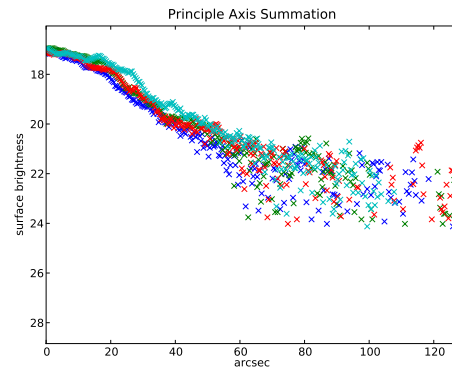
(a) r' band image



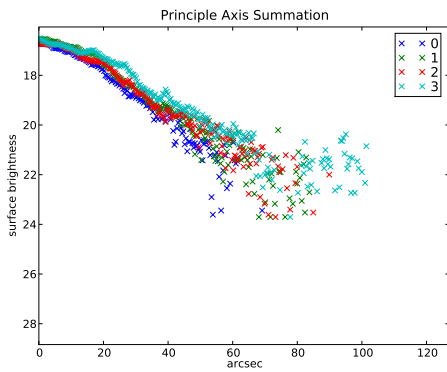
(b) low luminosity r' band image



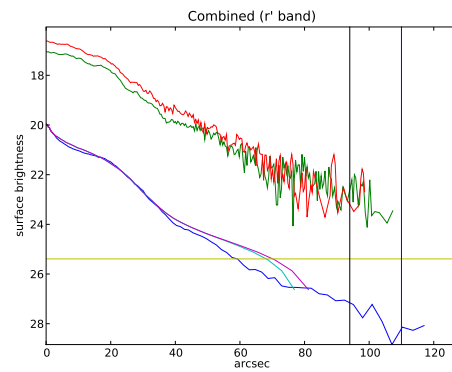
(c) Equivalent Profiles



(d) Axial Summation of 4 Quadrants

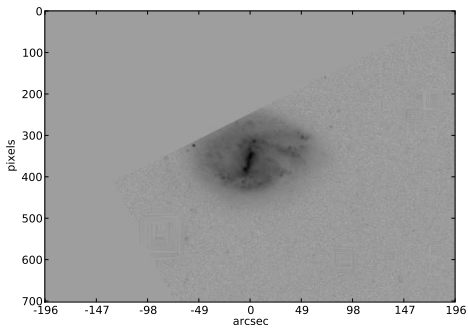


(e) Axial Summation of 4 Quadrants

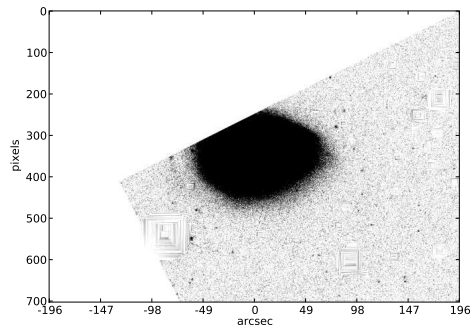


(f) Combined

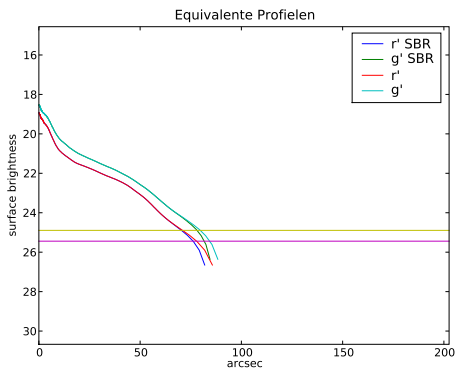
Figure A.43: *Galaxy NGC 4668* - Pohlen en Trujillo have classified this galaxy as Type III. No truncation is seen. The underlimit is set at 80 arcseconds.



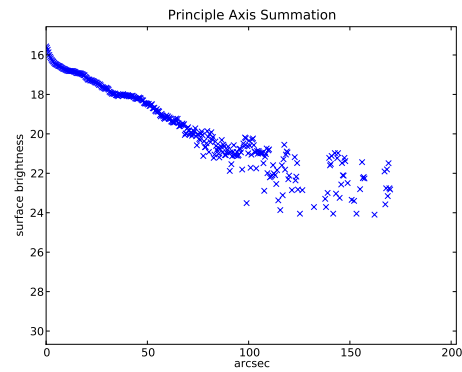
(a) r' band image



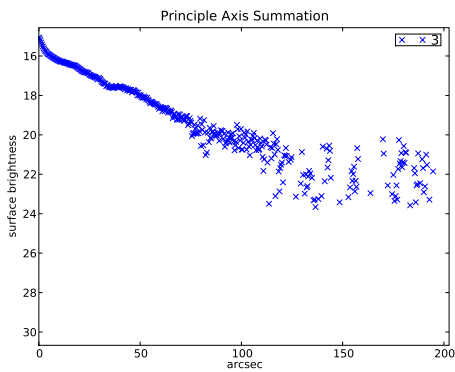
(b) low luminosity r' band image



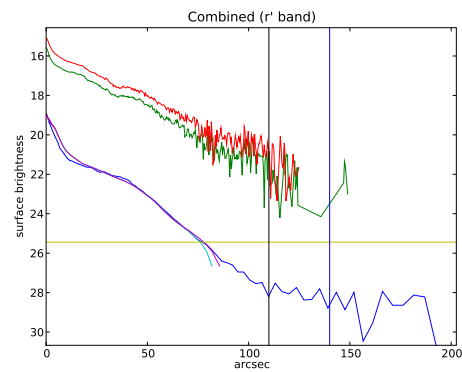
(c) Equivalent Profiles



(d) Axial Summation of 4 Quadrants

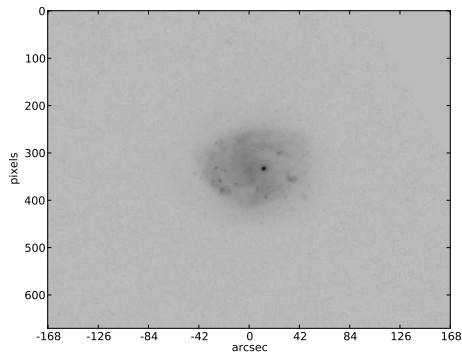


(e) Axial Summation of 4 Quadrants

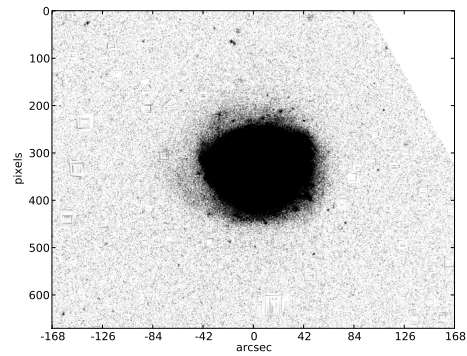


(f) Combined

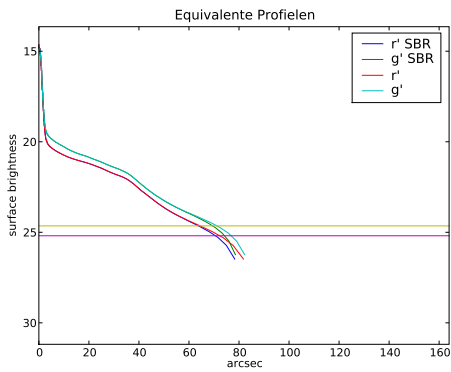
Figure A.44: *Galaxy NGC 4904* - Pohlen en Trujillo have classified this galaxy as Type II.o-OLR + III. A possible truncation at 120 arcseconds. This might also stem from the observed asymmetry.



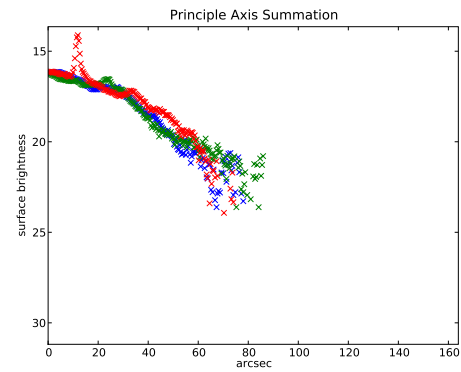
(a) r' band image



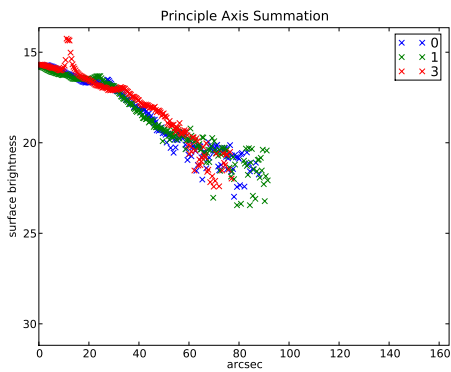
(b) low luminosity r' band image



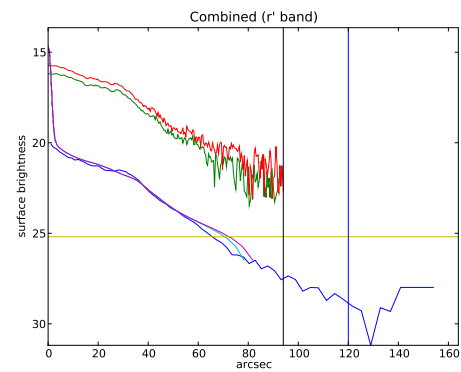
(c) Equivalent Profiles



(d) Axial Summation of 4 Quadrants

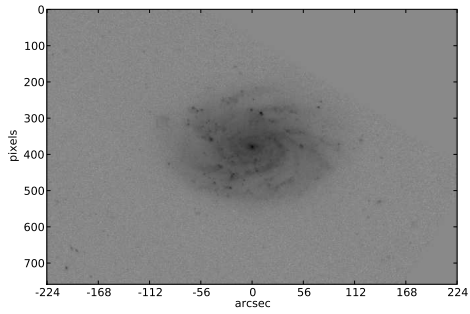


(e) Axial Summation of 4 Quadrants

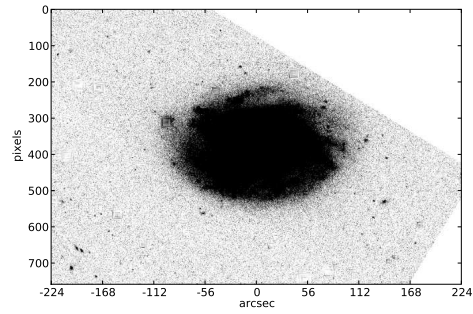


(f) Combined

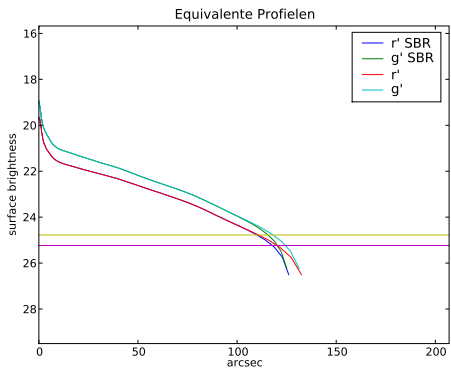
Figure A.45: *Galaxy NGC 5147* - Pohlen en Trujillo have classified this galaxy as Type II.o-OLR + III. No truncation is seen and the underlimit is set at 90 arcseconds. Again the type III classification in relation with an asymmetric galaxy.



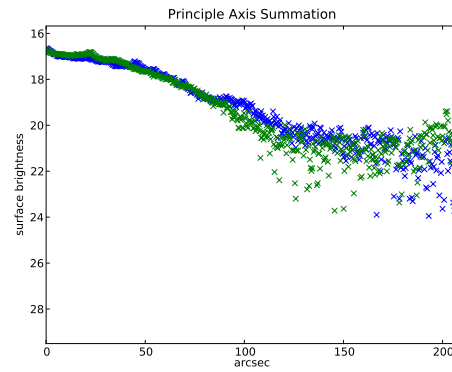
(a) r' band image



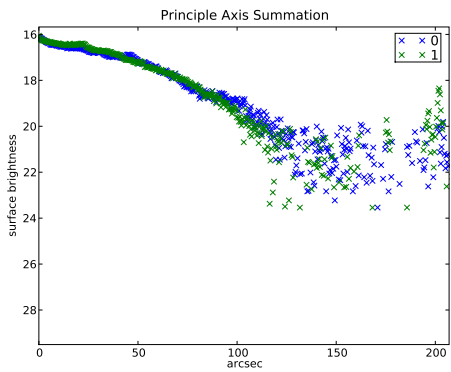
(b) low luminosity r' band image



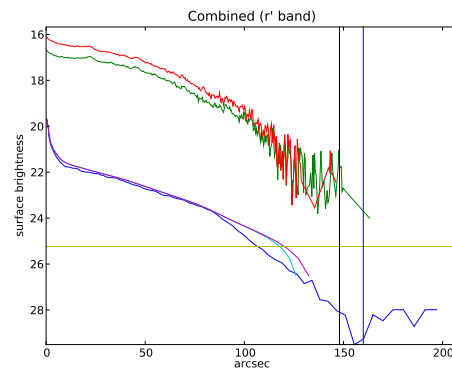
(c) Equivalent Profiles



(d) Axial Summation of 4 Quadrants

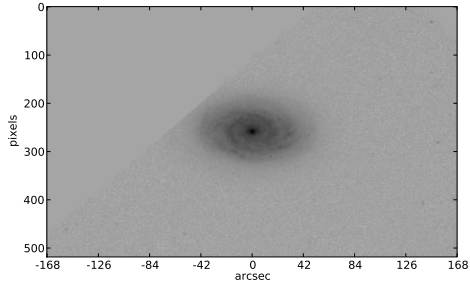


(e) Axial Summation of 4 Quadrants

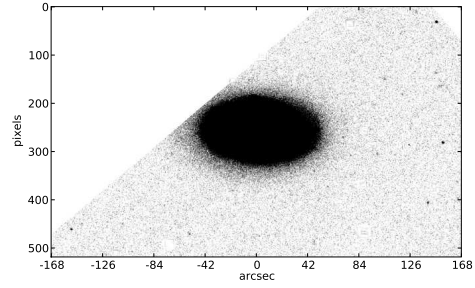


(f) Combined

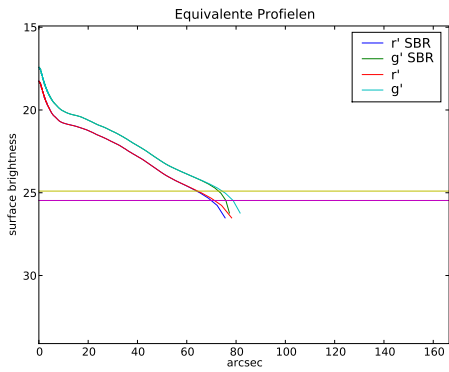
Figure A.46: *Galaxy NGC 5300* - Pohlen en Trujillo have classified this galaxy as Type II.o-CT. A truncation is seen at 140 arcseconds.



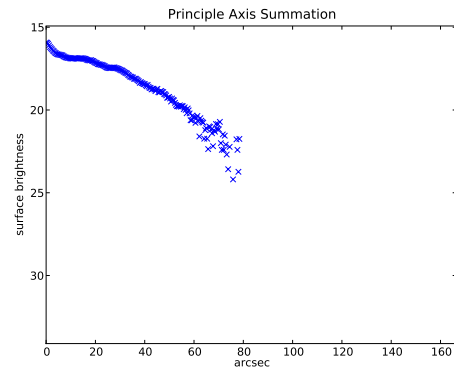
(a) r' band image



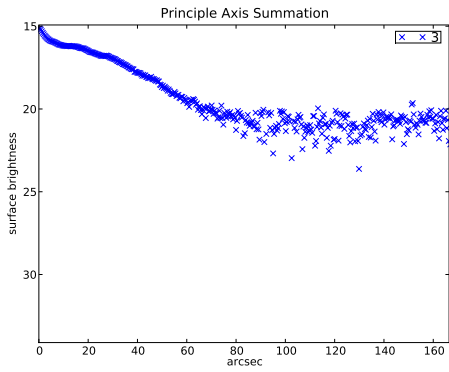
(b) low luminosity r' band image



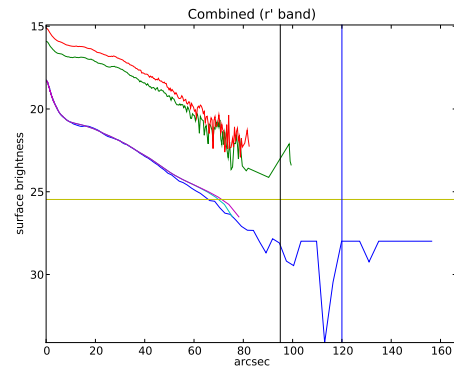
(c) Equivalent Profiles



(d) Axial Summation of 4 Quadrants

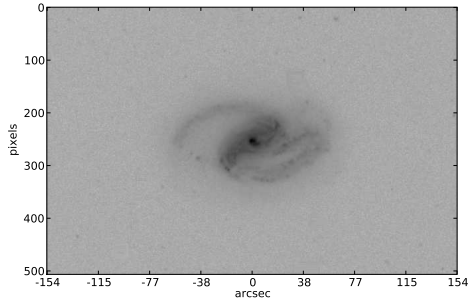


(e) Axial Summation of 4 Quadrants

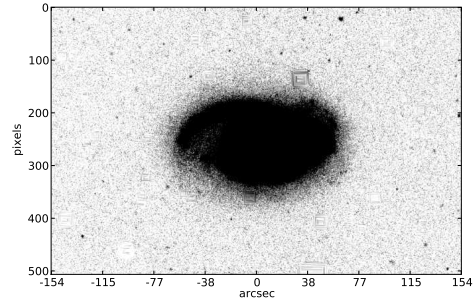


(f) Combined

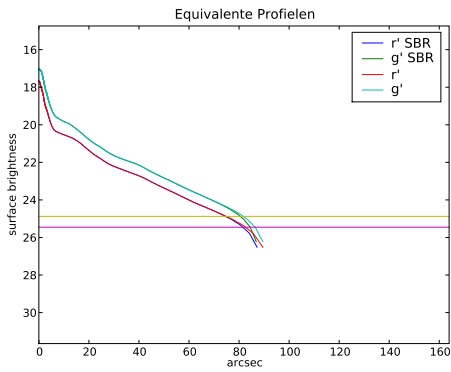
Figure A.47: *Galaxy NGC 5376* - Pohlen en Trujillo have classified this galaxy as Type II.o-OLR. No truncation is seen and the underlimit is set at 80 arcseconds.



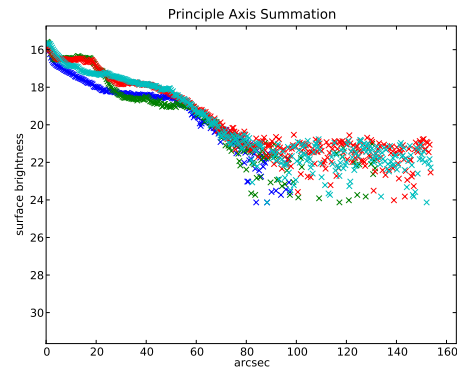
(a) r' band image



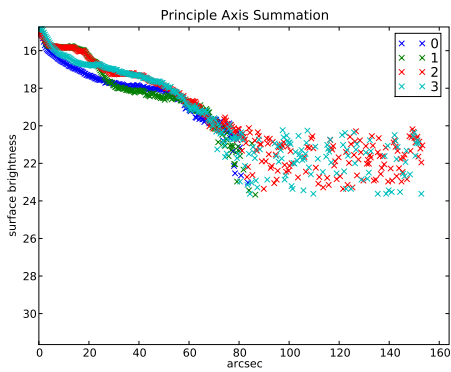
(b) low luminosity r' band image



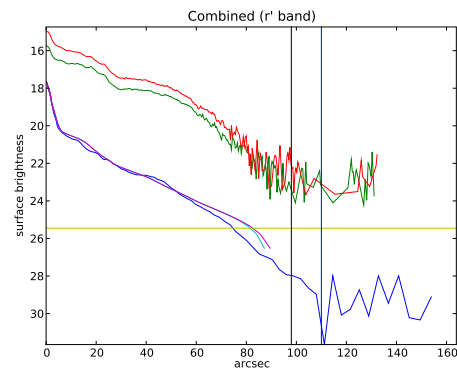
(c) Equivalent Profiles



(d) Axial Summation of 4 Quadrants

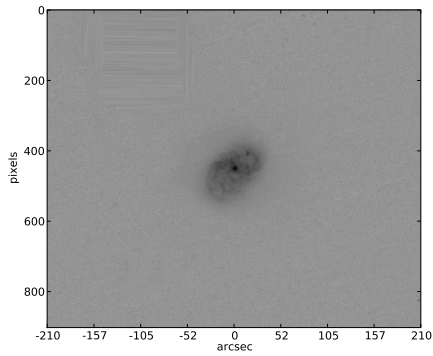


(e) Axial Summation of 4 Quadrants

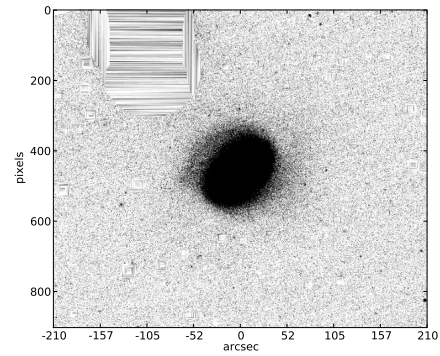


(f) Combined

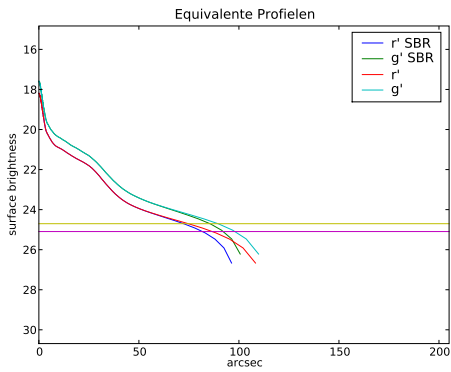
Figure A.48: *Galaxy NGC 5430* - Pohlen en Trujillo have classified this galaxy as Type II.o-OLR. A possible truncation is seen at 90 arcseconds.



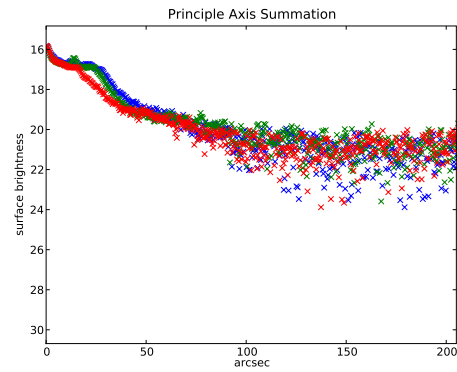
(a) r' band image



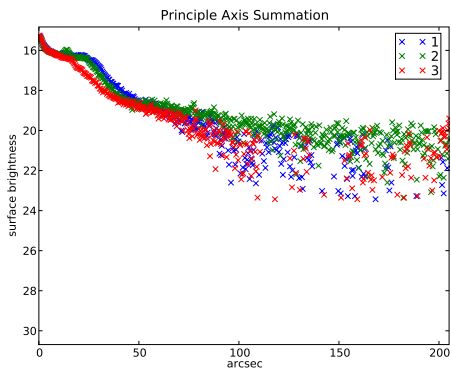
(b) low luminosity r' band image



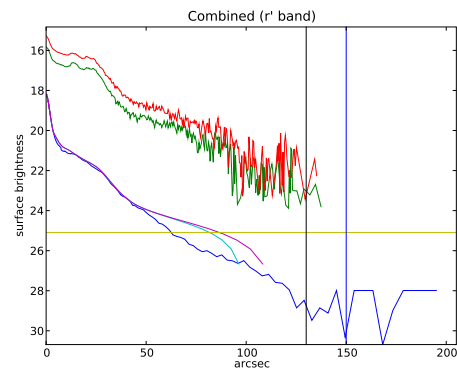
(c) Equivalent Profiles



(d) Axial Summation of 4 Quadrants

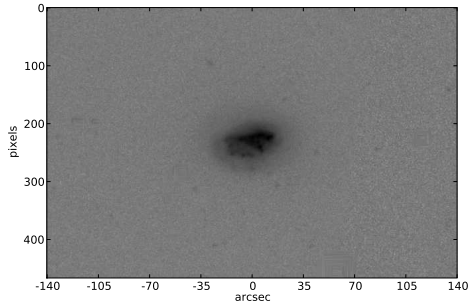


(e) Axial Summation of 4 Quadrants

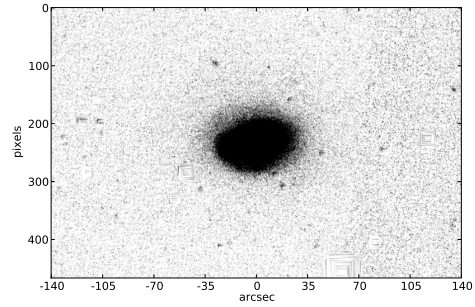


(f) Combined

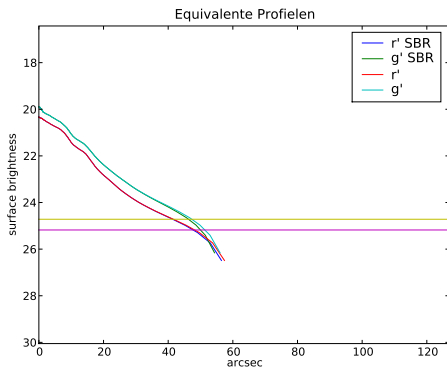
Figure A.49: *Galaxy NGC 5480* - Pohlen en Trujillo have classified this galaxy as Type III-d. The underlimit is set at 130 arcseconds as no truncation is seen.



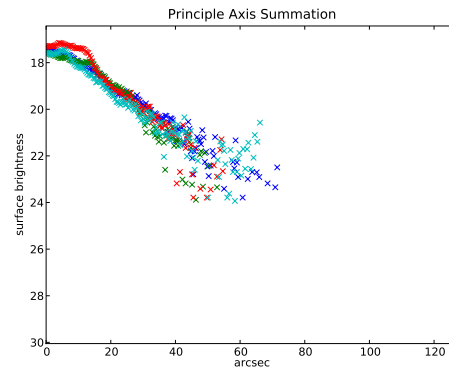
(a) r' band image



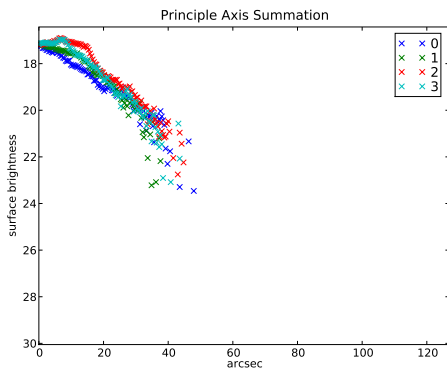
(b) low luminosity r' band image



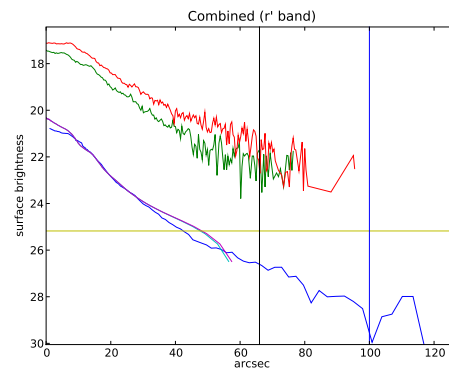
(c) Equivalent Profiles



(d) Axial Summation of 4 Quadrants

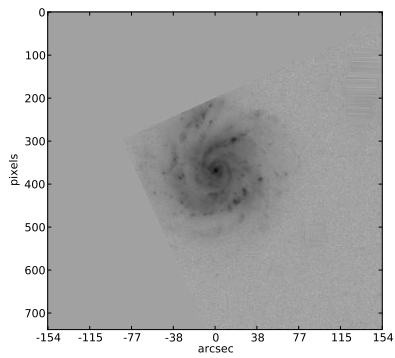


(e) Axial Summation of 4 Quadrants

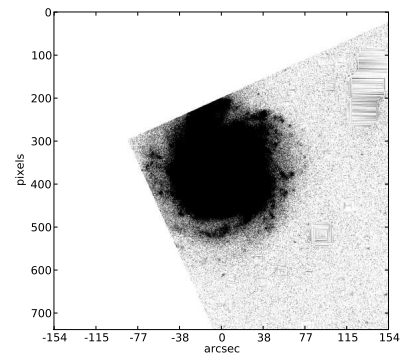


(f) Combined

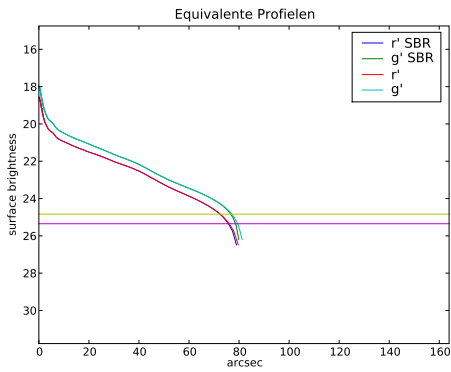
Figure A.50: *Galaxy NGC 5624* - Pohlen en Trujillo have classified this galaxy as Type III. No truncation is seen and the underlimit is set at 70 arcseconds.



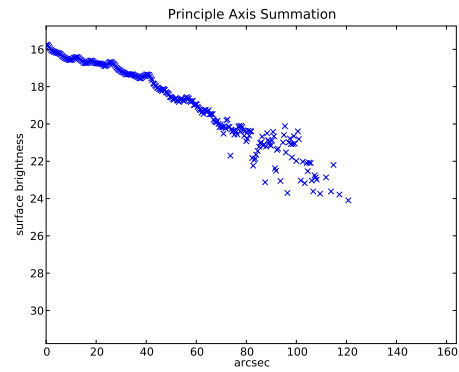
(a) r' band image



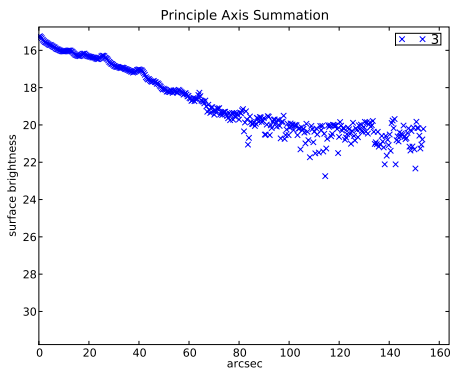
(b) low luminosity r' band image



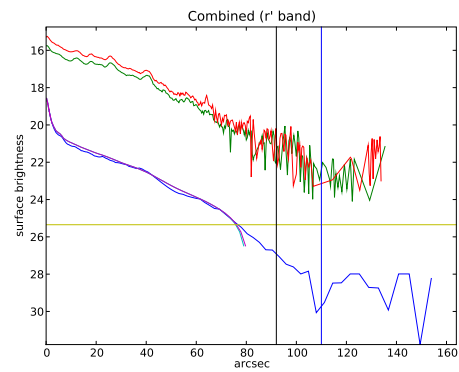
(c) Equivalent Profiles



(d) Axial Summation of 4 Quadrants

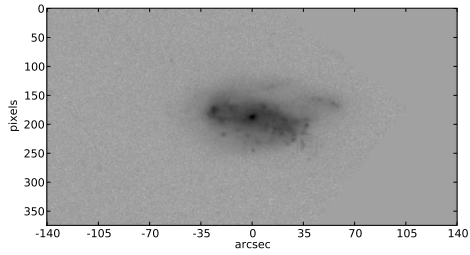


(e) Axial Summation of 4 Quadrants

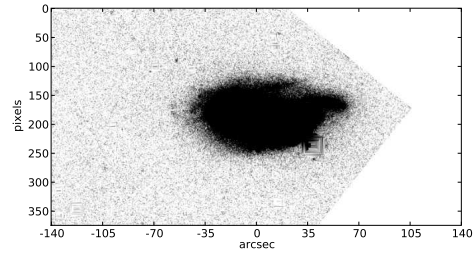


(f) Combined

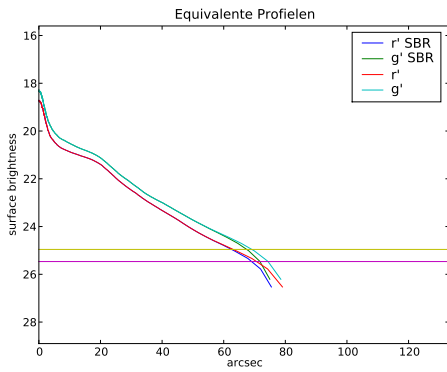
Figure A.51: *Galaxy NGC 5660* - Pohlen en Trujillo have classified this galaxy as Type II-CT. A truncation is seen at 100 arcseconds.



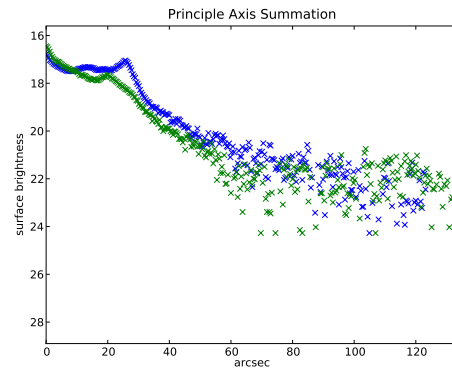
(a) r' band image



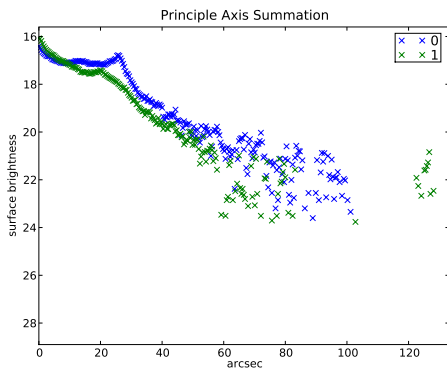
(b) low luminosity r' band image



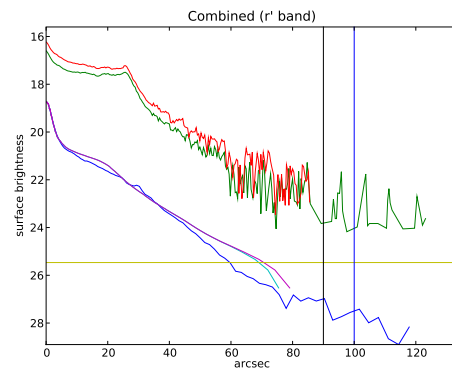
(c) Equivalent Profiles



(d) Axial Summation of 4 Quadrants

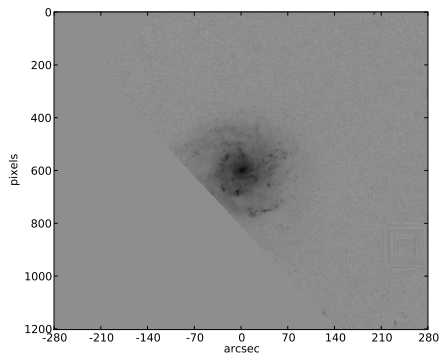


(e) Axial Summation of 4 Quadrants

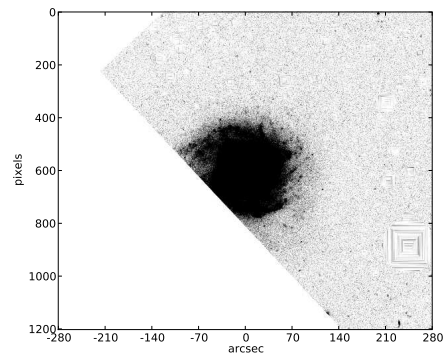


(f) Combined

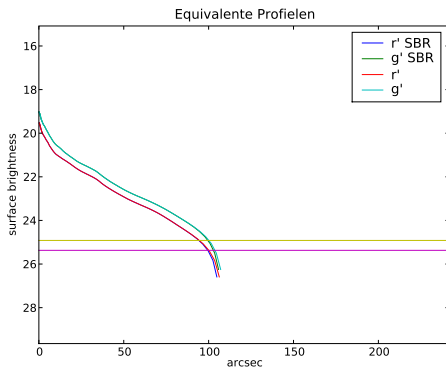
Figure A.52: *Galaxy NGC 5667* - Pohlen en Trujillo have classified this galaxy as Type II.i + III. A truncation is seen at 80 arcseconds.



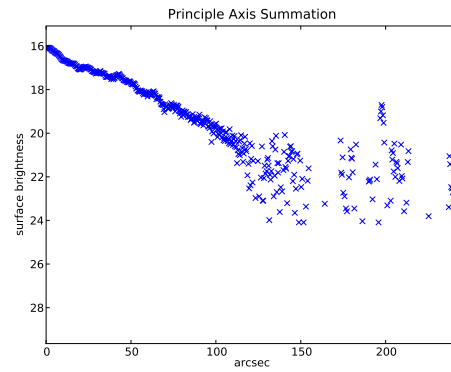
(a) r' band image



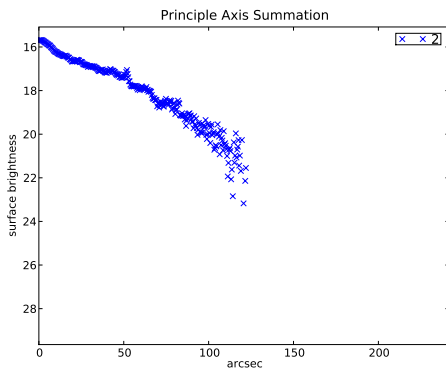
(b) low luminosity r' band image



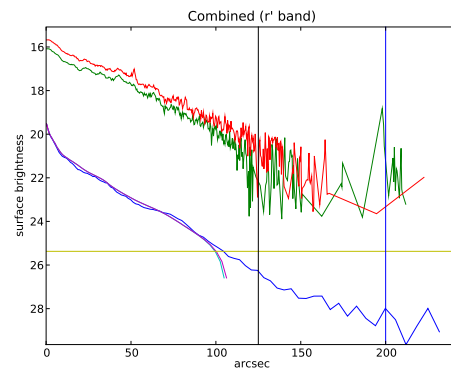
(c) Equivalent Profiles



(d) Axial Summation of 4 Quadrants

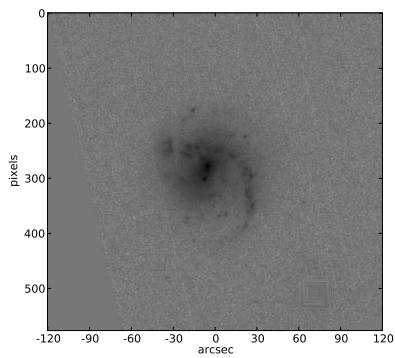


(e) Axial Summation of 4 Quadrants

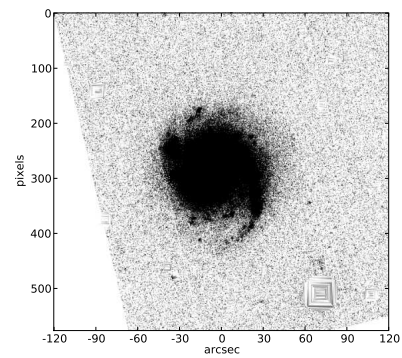


(f) Combined

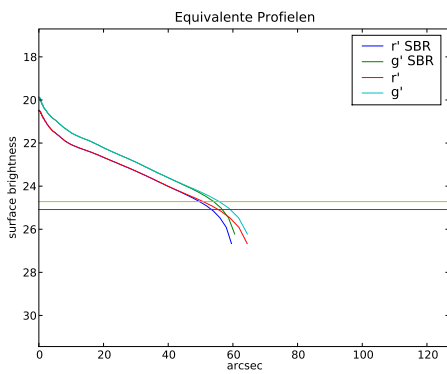
Figure A.53: *Galaxy NGC 5668* - Pohlen en Trujillo have classified this galaxy as Type I. No truncation is seen and the underlimit is placed at 130 arcseconds.



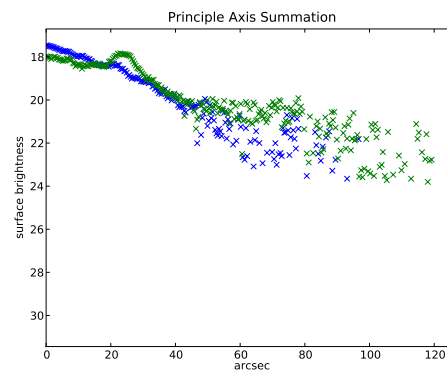
(a) r' band image



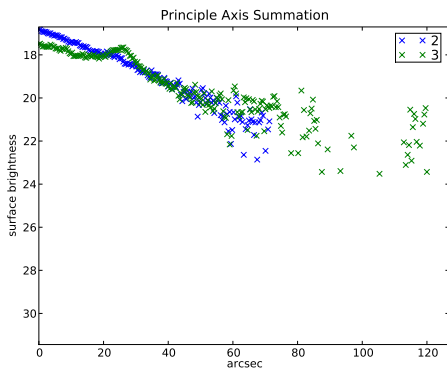
(b) low luminosity r' band image



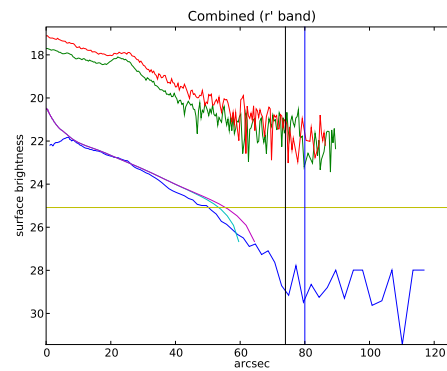
(c) Equivalent Profiles



(d) Axial Summation of 4 Quadrants

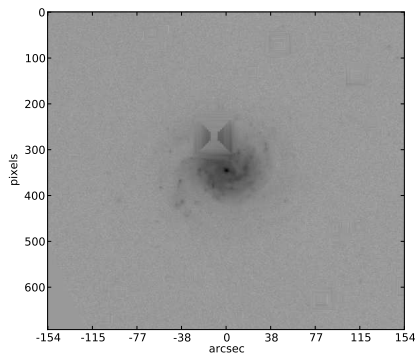


(e) Axial Summation of 4 Quadrants

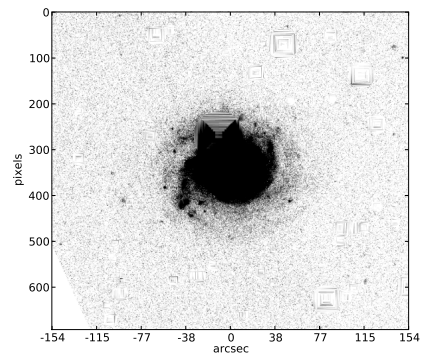


(f) Combined

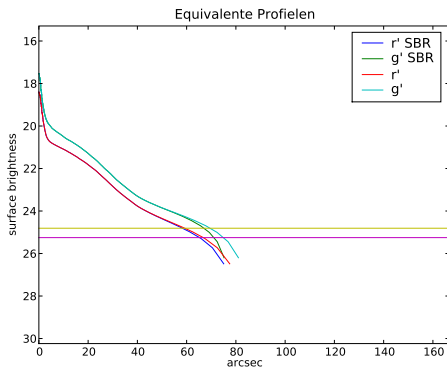
Figure A.54: *Galaxy NGC 5693* - Pohlen en Trujillo have classified this galaxy as Type II-AB. No truncation is seen and the truncation underlimit is set at 50 arcseconds.



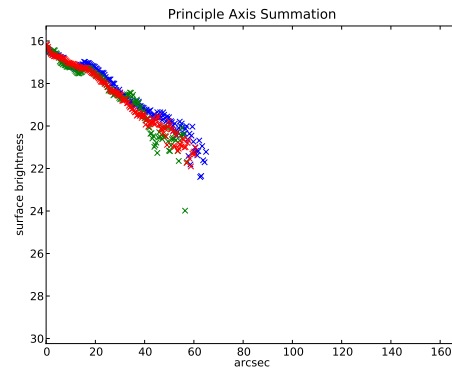
(a) r' band image



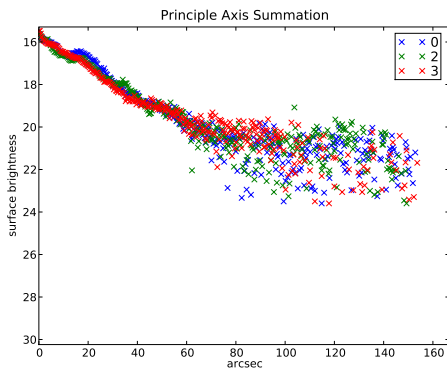
(b) low luminosity r' band image



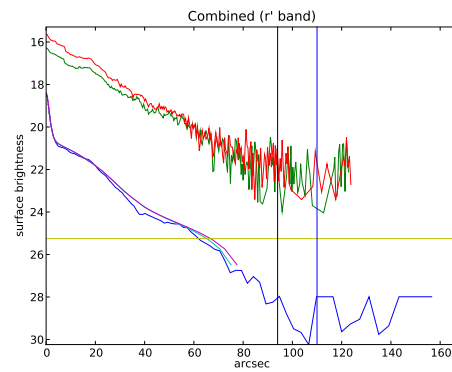
(c) Equivalent Profiles



(d) Axial Summation of 4 Quadrants

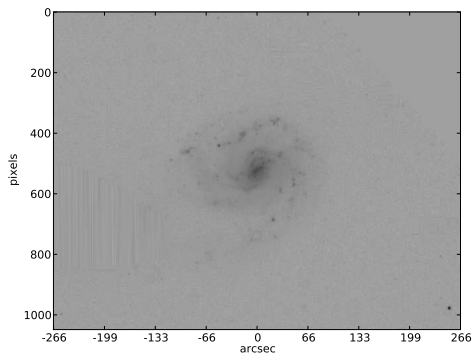


(e) Axial Summation of 4 Quadrants

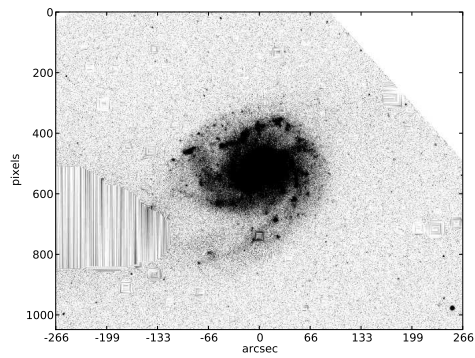


(f) Combined

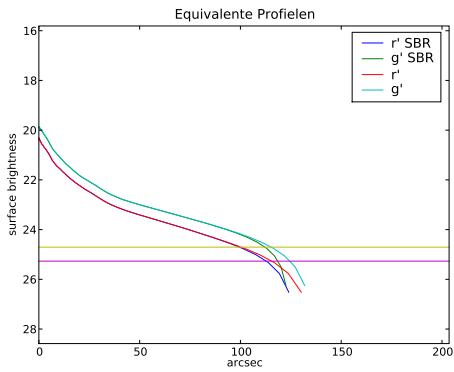
Figure A.55: *Galaxy NGC 5768* - Pohlen en Trujillo have classified this galaxy as Type I. No truncation is seen and the underlimit is set at 90 arcseconds.



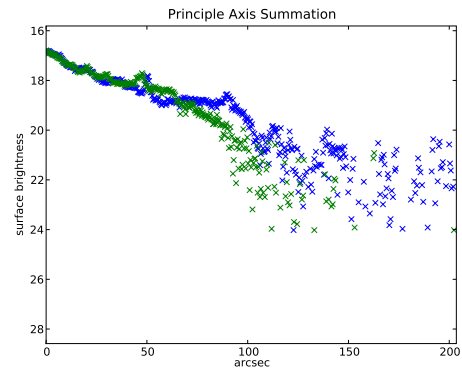
(a) r' band image



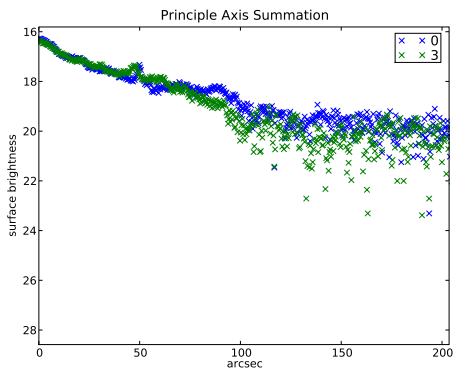
(b) low luminosity r' band image



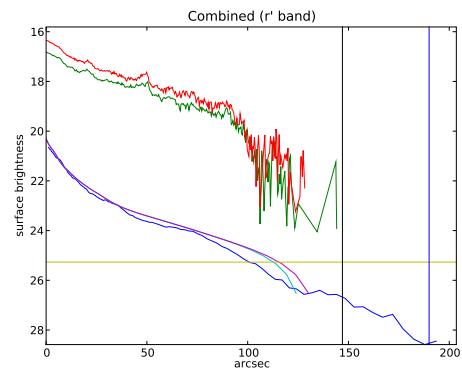
(c) Equivalent Profiles



(d) Axial Summation of 4 Quadrants

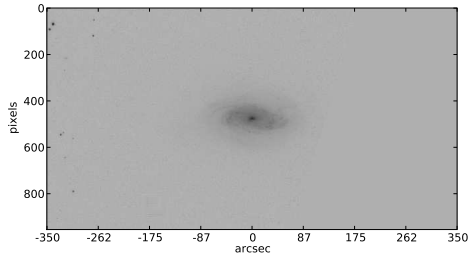


(e) Axial Summation of 4 Quadrants

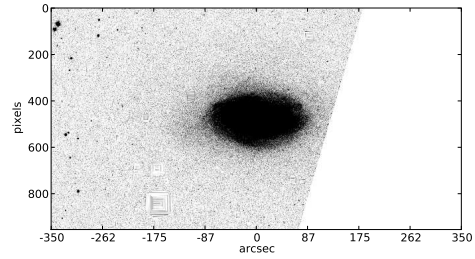


(f) Combined

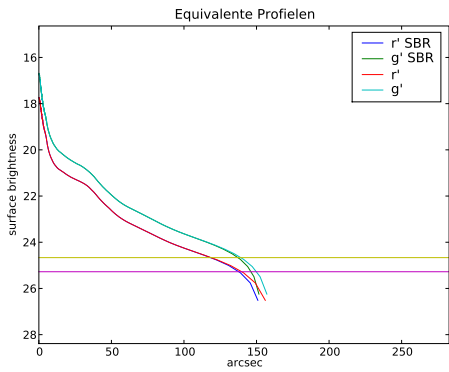
Figure A.56: *Galaxy NGC 5774* - Pohlen en Trujillo have classified this galaxy as Type II.o-OLR + III. A truncation is seen at 110 arcseconds.



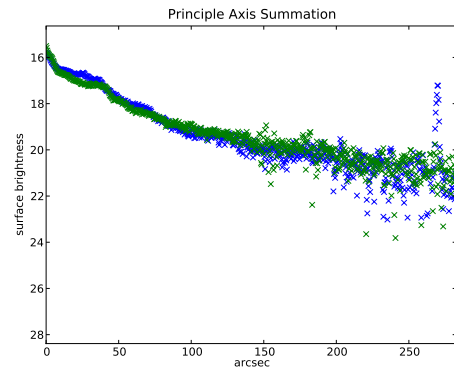
(a) r' band image



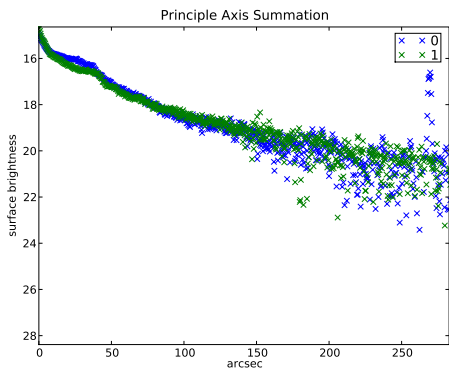
(b) low luminosity r' band image



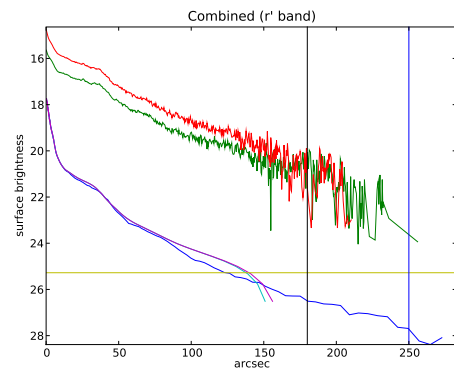
(c) Equivalent Profiles



(d) Axial Summation of 4 Quadrants

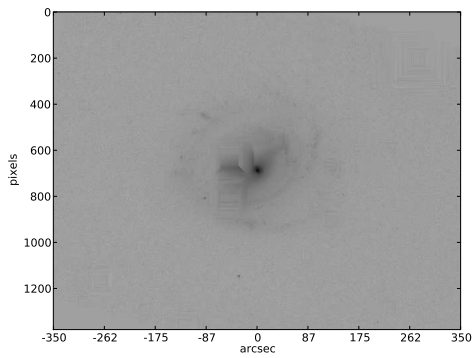


(e) Axial Summation of 4 Quadrants

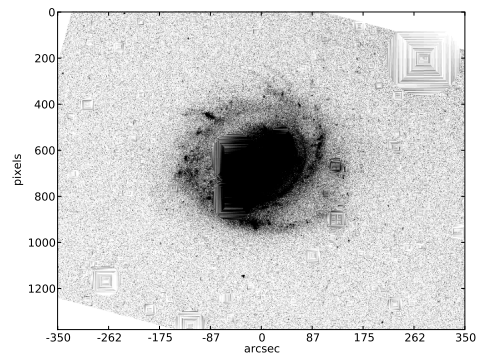


(f) Combined

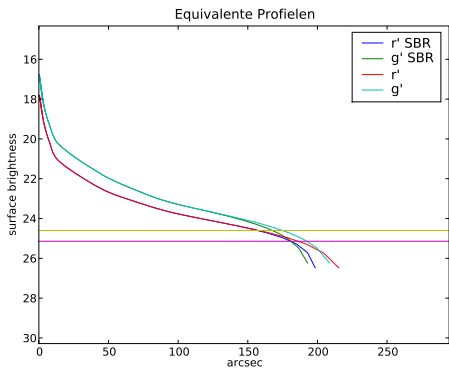
Figure A.57: *Galaxy NGC 5806* - Pohlen en Trujillo have classified this galaxy as Type III. No truncation is seen. The underlimit is set at 180 arcseconds.



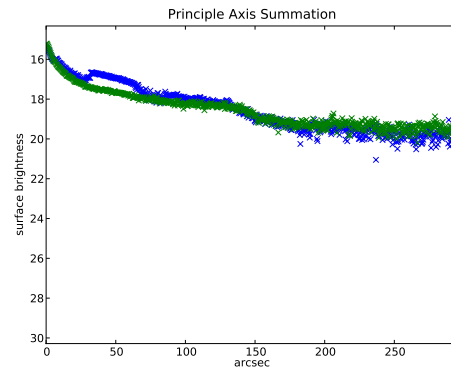
(a) r' band image



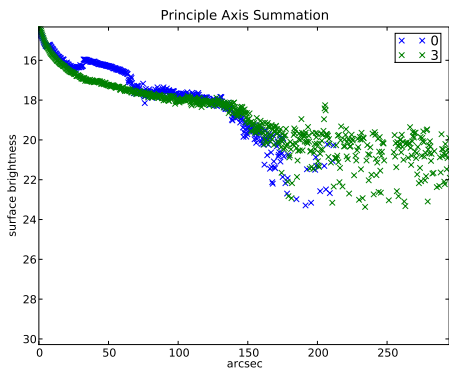
(b) low luminosity r' band image



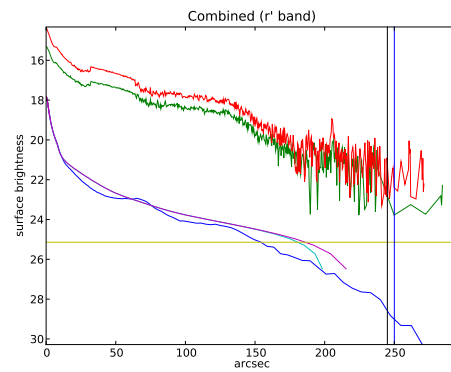
(c) Equivalent Profiles



(d) Axial Summation of 4 Quadrants

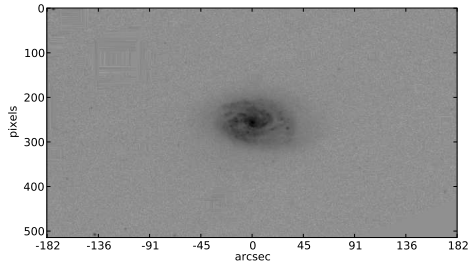


(e) Axial Summation of 4 Quadrants

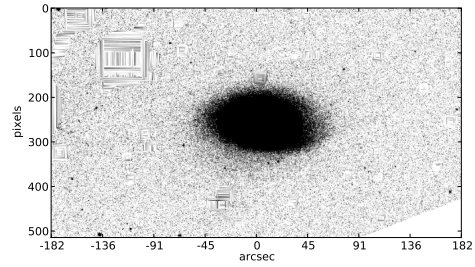


(f) Combined

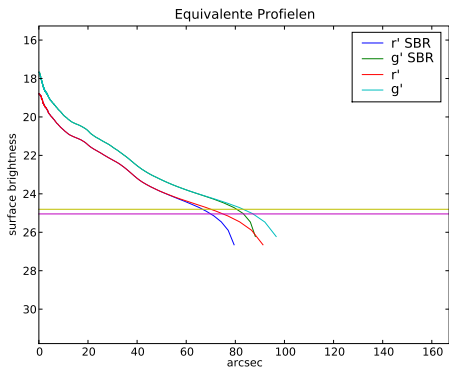
Figure A.58: *Galaxy NGC 5850* - Pohlen en Trujillo have classified this galaxy as Type II.o-OLR. A possible truncation is seen at 180 arcseconds.



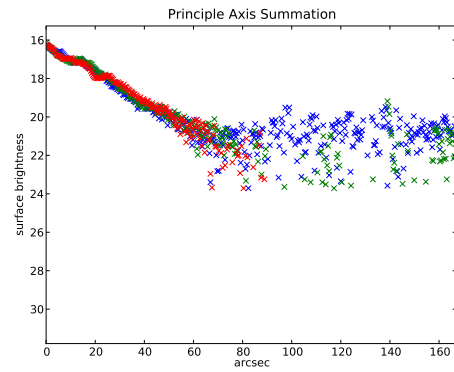
(a) r' band image



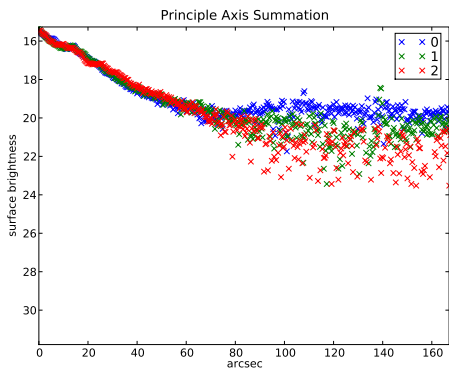
(b) low luminosity r' band image



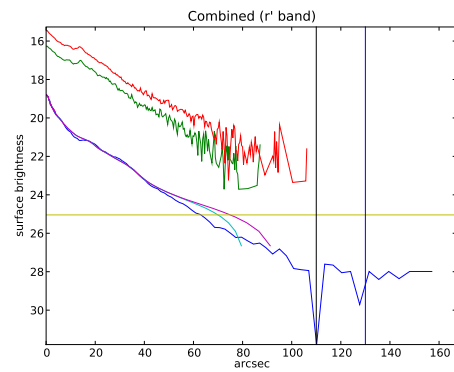
(c) Equivalent Profiles



(d) Axial Summation of 4 Quadrants

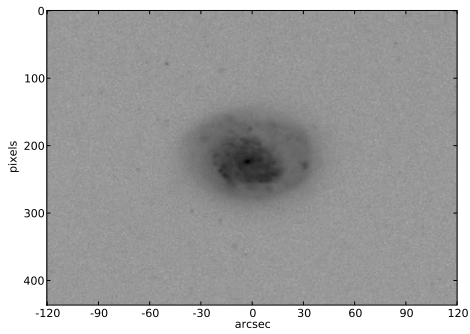


(e) Axial Summation of 4 Quadrants

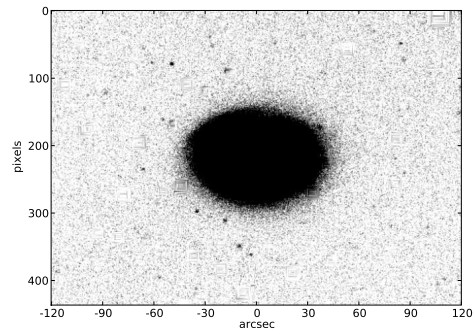


(f) Combined

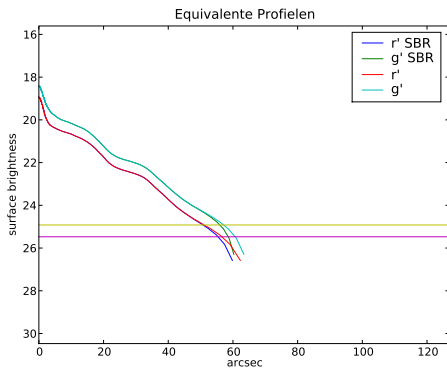
Figure A.59: *Galaxy NGC 5937* - Pohlen en Trujillo have classified this galaxy as Type III. No signs of a truncation. The underlimit is set at 80 arcseconds.



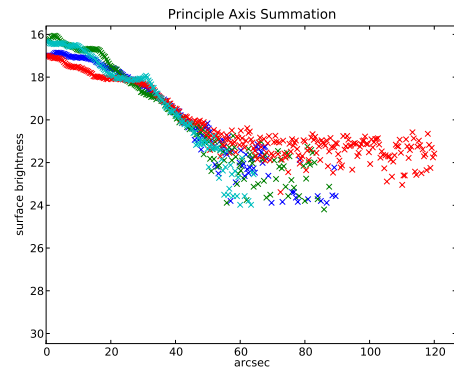
(a) r' band image



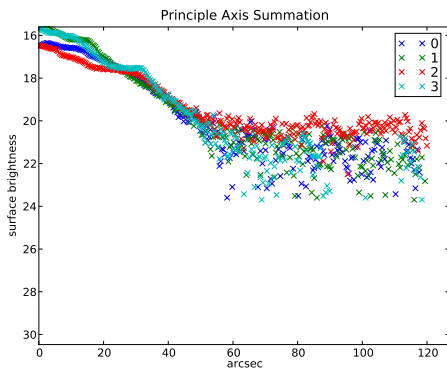
(b) low luminosity r' band image



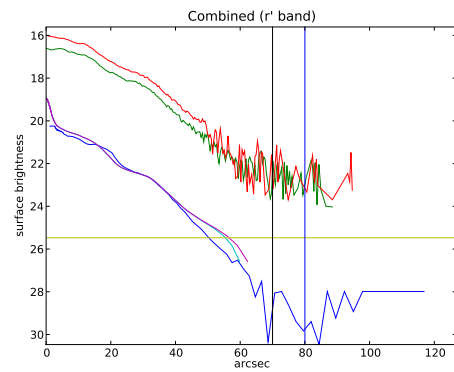
(c) Equivalent Profiles



(d) Axial Summation of 4 Quadrants

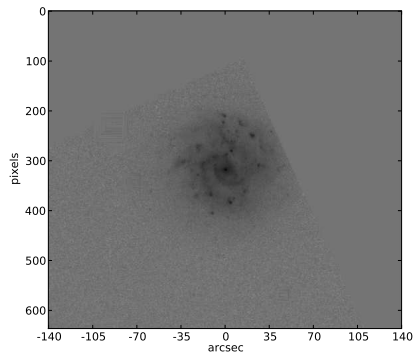


(e) Axial Summation of 4 Quadrants

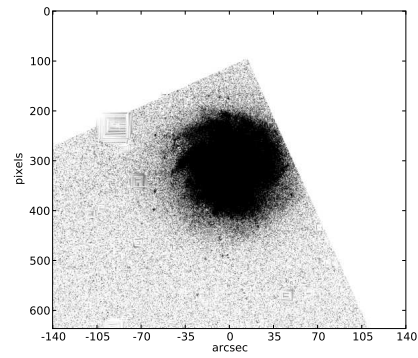


(f) Combined

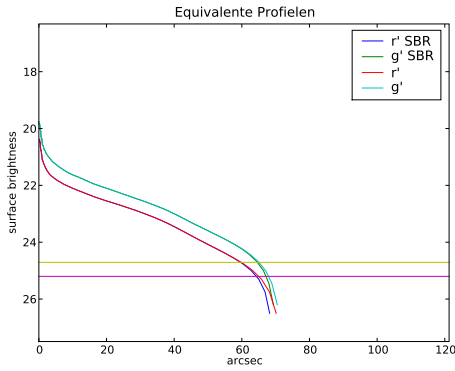
Figure A.60: *Galaxy NGC 6155* - Pohlen en Trujillo have classified this galaxy as Type II-AB. No truncation is seen. The underlimit is set at 70 arcseconds.



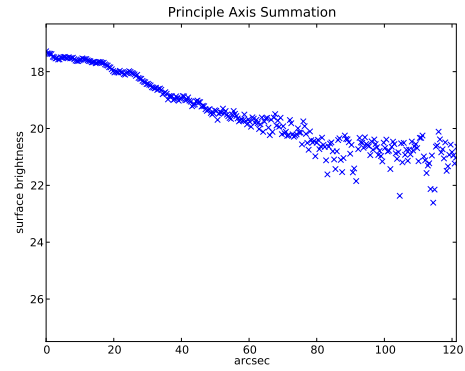
(a) r' band image



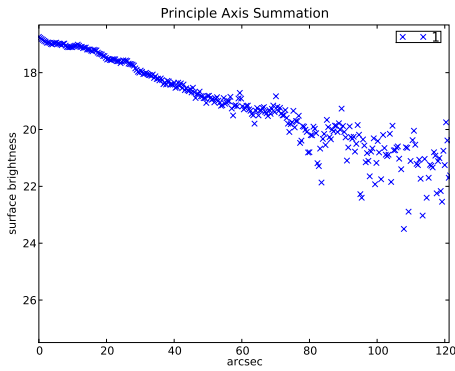
(b) low luminosity r' band image



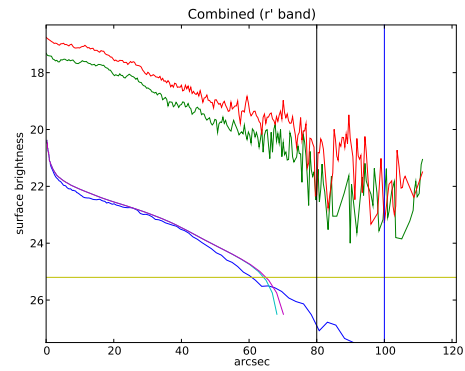
(c) Equivalent Profiles



(d) Axial Summation of 4 Quadrants

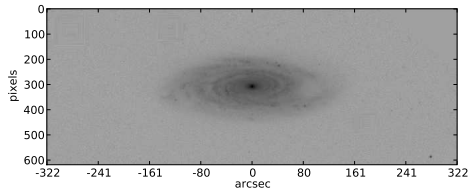


(e) Axial Summation of 4 Quadrants

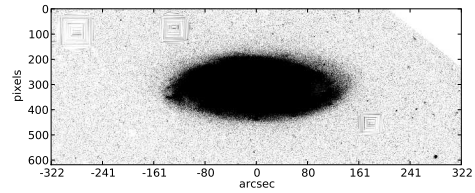


(f) Combined

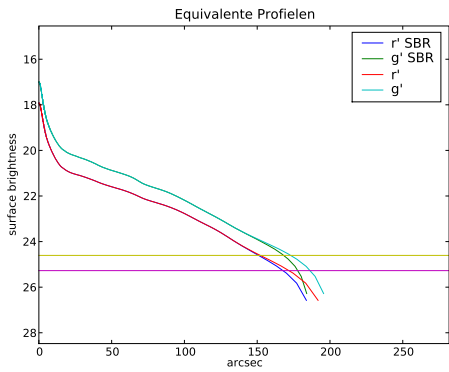
Figure A.61: *Galaxy NGC 7437* - Pohlen en Trujillo have classified this galaxy as Type II-CT. Only one quadrant can be used in the classification. No evidence is seen for a truncation and the underlimit is set at 80 arcseconds.



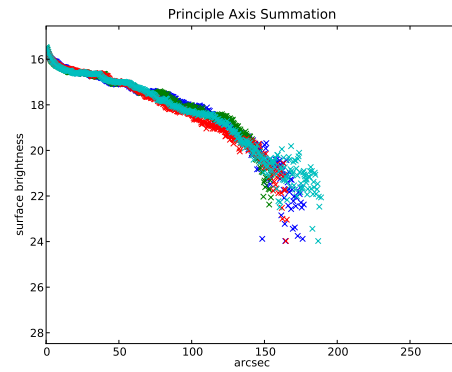
(a) r' band image



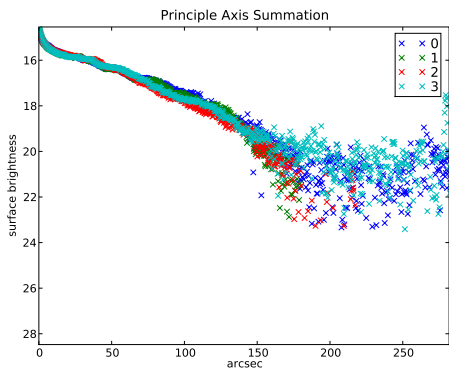
(b) low luminosity r' band image



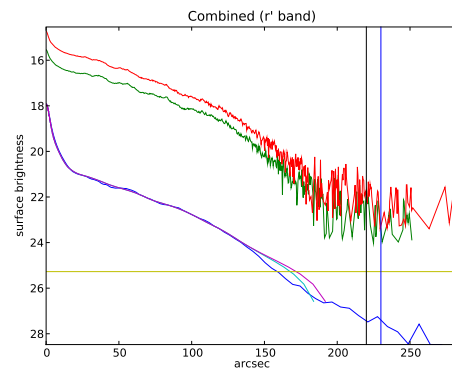
(c) Equivalent Profiles



(d) Axial Summation of 4 Quadrants

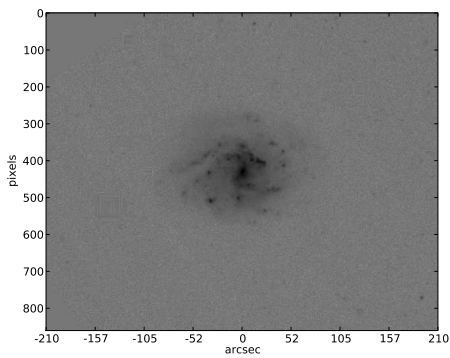


(e) Axial Summation of 4 Quadrants

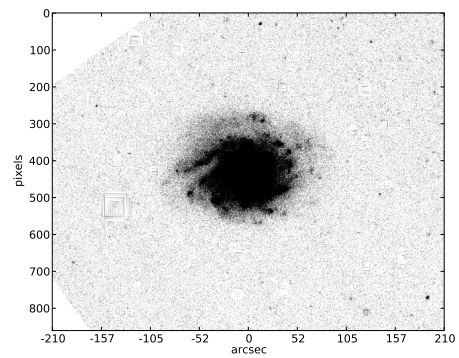


(f) Combined

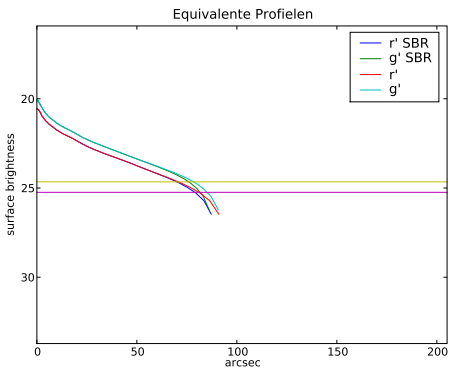
Figure A.62: *Galaxy NGC 7606* - Pohlen en Trujillo have classified this galaxy as Type II-CT. A huge galaxy with a possible truncation at 180 arcseconds.



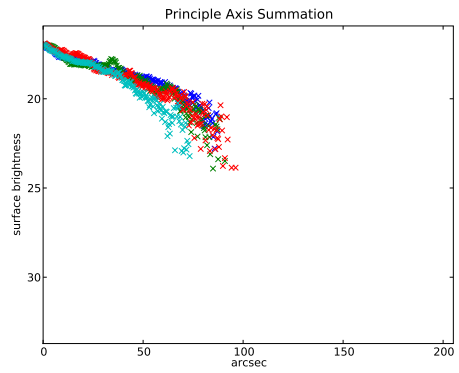
(a) r' band image



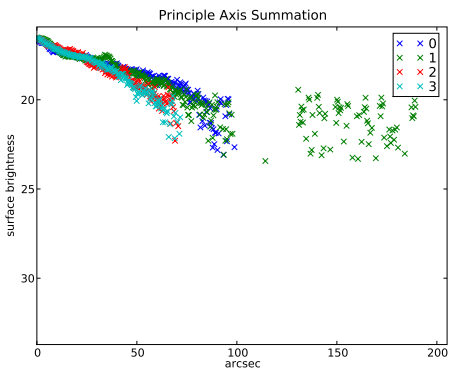
(b) low luminosity r' band image



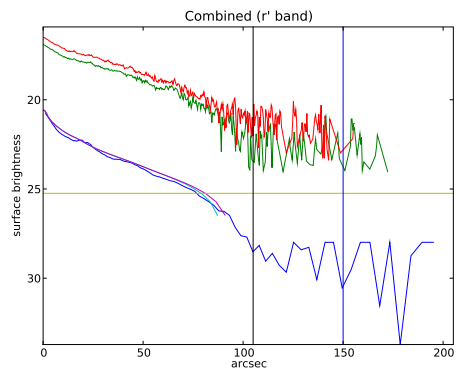
(c) Equivalent Profiles



(d) Axial Summation of 4 Quadrants

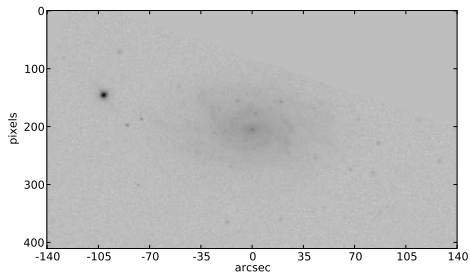


(e) Axial Summation of 4 Quadrants

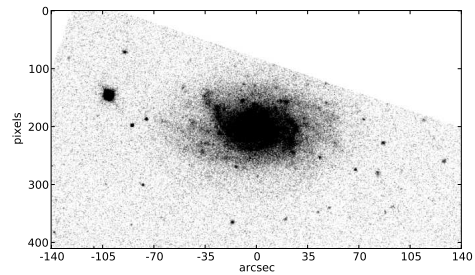


(f) Combined

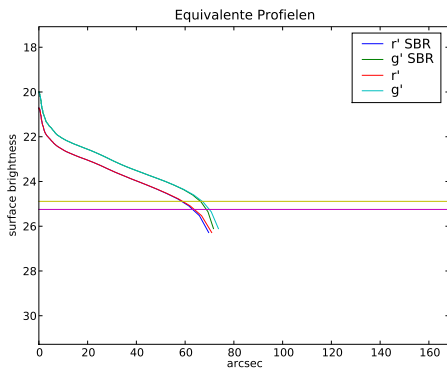
Figure A.63: *Galaxy PGC 006667* - Pohlen en Trujillo have classified this galaxy as Type II-AB. No truncation is seen and the galaxy underlimit is set at 100 arcseconds.



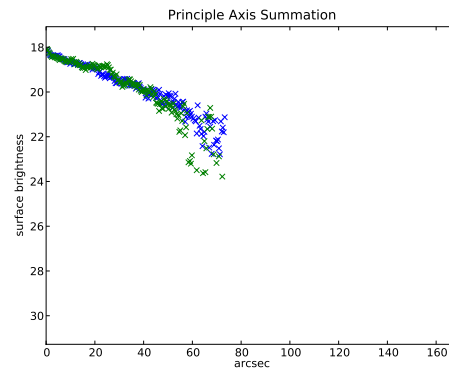
(a) r' band image



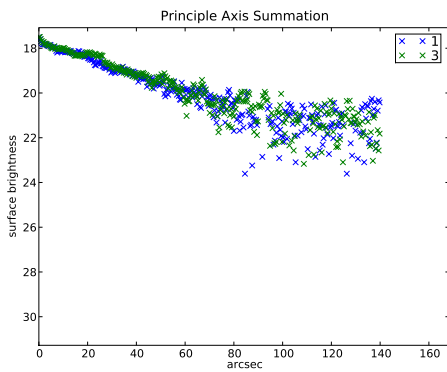
(b) low luminosity r' band image



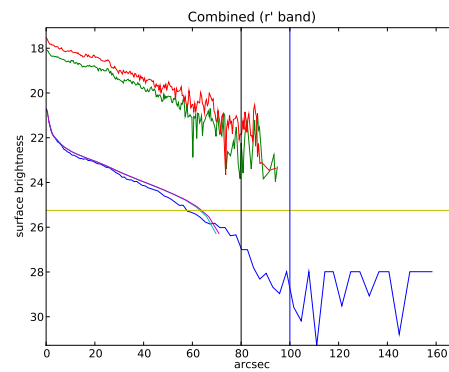
(c) Equivalent Profiles



(d) Axial Summation of 4 Quadrants

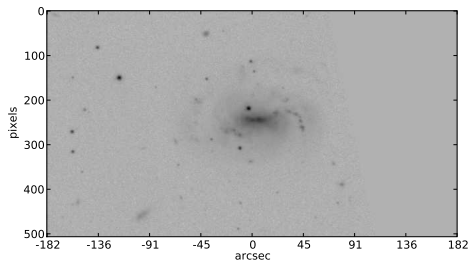


(e) Axial Summation of 4 Quadrants

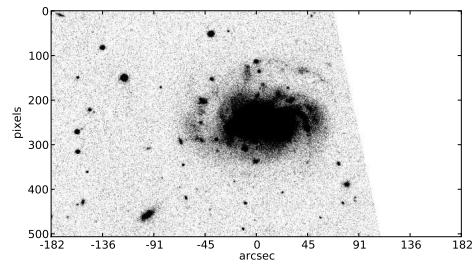


(f) Combined

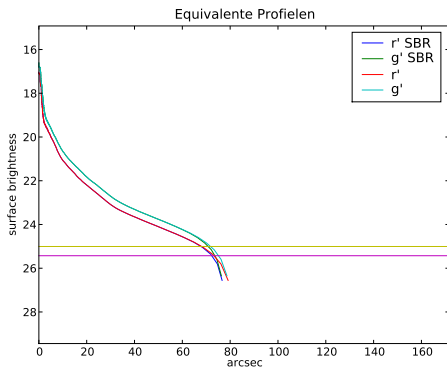
Figure A.64: *Galaxy UGC 02081* - Pohlen en Trujillo have classified this galaxy as Type II.CT. Masking failed horribly in this galaxy. Still a possible truncation may be seen at 80 arcseconds.



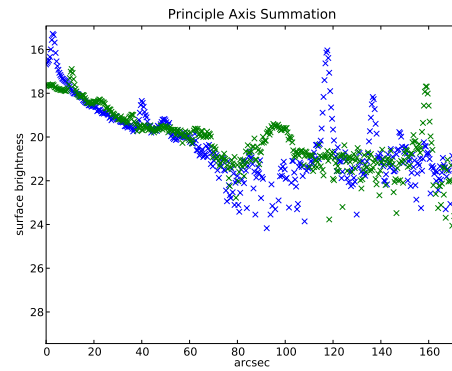
(a) r' band image



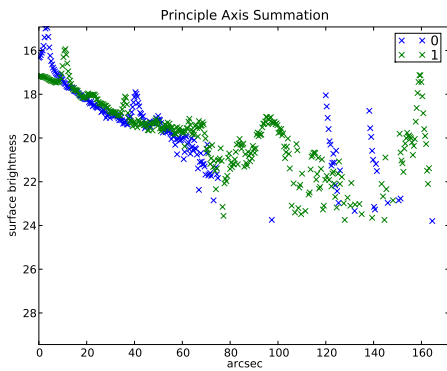
(b) low luminosity r' band image



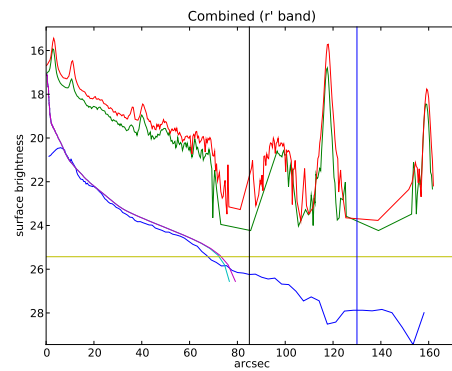
(c) Equivalent Profiles



(d) Axial Summation of 4 Quadrants

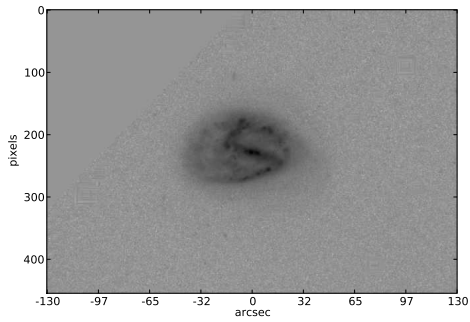


(e) Axial Summation of 4 Quadrants

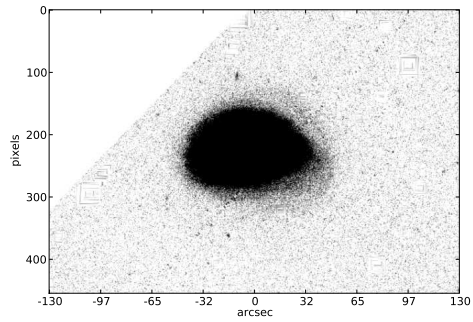


(f) Combined

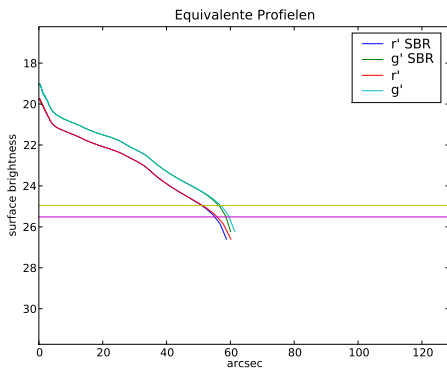
Figure A.65: *Galaxy UGC 04393* - Pohlen en Trujillo have classified this galaxy as Type I. Masking failed in this galaxy. A possible truncation is seen at 70 arcseconds.



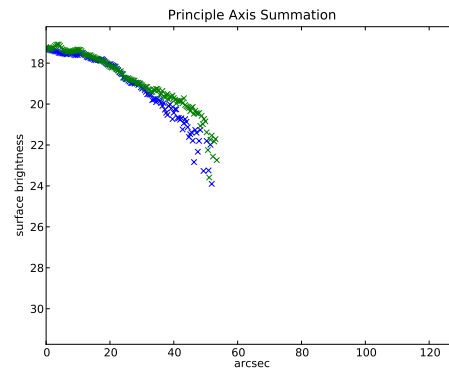
(a) r' band image



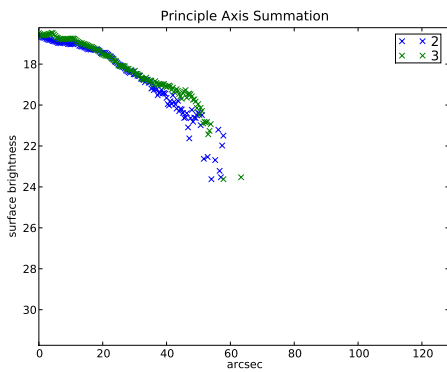
(b) low luminosity r' band image



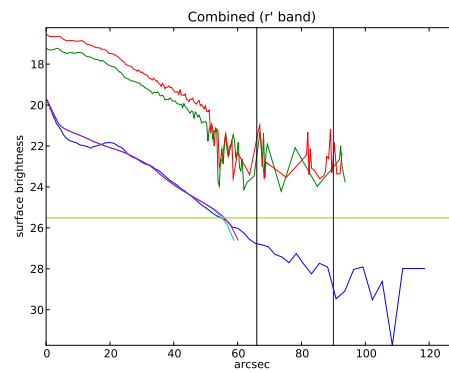
(c) Equivalent Profiles



(d) Axial Summation of 4 Quadrants

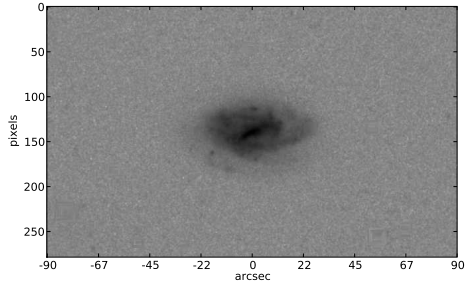


(e) Axial Summation of 4 Quadrants

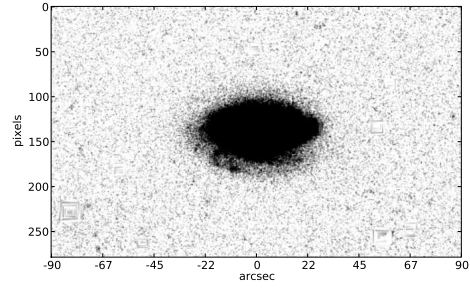


(f) Combined

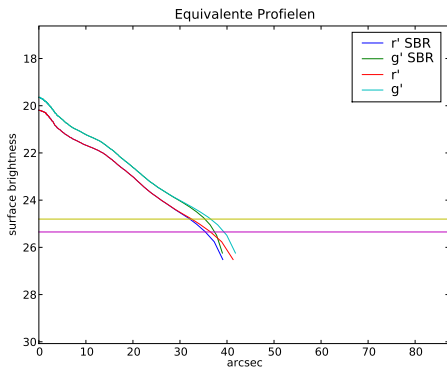
Figure A.66: *Galaxy UGC 06309* - Pohlen en Trujillo have classified this galaxy as Type II.i. A possible truncation at 60 arcseconds. Figure *b* shows a clear asymmetry and leads to doubts about the reliability of the data.



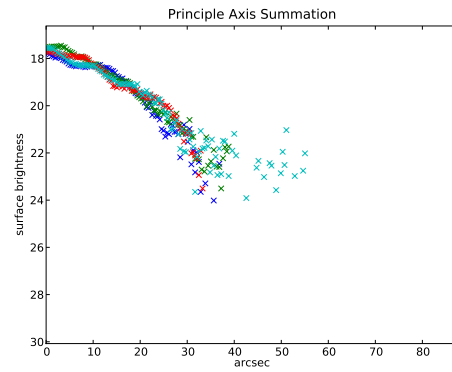
(a) r' band image



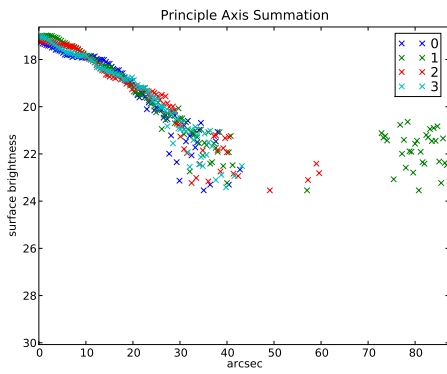
(b) low luminosity r' band image



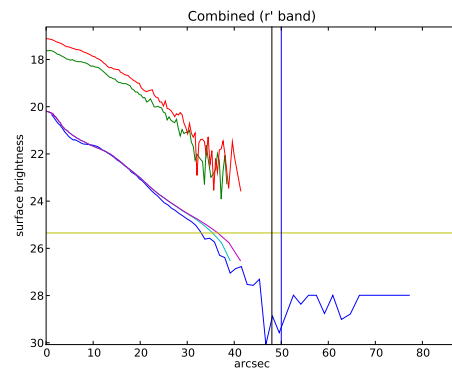
(c) Equivalent Profiles



(d) Axial Summation of 4 Quadrants

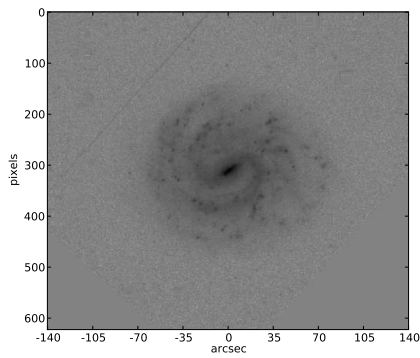


(e) Axial Summation of 4 Quadrants

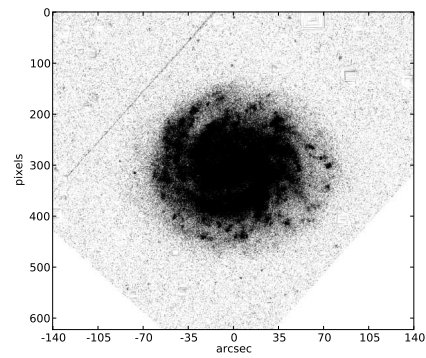


(f) Combined

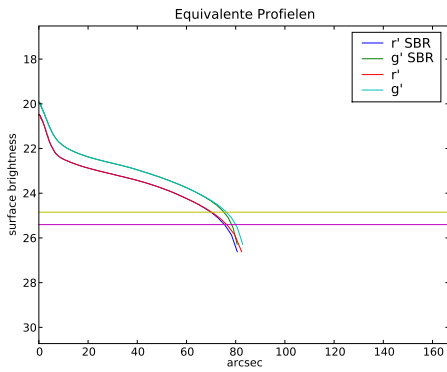
Figure A.67: *Galaxy UGC 06518* - Pohlen en Trujillo have classified this galaxy as Type II.i. A clear truncation at 40 arcseconds.



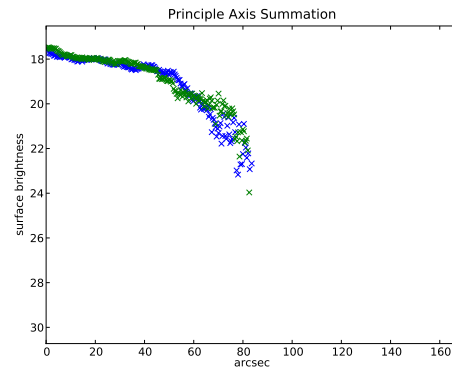
(a) r' band image



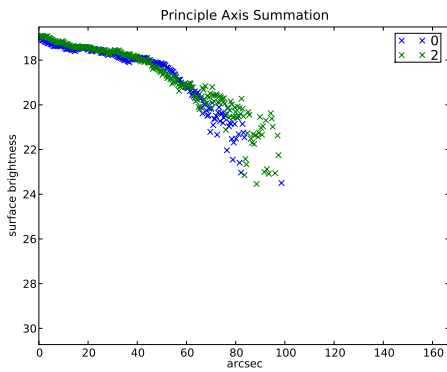
(b) low luminosity r' band image



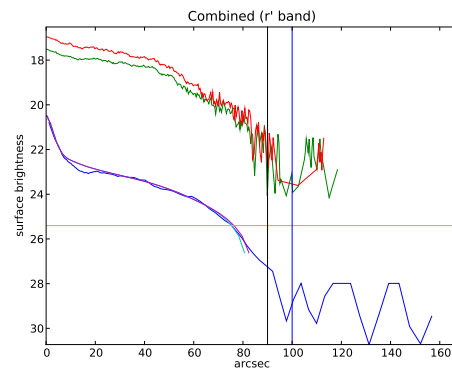
(c) Equivalent Profiles



(d) Axial Summation of 4 Quadrants

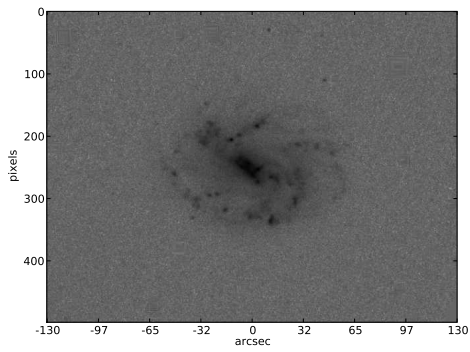


(e) Axial Summation of 4 Quadrants

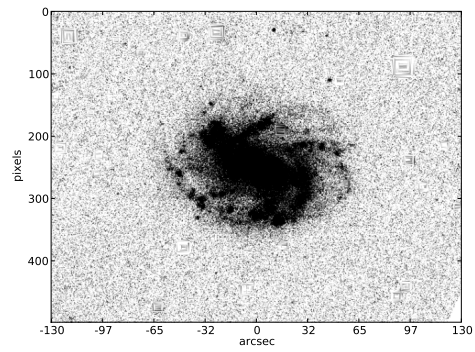


(f) Combined

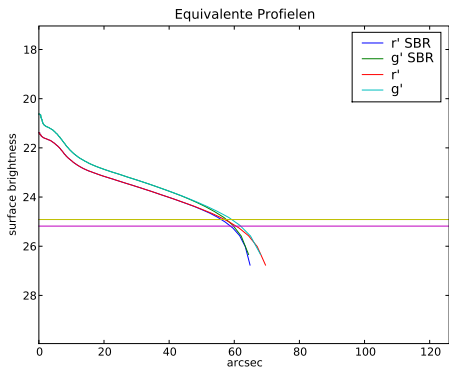
Figure A.68: *Galaxy UGC 06903* - Pohlen en Trujillo have classified this galaxy as Type II.o-CT. A clear truncation at 90 arcseconds.



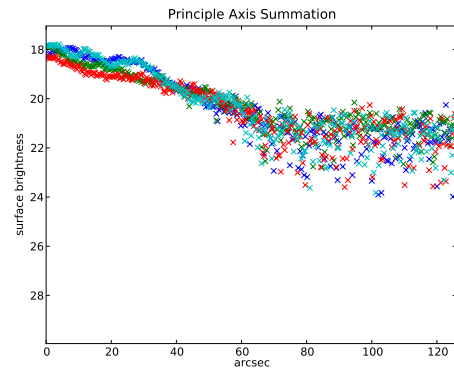
(a) r' band image



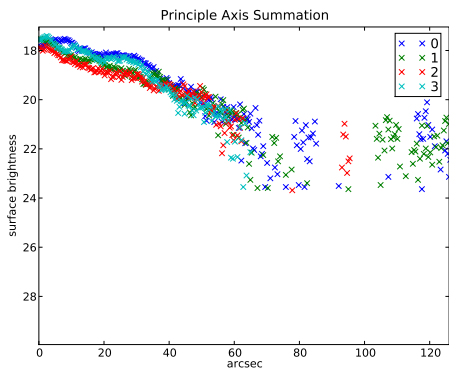
(b) low luminosity r' band image



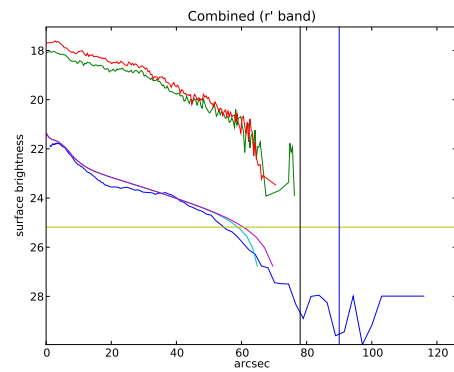
(c) Equivalent Profiles



(d) Axial Summation of 4 Quadrants

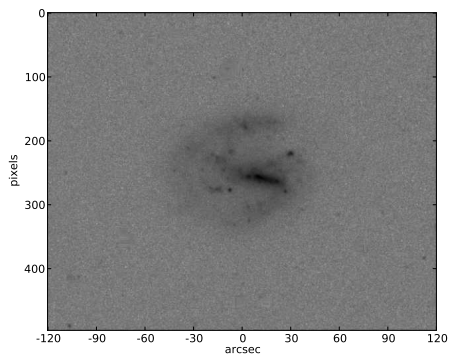


(e) Axial Summation of 4 Quadrants

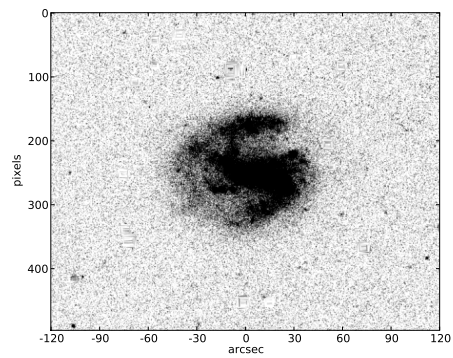


(f) Combined

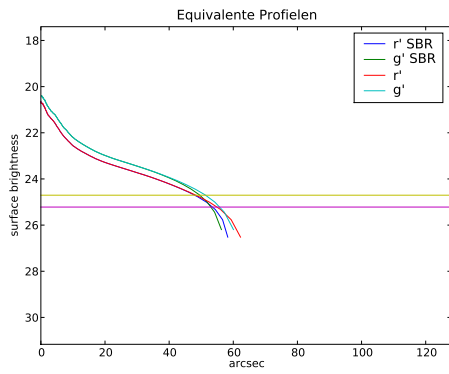
Figure A.69: *Galaxy UGC 07700* - Pohlen en Trujillo have classified this galaxy as Type II.o-CT. A clear truncation at 70 arcseconds.



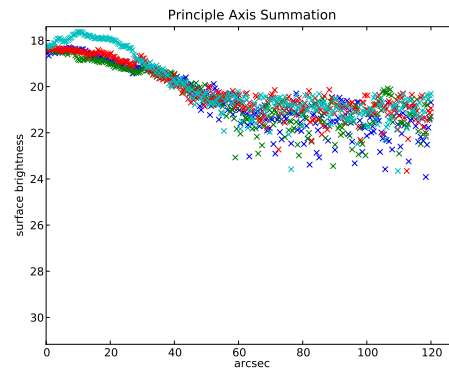
(a) r' band image



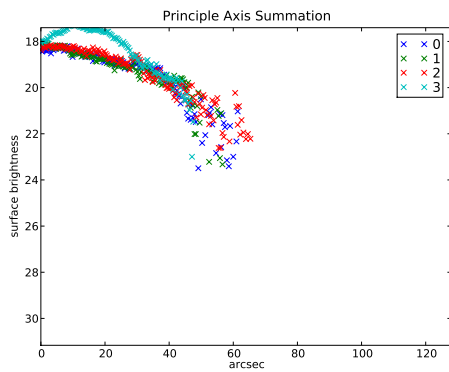
(b) low luminosity r' band image



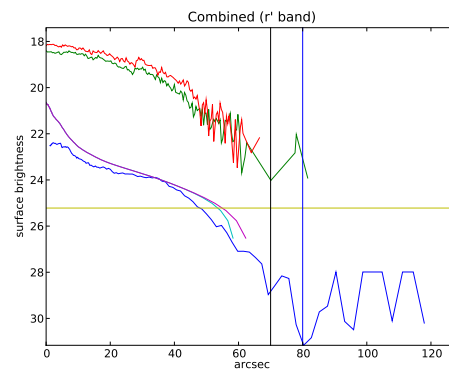
(c) Equivalent Profiles



(d) Axial Summation of 4 Quadrants

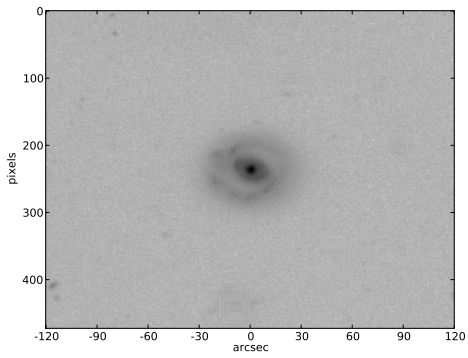


(e) Axial Summation of 4 Quadrants

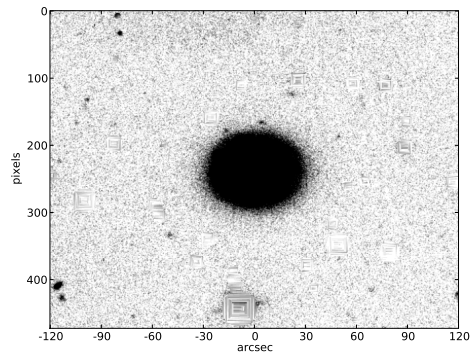


(f) Combined

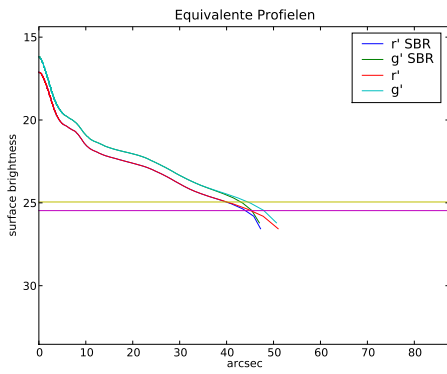
Figure A.70: *Galaxy UGC 08084* - Pohlen en Trujillo have classified this galaxy as Type II.o-OLR. This galaxy might show a truncation at 60 arcseconds. But as can be seen from *b* it is horribly unsymmetrical.



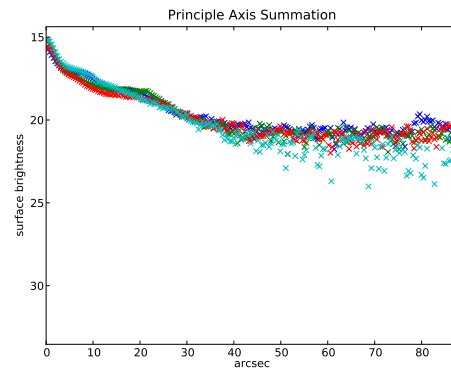
(a) r' band image



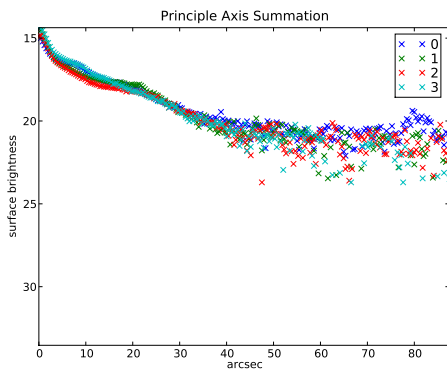
(b) low luminosity r' band image



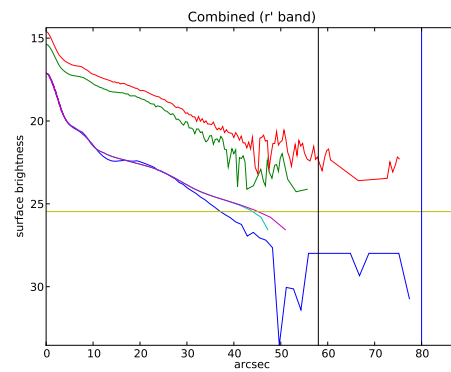
(c) Equivalent Profiles



(d) Axial Summation of 4 Quadrants

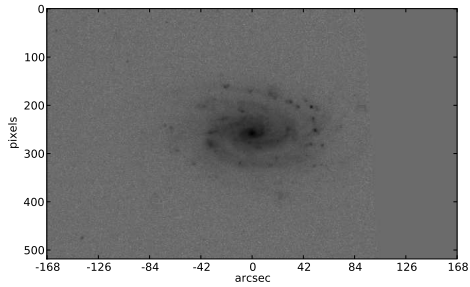


(e) Axial Summation of 4 Quadrants

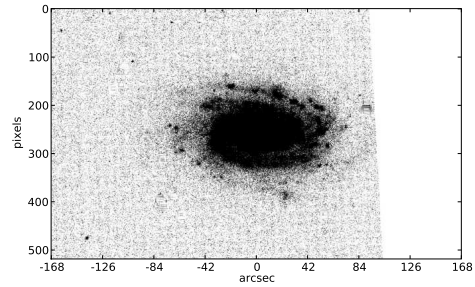


(f) Combined

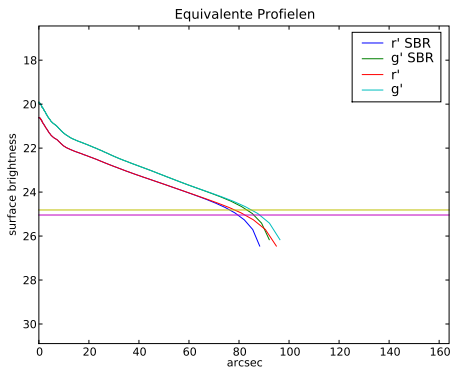
Figure A.71: *Galaxy UGC 08237* - Pohlen en Trujillo have classified this galaxy as Type II.o-OLR. No clear truncation is seen in the r' band. The g' band might possibly show a truncation. Underlimit is set at 50 arcsec.



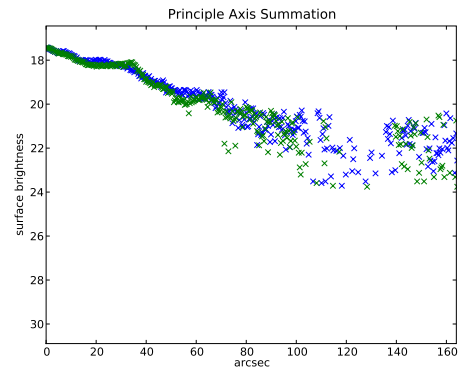
(a) r' band image



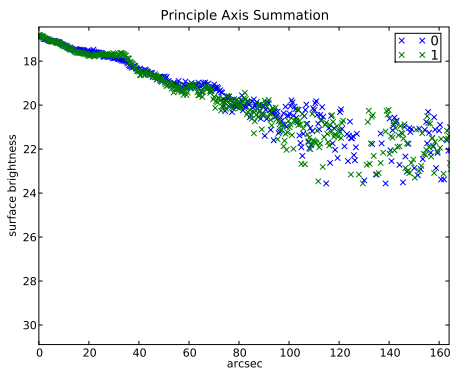
(b) low luminosity r' band image



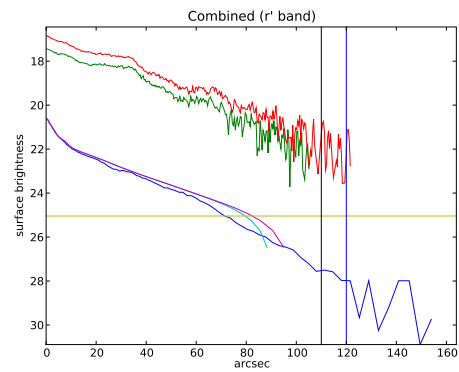
(c) Equivalent Profiles



(d) Axial Summation of 4 Quadrants

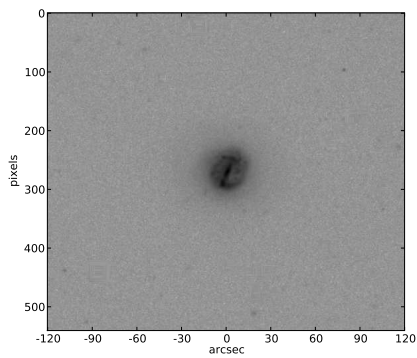


(e) Axial Summation of 4 Quadrants

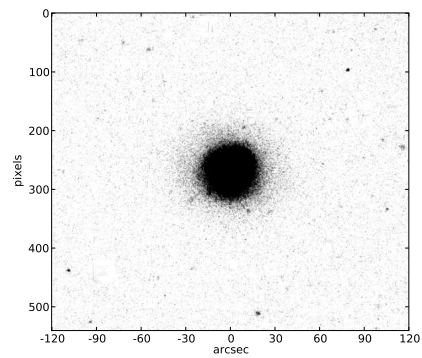


(f) Combined

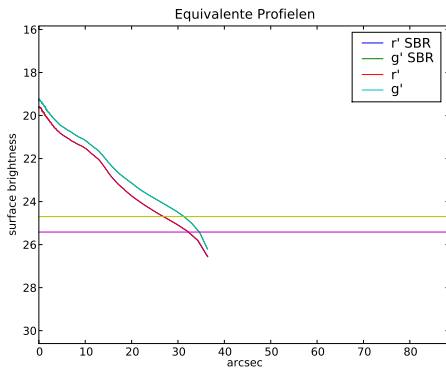
Figure A.72: *Galaxy UGC 08658* - Pohlen en Trujillo have classified this galaxy as Type II-CT. No truncation is found. The underlimit is set at 110 arcseconds.



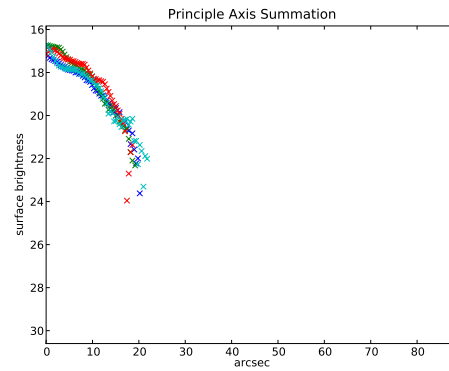
(a) r' band image



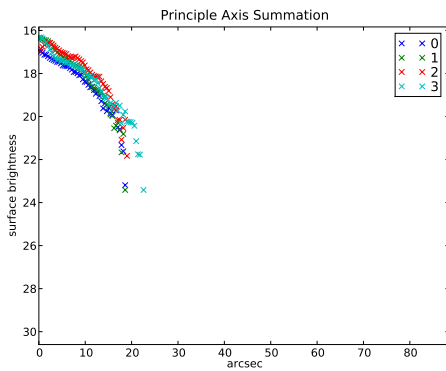
(b) low luminosity r' band image



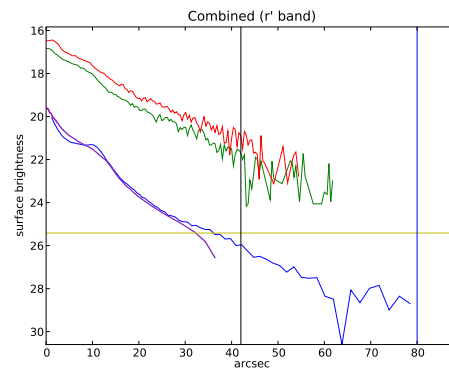
(c) Equivalent Profiles



(d) Axial Summation of 4 Quadrants

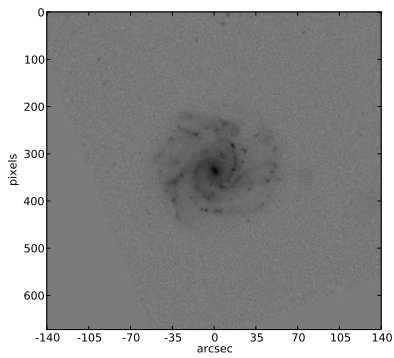


(e) Axial Summation of 4 Quadrants

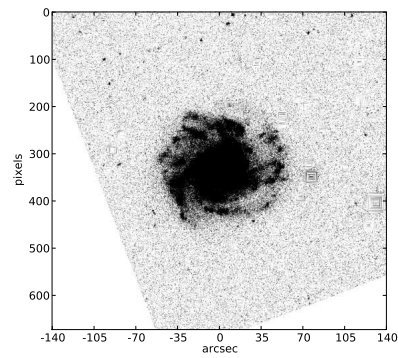


(f) Combined

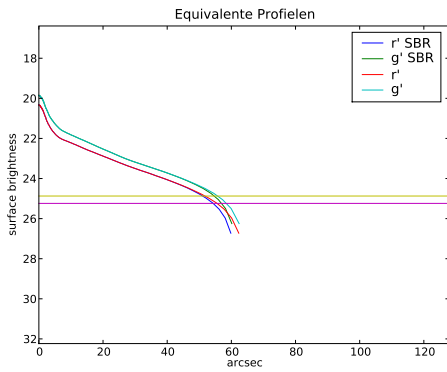
Figure A.73: *Galaxy UGC 09741* - Pohlen en Trujillo have classified this galaxy as Type III. The galaxy is not perfectly circular. A truncation is seen at 50 arcseconds.



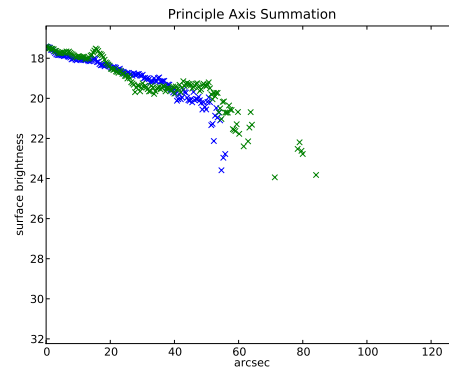
(a) r' band image



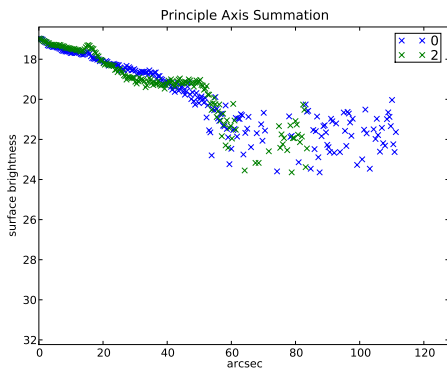
(b) low luminosity r' band image



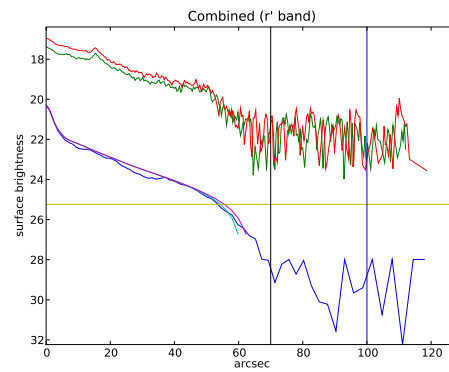
(c) Equivalent Profiles



(d) Axial Summation of 4 Quadrants

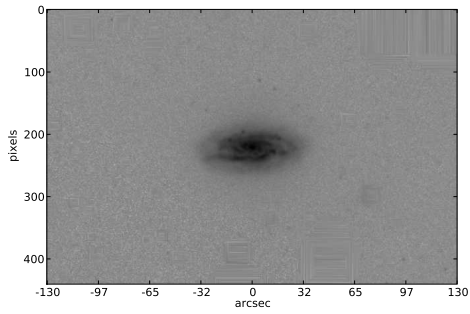


(e) Axial Summation of 4 Quadrants

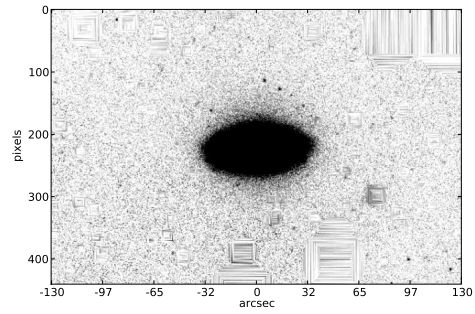


(f) Combined

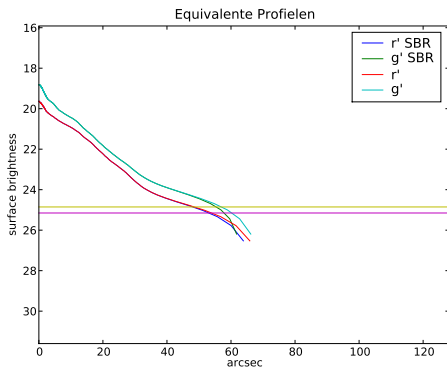
Figure A.74: *Galaxy UGC 09837* - Pohlen en Trujillo have classified this galaxy as Type II-CT. A clear truncation is seen at 70 arcsec.



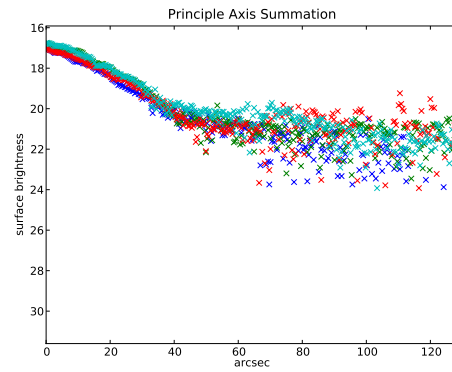
(a) r' band image



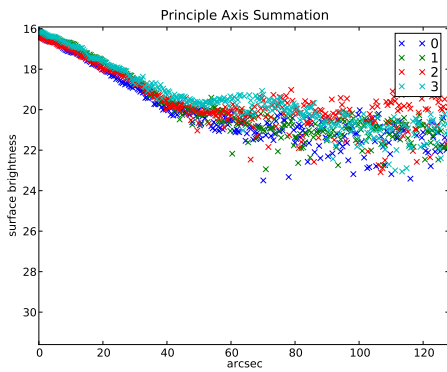
(b) low luminosity r' band image



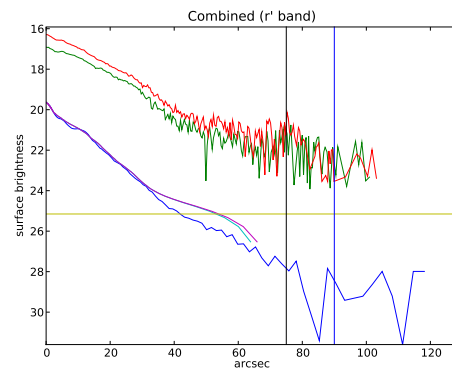
(c) Equivalent Profiles



(d) Axial Summation of 4 Quadrants

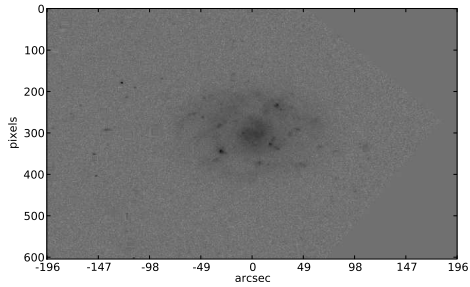


(e) Axial Summation of 4 Quadrants

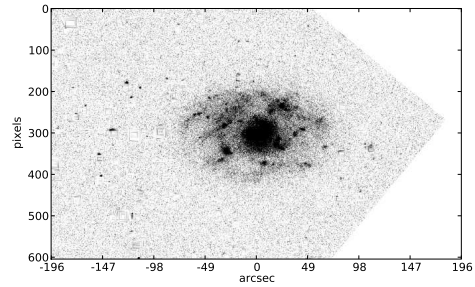


(f) Combined

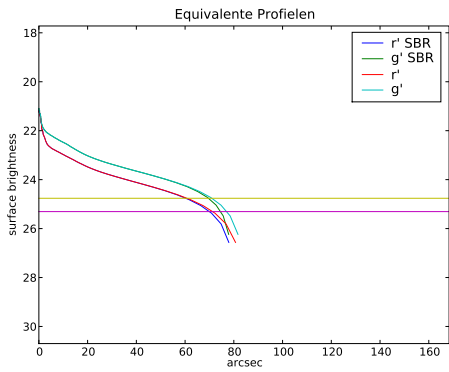
Figure A.75: *Galaxy UGC 10721* - Pohlen en Trujillo have classified this galaxy as Type III. Again a disturbance is seen. A truncation is seen at 80 arcsec.



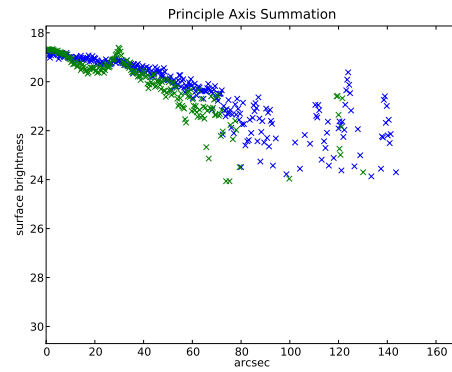
(a) r' band image



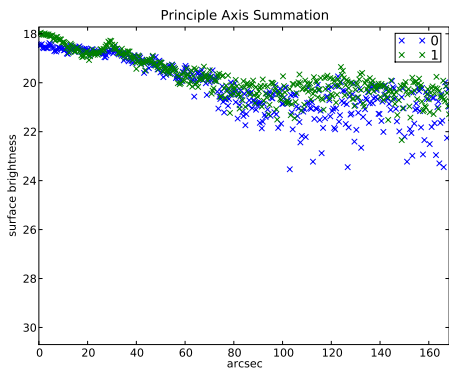
(b) low luminosity r' band image



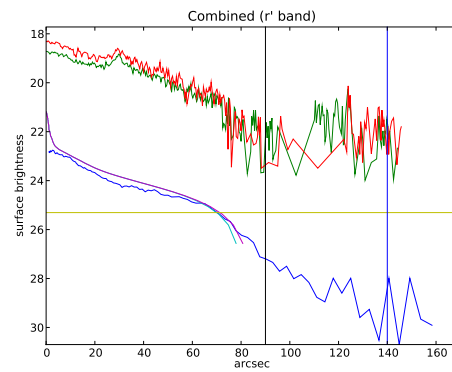
(c) Equivalent Profiles



(d) Axial Summation of 4 Quadrants



(e) Axial Summation of 4 Quadrants



(f) Combined

Figure A.76: *Galaxy UGC 12709* - Pohlen en Trujillo have classified this galaxy as Type II-CT. The profile is too contaminated for any conclusions to be drawn.